

Thermal quenches in $\mathcal{N} = 2^*$ plasmas

Alex Buchel,^{1,2} Luis Lehner^{1,3} and Robert C. Myers¹

¹ *Perimeter Institute for Theoretical Physics
Waterloo, Ontario N2J 2W9, Canada*

² *Department of Applied Mathematics, University of Western Ontario
London, Ontario N6A 5B7, Canada*

³ *Department of Physics, University of Guelph
Guelph, Ontario N1G 2W1, Canada*

Abstract

We exploit gauge/gravity duality to study ‘thermal quenches’ in a plasma of the strongly coupled $\mathcal{N} = 2^*$ gauge theory. Specifically, we consider the response of an initial thermal equilibrium state of the theory under variations of the bosonic or fermionic mass, to leading order in $m/T \ll 1$. When the masses are made to vary in time, novel new counterterms must be introduced to renormalize the boundary theory. We consider transitions the conformal super-Yang-Mills theory to the mass deformed gauge theory and also the reverse transitions. By construction, these transitions are controlled by a characteristic time scale \mathcal{T} and we show how the response of the system depends on the ratio of this time scale to the thermal time scale $1/T$. The response shows interesting scaling behaviour both in the limit of fast quenches with $T\mathcal{T} \ll 1$ and slow quenches with $T\mathcal{T} \gg 1$. In the limit that $T\mathcal{T} \rightarrow \infty$, we observe the expected adiabatic response. For fast quenches, the relaxation to the final equilibrium is controlled by the lowest quasinormal mode of the bulk scalar dual to the quenched operator. For slow quenches, the system relaxes with a (nearly) adiabatic response that is governed entirely by the late time profile of the mass. We describe new renormalization scheme ambiguities in defining gauge invariant observables for the theory with time dependant couplings.

June 28, 2012

Contents

1	Introduction	2
2	Gravitational description of $\mathcal{N} = 2^*$ gauge theory	6
2.1	Holographic renormalization	10
2.1.1	Renormalization of $m^2 = -3$ bulk scalar	11
2.1.2	Renormalization of $m^2 = -4$ bulk scalar	14
2.2	High temperature equilibrium thermodynamics	16
3	Holographic mass quenches at high temperatures	20
3.1	Physical observables and ambiguities	23
3.1.1	$m^2 = -3$	24
3.1.2	$m^2 = -4$	29
4	Numerical procedure	34
4.1	$m^2 = -3$	35
4.2	$m^2 = -4$	35
5	Results	36
5.1	Quenches with \mathcal{O}_3	37
5.2	Quenches with \mathcal{O}_2	46
6	Conclusions	54
A	Discretization of the evolution equation	69

1 Introduction

Consider quantum mechanics with a Hamiltonian which depends on some external parameter λ ,

$$H_\lambda = H_0 + \lambda \delta H. \tag{1.1}$$

The dynamics of the system induced by variations in λ is well-understood, *e.g.*, see [1]. In particular, consider beginning with $\lambda = 0$ and preparing the system in an energy eigenstate of the Hamiltonian H_0 . If the new coupling is turned on adiabatically, the system continues in an eigenstate with a time-dependent energy which simply traces

the changes in $\lambda(t)$. In contrast, if the coupling is abruptly turned on, *e.g.*, $\lambda = \lambda_0 \theta(t)$, the system would evolve forward in a complicated linear superposition of eigenstates of the new Hamiltonian. While the description of adiabatically evolving couplings is easily adapted to quantum field theory (QFT) [2], the description of the latter ‘quantum quenches’ is less well understood in the context. However, it has become the subject of a vigorous research program motivated by the recent advances in cold atom experiments [3–5].

Gauge/gravity duality [6] provides a remarkable framework for the study of certain strongly coupled gauge theories. Although the most applications of this correspondence have been directed at analyzing the static properties of the boundary theories, there is no conceptual obstacle in applying this holographic framework to time dependant problems and in particular, to the study of quantum quenches [7]. In fact, early attention was given to the related question of describing ‘thermalization’ within this holographic framework [8] and motivated by connections with the strongly coupled quark-gluon plasma, there has been a renewed interest in this subject [9–12]. However, given the complexities of the bulk description of rapid changes in the boundary theory, numerical relativity is increasingly being applied to study these ‘far from equilibrium’ situations [13–19].

In this paper we begin a study of quenches in the strongly couple $\mathcal{N} = 2^*$ gauge theory [20–22] applying the techniques of numerical relativity. Recall that $\mathcal{N} = 2^*$ gauge theory is obtained as a deformation of the $\mathcal{N} = 4$ super-Yang-Mills (SYM), where a $\mathcal{N} = 2$ hypermultiplet acquires a mass m . For technical reasons, we will limit our present investigation to ‘thermal quenches,’ where the initial state is a thermal state, *i.e.*, the $\mathcal{N} = 2^*$ theory is prepared in a microcanonical ensemble, and we work to leading order in in a high temperature expansion with $m \ll T$.¹ As explained in [25], in such a thermal state, we can split the masses of the bosonic and the fermionic components of the massive hypermultiplet. Hence we investigate two separate classes of thermal quenches with

$$\mathcal{L}_{SYM} + \lambda_{\Delta}(t) \mathcal{O}_{\Delta}, \tag{1.2}$$

where we may have either the bosonic mass operator \mathcal{O}_2 or the fermionic mass operator \mathcal{O}_3 (with dimensions $\Delta = 2$ and 3 , respectively). Of course, the couplings which vary in time are then simply the corresponding masses, *i.e.*, $\lambda_2 = m_b^2$ and $\lambda_3 = m_f$. In

¹Thermodynamics of $\mathcal{N} = 2^*$ plasma was discussed in [23–26].

particular, we will consider the following specific profiles for these couplings

$$\lambda_{\Delta}(t) = \frac{1}{2} \lambda_{\Delta}^0 \left[1 \pm \tanh(t/\mathcal{T}) \right]. \quad (1.3)$$

Note that the profile in eq. (1.3) with the + sign has $\lambda_{\Delta}(t \rightarrow -\infty) = 0$ and $\lambda_{\Delta}(t \rightarrow +\infty) = \lambda_{\Delta}^0$. Hence it produces a transition from an initial thermal state in the conformal SYM gauge theory to a final state of a massive gauge theory. Meanwhile the profile with the - sign then corresponds to the reverse transition from the massive theory to the conformal theory.

We have introduced the time scale \mathcal{T} in eq. (1.3) to control the rate of these transitions. This will allow us to consider not only abrupt quenches (with $\mathcal{T} \rightarrow 0$) but also transitions made over a finite time. In particular, we will also consider the adiabatic limit where $\mathcal{T} \rightarrow \infty$. We will find that the response to these different quenches will depend on how \mathcal{T} compares to the thermal time scale $1/T$. Hence it will be convenient in the following to define the dimensionless ratio $\alpha \equiv \pi T_i \mathcal{T}$, where T_i is the temperature of the initial state. Note that while our calculations of these thermal quenches are perturbative in m/T_i , they are no restrictions² on the rate controlling ratio $T_i \mathcal{T}$.

The holographic dual of the $\mathcal{N} = 2^*$ gauge theory consists of Einstein gravity coupled to two massive scalar fields in five dimensions, as will be described in detail in the next section. Of course, within this framework, the initial thermal state is described by an asymptotically anti-de Sitter (AdS) black hole and the quenches are realized by varying the asymptotic behaviour of the corresponding scalar with the given profile (1.3). This variation essentially excites the bulk scalar with a wave packet that falls down into the horizon from the asymptotic boundary. Our numerical simulations evaluate the evolution of these scalar excitations in detail and in particular, allow us to determine the response of the boundary theory, as measured by the expectation values of the stress energy $\langle T_{ij} \rangle$ and the operator $\langle \mathcal{O}_{\Delta} \rangle$. Our main focus is to study the transitions from the massive theory to the conformal theory, however, as we will explain, the results for the reverse transitions readily follows from the previous case, in the high temperature limit.

Before proceeding, let us summarize the results of our study:

- New ultraviolet divergences appear into the quantum field theory when the couplings are made to vary in time, as for the quenches described above. Holography provides a well-defined approach to regulating these new divergences and renormalizing the

²One caveat to this statement will be discussed in section 6.

boundary theory, even in the presence of such time varying couplings. In particular, the necessary new counterterms are readily identified.

- The response to fast quenches with $\alpha \ll 1$ exhibits an interesting scaling behaviour in α , similar to that noted previously in [9, 13]. This scaling is apparent both in the immediate response of the observables, *e.g.*, $\langle \mathcal{O}_\Delta(t) \rangle$, and in the comparison of the initial and final state, *e.g.*, the overall change in the energy density. These scalings are particularly dramatic in the case of the dimension three operator, where the immediate response scales as $\alpha^{-2} \ln(1/\alpha)$ as $\alpha \rightarrow 0$. For both operators, this scaling behaviour is divergent and naively suggests that an abrupt quench with $\alpha = 0$ is unphysical. However, our present perturbative analysis is not sufficient to reliably confirm this conclusion.
- For very slow transitions with $\alpha \gg 1$, the system essentially maintains thermodynamic equilibrium throughout the process and the response simply tracks the change in the coupling. The approach to the adiabatic limit with $\alpha \rightarrow \infty$ also exhibits an interesting scaling behaviour with α . As expected the entropy production goes to zero in this limit confirming that the adiabatic quenches are reversible.
- The relaxation of the system after a thermal quench of the coupling is sensitive to whether the ratio of the characteristic time-scale \mathcal{T} to the thermal scale $1/T_i$ is larger or smaller than one, *i.e.*, whether $\alpha \gtrsim 1$ or $\alpha \lesssim 1$. For fast quenches (with $\alpha \ll 1$), the relaxation is dominated by the lowest quasinormal mode of the bulk scalar. This behaviour indicates that the relaxation after fast quenches is universally controlled by the characteristic thermal time scale $1/T_i$, as has been observed previously in [13, 16, 18]. In contrast, for slow quenches (with $\alpha \gg 1$), the system relaxes with a (nearly) adiabatic response and so the relaxation is governed entirely by the late time profile of the coupling.
- The holographic renormalization of the boundary theory with time-dependent couplings introduces new scheme-dependent ambiguities. This situation is rather reminiscent of the ambiguities that arise in studying QFT in curved spacetime [27]. All of these new ambiguities only play a role while the couplings are varying and so they are not important after the coupling has achieved its final value.

The remainder is organized as follows: In section 2, we review the dual gravitational description of strongly coupled $\mathcal{N} = 2^*$ gauge theory, its holographic renormalization for arbitrary sources, and the high-temperature equilibrium thermodynamics. In sec-

tion 3, we derive the bulk equations of motion describing the gravitational dual of the mass quenches (1.3). We also compute the expectation values of the stress-energy tensor and the operator \mathcal{O}_Δ throughout the quench. Our numerical procedure is outlined in section 4. In section 5, we provide a detailed discussion of the results of our numerical simulations. We conclude with further comments and future directions in section 6. Further details of the analysis, as well as the description of the discretization of the evolution equations, are discussed in appendix A.

2 Gravitational description of $\mathcal{N} = 2^*$ gauge theory

In this paper, we will use holography to study quenches of the masses for the $\mathcal{N} = 2^*$ gauge theory at strong coupling [20–22]. However, to begin let us recall the field theoretic description of the mass deformation of the $\mathcal{N} = 4$ SYM which yields the $\mathcal{N} = 2^*$ theory. The field content of the $\mathcal{N} = 4$ SYM theory includes the gauge field A_μ , four Majorana fermions ψ_a and three complex scalars ϕ_i , where all of these fields are in the adjoint representation. Now the SYM theory can be deformed by adding two independent ‘mass’ terms [26]

$$\delta\mathcal{L} = -2 \int d^4x \left[m_b^2 \mathcal{O}_2 + m_f \mathcal{O}_3 \right] \quad (2.1)$$

where

$$\mathcal{O}_2 = \frac{1}{3} \text{Tr} \left(|\phi_1|^2 + |\phi_2|^2 - 2|\phi_3|^2 \right), \quad (2.2)$$

$$\begin{aligned} \mathcal{O}_3 = & -\text{Tr} \left(i \psi_1 \psi_2 - \sqrt{2} g_{\text{YM}} \phi_3 [\phi_1, \phi_1^\dagger] + \sqrt{2} g_{\text{YM}} \phi_3 [\phi_2^\dagger, \phi_2] + \text{h.c.} \right) \\ & + \frac{2}{3} m_f \text{Tr} \left(|\phi_1|^2 + |\phi_2|^2 + |\phi_3|^2 \right). \end{aligned} \quad (2.3)$$

If one fixes $m_b = m_f$, the effect is to give masses to an $\mathcal{N} = 2$ hypermultiplet consisting of $\lambda_{1,2}$ and $\phi_{1,2}$, *i.e.*, the resulting theory still preserves $\mathcal{N} = 2$ supersymmetry. Note that beyond a fermion mass term, the dimension-3 operator contains trilinear couplings between the hypermultiplet scalars and ϕ_3 , as well as a mass term for all three scalars. Note that the latter is a coupling-dependent correction induced at finite mass, *i.e.*, so that $m_f \mathcal{O}_3$ contains a contribution of order m_f^2 . The presence of these additional interactions is dictated by the supersymmetry algebra and the latter mass terms can be distinguished from those in \mathcal{O}_2 by their transformation properties under the $SO(6)_R$ symmetry of the $\mathcal{N} = 4$ theory [26]. Further note that the dimension-2 operator

\mathcal{O}_2 contains an unstable mass term for the scalar ϕ_3 , which is in the $\mathcal{N} = 2$ vector multiplet, as well as positive masses for the two scalars in the hypermultiplet. The two mass contributions for ϕ_3 only cancel with $m_b = m_f$, leaving this scalar massless in the supersymmetric theory. In the following study of mass quenches, we will vary m_b and m_f independently and so we are not restricting our analysis to the supersymmetric theory. Our assumption will be that the structure of the two independent operators remains as described above. However, one should worry then that the theory may be unstable,³ *i.e.*, when $m_b > m_f$, however, we will also be working at finite temperature with $m_{b,f}/T \ll 1$. In this case, ‘large’ positive thermal masses will be induced for all of the scalars, in particular ϕ_3 , which will prevent any such instabilities from arising.

As we next describe, the holographic dual of these mass deformations is well understood [20–22]. In the dual five-dimensional supergravity, we can restrict our attention to a pair of scalars, which we denote α and χ . This construction and its ‘uplift’ to ten dimensions was originally elucidated by Pilch and Warner [20]. In the full ten-dimensional type IIb supergravity, the two scalars are Kaluza-Klein modes which deform the original $AdS_5 \times S^5$ geometry dual to the $\mathcal{N} = 4$ SYM theory. According to the general framework of holographic RG flows [6], the asymptotic boundary behaviour of the supergravity scalars contains information about the couplings and expectation values of the dual operators in the boundary theory. Here, these are the mass parameters and the two operators presented in eq. (2.1). Our nomenclature will be that the scalar α is dual to the ‘*bosonic*’ mass term \mathcal{O}_2 , in eq. (2.2), while χ is dual to the ‘*fermionic*’ mass term \mathcal{O}_3 in eq. (2.3).

The appropriate terms in the five-dimensional supergravity action, including the scalars α and χ , can be written as

$$I_5 = \int_{\mathcal{M}_5} d\xi^5 \sqrt{-g} \mathcal{L}_5 = \frac{1}{4\pi G_5} \int_{\mathcal{M}_5} d\xi^5 \sqrt{-g} \left[\frac{1}{4} R - 3(\partial\alpha)^2 - (\partial\chi)^2 - \mathcal{V}(\alpha, \chi) \right], \quad (2.4)$$

where the potential takes the form

$$\mathcal{V}(\alpha, \chi) = -e^{-4\alpha} - 2e^{2\alpha} \cosh(2\chi) + \frac{1}{4} e^{8\alpha} \sinh^2(2\chi). \quad (2.5)$$

Implicitly here, we set have the curvature radius of the five-dimensional AdS vacuum to be unity, *i.e.*, $L = 1$. With these conventions, the five-dimensional Newton’s constant

³A full description of these instabilities (including their end-point) at strong coupling would require extending the holographic framework described below and may well require considering the full ten-dimensional string theory in the bulk.

becomes

$$G_5 \equiv \frac{\pi}{2N^2}. \quad (2.6)$$

The resulting Einstein equations can be written as

$$R_{\mu\nu} = 12\partial_\mu\alpha\partial_\nu\alpha + 4\partial_\mu\chi\partial_\nu\chi + \frac{4}{3}g_{\mu\nu}\mathcal{V}, \quad (2.7)$$

while the equations of motion for the scalars become

$$\square\alpha = \frac{1}{6}\frac{\partial\mathcal{V}}{\partial\alpha} \quad \text{and} \quad \square\chi = \frac{1}{2}\frac{\partial\mathcal{V}}{\partial\chi}. \quad (2.8)$$

As commented above, we are considering quenches of the mass parameters at finite temperature and in the regime $m_{b,f}/T \ll 1$. This means that the dual holographic background will be an asymptotically AdS black hole and we will work perturbatively in the amplitude of the bulk scalars. In this case, the scalar sector of the effective action (2.4) can be expanded up to quadratic order in α and χ . Furthermore, since the potential (2.5) does not contain a quadratic term mixing the two scalars, each of them can be treated independently, *i.e.*, we study quenches in

$$I_5 = \frac{1}{16\pi G_5} \int d^5\xi \sqrt{-g} \left(R + 12 - \frac{1}{2}(\partial\phi)^2 - \frac{1}{2}m^2\phi^2 + \mathcal{O}(\phi^3) \right), \quad (2.9)$$

with

$$m^2 = \begin{cases} -3, & \text{if } \phi = 2\sqrt{2}\chi \iff \text{fermionic mass operator } \mathcal{O}_3, \\ -4, & \text{if } \phi = 2\sqrt{6}\alpha \iff \text{bosonic mass operator } \mathcal{O}_2. \end{cases} \quad (2.10)$$

The quenches which we study will be homogeneous and isotropic in the spatial directions on the boundary. Hence our ansatz for both the background metric and the bulk scalar field depend only⁴ on a radial coordinate r and a time v :

$$ds_5^2 = -A(v, r) dv^2 + \Sigma(v, r)^2 d\vec{x}^2 + 2 dr dv, \quad \phi = \phi(v, r). \quad (2.11)$$

The metric ansatz is adapted to infalling Eddington-Finkelstein (EF) coordinates, which has proven useful in holographic investigations of the dynamics of thermal systems [13, 14, 28]. With this ansatz, we will assume that the asymptotic AdS boundary occurs at $r \rightarrow \infty$ with

$$A(v, r) \rightarrow r^2 \quad \text{and} \quad \Sigma \rightarrow r. \quad (2.12)$$

⁴Some limitations of this approximation are discussed in section 6.

Given eq. (2.11), we obtain the following equations of motion:

$$0 = \frac{2}{A} \partial_r(\dot{\phi}) + \frac{3 \partial_r \Sigma}{\Sigma A} \dot{\phi} + \frac{3 \partial_r \phi}{\Sigma A} \dot{\Sigma} - \frac{m^2}{A} \phi, \quad (2.13)$$

$$0 = \Sigma \partial_r(\dot{\Sigma}) + 2 \dot{\Sigma} \partial_r \Sigma - 2 \Sigma^2 + \frac{1}{12} m^2 \phi^2 \Sigma^2, \quad (2.14)$$

$$0 = \partial_r^2 A - \frac{12}{\Sigma^2} \dot{\Sigma} \partial_r \Sigma + 4 + \dot{\phi} \partial_r \phi - \frac{1}{6} m^2 \phi^2, \quad (2.15)$$

$$0 = \ddot{\Sigma} - \frac{1}{2} \partial_r A \dot{\Sigma} + \frac{1}{6} \Sigma (\dot{\phi})^2, \quad (2.16)$$

$$0 = \partial_r^2 \Sigma + \frac{1}{6} \Sigma (\partial_r \phi)^2, \quad (2.17)$$

where we have defined for any function $h(r, v)$,

$$\dot{h} \equiv \partial_v h + \frac{1}{2} A \partial_r h. \quad (2.18)$$

Note that eqs. (2.16) and (2.17) are constraint equations. In particular, the radial derivative of eq. (2.16) and the time derivative of eq. (2.17) are both implied by the first three equations. Note also that the form of the metric (2.11) is invariant under the residual diffeomorphism [13]

$$r \rightarrow r + f(v), \quad (2.19)$$

for an arbitrary function $f(v)$ — we use this as a check in our analysis below.

Given eq. (2.12), it is straightforward to find the asymptotic solution to eqs. (2.13–2.17):

■ When $m^2 = -3$,

$$\begin{aligned} \phi &= \frac{1}{r} p_0 + \frac{1}{r^2} \left(-\frac{1}{2} p_0 a_1 + p'_0 \right) + \frac{1}{r^3} \left(p_2 - \left(\frac{1}{2} p_0'' + \frac{1}{6} p_0^3 \right) \ln r \right) + \mathcal{O}(r^{-4} \ln r), \\ \Sigma &= r + \frac{1}{2} a_1 + \mathcal{O}(r^{-1}), \\ A &= r^2 + a_1 r + \frac{1}{4} a_1^2 - \frac{1}{6} p_0^2 - a_1' + \frac{1}{r^2} \left(a_4 + \left(\frac{1}{6} p_0 p_0'' + \frac{1}{36} p_0^4 - \frac{1}{6} (p_0')^2 \right) \ln r \right) \\ &\quad + \mathcal{O}(r^{-3} \ln r), \end{aligned} \quad (2.20)$$

where $\{p_0, p_2, a_1, a_4\}$ are functions of the time v and we have defined $h' \equiv \partial_v h$ for any function $h(v)$. In addition, on the boundary, the constraint (2.16) becomes

$$\begin{aligned} 0 &= -2a_4' + \frac{2}{3} (p_0')^2 a_1 + \frac{5}{27} p_0^3 p_0' - \frac{2}{3} p_0 a_1 p_0'' + \frac{2}{3} p_0' p_2 - \frac{2}{3} p_0 p_2' - \frac{1}{9} p_0' p_0'' + \frac{4}{9} p_0 p_0''' \\ &\quad - \frac{2}{3} p_0 a_1' p_0' + \frac{1}{3} a_1' p_0^2 a_1. \end{aligned} \quad (2.21)$$

Note that if this constraint is imposed on the boundary (*i.e.*, at $r \rightarrow \infty$) then eq. (2.16) will be satisfied at all values of r when the equations of motion (2.13–2.15) are satisfied. Finally, we observe that under the residual diffeomorphism (2.19) one has

$$\begin{pmatrix} p_0 \\ p_2 \\ a_1 \\ a_4 \end{pmatrix} \rightarrow \begin{pmatrix} p_0 \\ p_2 + p_0(f^2 + fa_1) - 2fp'_0 \\ a_1 + 2f \\ a_4 \end{pmatrix}. \quad (2.22)$$

We emphasize that this transformation will allow us to choose a gauge where $a_1 = 0$, which will do in section 3. Further, we note that the constraint (2.21) is invariant under the transformation (2.22).

■ When $m^2 = -4$,

$$\begin{aligned} \phi &= \frac{1}{r^2} (p_0 + p_0^l \ln r) + \mathcal{O}(r^{-3} \ln r), \\ \Sigma &= r + \frac{1}{2}a_1 + \mathcal{O}(r^{-3} \ln^2 r), \\ A &= r^2 + a_1 r + \frac{1}{4}a_1^2 - a'_1 + \frac{1}{r^2} \left(a_4 - \left(\frac{1}{54}(p_0^l)^2 + \frac{2}{9}p_0 p_0^l \right) \ln r - \frac{1}{9}(p_0^l)^2 \ln^2 r \right) \\ &\quad + \mathcal{O}(r^{-3} \ln r), \end{aligned} \quad (2.23)$$

where $\{p_0, p_0^l, a_1, a_4\}$ are functions of v . In this case, the boundary constraint provided by eq. (2.16) is,

$$0 = -2a'_4 - \frac{20}{81}p_0^l(p_0^l)' + \frac{8}{27}p_0(p_0^l)' - \frac{10}{27}p_0^l p_0' - \frac{4}{9}p_0 p_0'. \quad (2.24)$$

Under residual diffeomorphism (2.19) one has

$$\begin{pmatrix} p_0^l \\ p_0 \\ a_1 \\ a_4 \end{pmatrix} \rightarrow \begin{pmatrix} p_0^l \\ p_0 \\ a_1 + 2f \\ a_4 \end{pmatrix}. \quad (2.25)$$

Hence again, we can use this diffeomorphism to set $a_1 = 0$. Further, the constraint (2.24) is now trivially invariant under the transformation (2.25).

2.1 Holographic renormalization

The physical observables of the boundary theory are the correlation functions of the gauge invariant operators. In the following analysis, we will consider the simplest of

these, namely, the one-point functions. That is, we will examine the response of $\langle T_{ij} \rangle$ and $\langle \mathcal{O}_\Delta \rangle$ to quenches in the mass couplings, as given by eq. (1.3). We will present our investigation of non-local probes of these quenches (*e.g.*, two-point functions, Wilson lines and entanglement entropy) elsewhere [29].

The holographic computation of these one-point functions is most easily implemented using Fefferman-Graham (FG) coordinates [30], which we write here as

$$ds_5^2 = \frac{d\rho^2}{\rho^2} + \frac{1}{\rho^2} G_{ij}(x^k, \rho) dx^i dx^j, \quad (2.26)$$

and

$$\phi = \phi(x^k, \rho). \quad (2.27)$$

The asymptotic AdS boundary now appears at $\rho \rightarrow 0$. As usual, to produce finite results in the holographic calculations, one regulates the bulk by introducing a cut-off surface at $\rho = \epsilon$, with some small ϵ . However, the one-point functions extracted directly from the action (2.9) would still diverge as this cut-off is removed, *i.e.*, as $\epsilon \rightarrow 0$, and thus these observables need to be holographically renormalized. The details of the holographic renormalization are sensitive to the conformal dimension of the particular boundary operator of interest, or correspondingly, to the mass m^2 of the bulk scalar ϕ in eq. (2.9). Hence we discuss the two cases for m^2 separately.

2.1.1 Renormalization of $m^2 = -3$ bulk scalar

First, we note that we are working with a flat boundary metric and thus in the FG metric (2.26),

$$\lim_{\rho \rightarrow 0} G_{ij} = \eta_{ij}. \quad (2.28)$$

Next we need to translate between the EF coordinates in eq. (2.11) and the FG coordinates in eq. (2.26). This coordinate transformation is easily constructed perturbatively for small ρ (large r) by comparing the asymptotic expansion of the bulk solutions of eqs. (2.13–2.15). Hence, using eq. (2.20) for $m^2 = -3$, we find

$$\begin{aligned} v &= t - \rho - \frac{1}{72}\rho^3 p_0(t)^2 + \frac{1}{144}\rho^4 p_0(t)p_0'(t) + \mathcal{O}(\rho^5 \ln \rho), \\ r &= \frac{1}{\rho} \left(1 - \frac{1}{2}\rho a_1(t) + \rho^2 \left(\frac{1}{2}a_1'(t) + \frac{1}{24}p_0(t)^2 \right) \right. \\ &\quad \left. + \rho^3 \left(-\frac{1}{4}a_1''(t) - \frac{1}{18}p_0(t)p_0'(t) \right) + \mathcal{O}(\rho^4 \ln \rho) \right). \end{aligned} \quad (2.29)$$

Note that as one approaches the boundary with $\rho \rightarrow 0$, the EF time v and the FG or boundary time t coincide, *i.e.*,

$$\lim_{\rho \rightarrow 0} v = t. \quad (2.30)$$

Now the relevant boundary counterterms are given by [24, 31, 32]:

$$I_{ct} = I_{ct}^{divergent} + I_{ct}^{finite} \quad (2.31)$$

where

$$I_{ct}^{divergent} = \frac{1}{16\pi G_5} \int_{\partial\mathcal{M}_{5,\rho=\epsilon}} d^4x \sqrt{-\gamma} \left(6 + \frac{1}{2}\phi^2 + \frac{1}{12}\phi^4 \ln \rho \right. \quad (2.32)$$

$$\left. + \frac{1}{2} \gamma^{ij} \partial_i \phi \partial_j \phi \ln \rho + \frac{1}{12} R^\gamma \phi^2 \ln \rho \right),$$

$$I_{ct}^{finite} = \frac{1}{16\pi G_5} \int_{\partial\mathcal{M}_{5,\rho=\epsilon}} d^4x \sqrt{-\gamma} \left(\delta_1 \phi^4 + \delta_2 \gamma^{ij} \partial_i \phi \partial_j \phi + \delta_3 R^\gamma \phi^2 \right). \quad (2.33)$$

These expressions are written using

$$\gamma_{ij} dx^j dx^j \equiv \rho^{-2} G_{ij}(x^k, \rho) dx^i dx^j. \quad (2.34)$$

Implicitly then, the boundary action contains many potentially divergent factors, *e.g.*, $\sqrt{-\gamma} = O(\epsilon^{-4})$. Above, we have separated the counterterms which diverge in the limit $\epsilon \rightarrow 0$ from the finite counterterms. Further R^γ is the Ricci scalar constructed from γ_{ij} treated as a four-dimensional metric with an external parameter ρ . Note that even though the boundary metric (2.28) is flat, the term proportional to $R^\gamma \phi^2$ contributes to the holographic renormalization in the presence of space-time varying sources [32]. As usual, the coefficients δ_i of the finite counterterms (2.33) are arbitrary constants, which are related to ambiguities in the renormalization scheme.

Combining all of these expressions to compute the renormalized one-point functions for

$$\langle T_{ij} \rangle \equiv \left(\mathcal{E}, \mathcal{P}, \mathcal{P}, \mathcal{P} \right), \quad (2.35)$$

and $\langle \mathcal{O}_3 \rangle$, we find

$$\begin{aligned}
8\pi G_5 \mathcal{E} &= -\frac{3}{2}a_4 - \frac{1}{12}(p'_0)^2 - \frac{1}{2}p_0 a_1 p'_0 + \frac{1}{8}p_0^2 a_1^2 - \frac{1}{2}p_0 p_2 + \frac{1}{3}p_0 p_0'' + \frac{7}{288}p_0^4 \\
&\quad + \mathcal{E}^{ambiguity}, \\
8\pi G_5 \mathcal{P} &= -\frac{1}{2}a_4 - \frac{1}{36}(p'_0)^2 + \frac{1}{6}p_0 a_1 p'_0 - \frac{1}{24}p_0^2 a_1^2 + \frac{1}{6}p_0 p_2 - \frac{1}{18}p_0 p_0'' + \frac{7}{864}p_0^4 \\
&\quad + \mathcal{P}^{ambiguity}, \\
16\pi G_5 \langle \mathcal{O}_3 \rangle &= \frac{1}{2}p_0'' - \frac{1}{12}p_0^3 - 2a_1 p'_0 + \frac{1}{2}p_0 a_1^2 - 2p_2 + \mathcal{O}_3^{ambiguity}.
\end{aligned} \tag{2.36}$$

Here we employ the superscript ‘*ambiguity*’ to denote renormalization scheme ambiguities introduced by the finite counterterms (2.33)

$$\begin{aligned}
\mathcal{E}^{ambiguity} &= \frac{1}{2}\delta_1 p_0^4 + \frac{1}{2}\delta_2 (p'_0)^2, \\
\mathcal{P}^{ambiguity} &= -2\delta_3 (p'_0)^2 - 2\delta_3 p_0 (p_0'') - \frac{1}{2}\delta_1 p_0^4 + \frac{1}{2}\delta_2 (p'_0)^2, \\
\mathcal{O}_3^{ambiguity} &= 4\delta_1 p_0^3 + 2\delta_2 p_0''.
\end{aligned} \tag{2.37}$$

As expected, the physical one-point functions in eq. (2.36) are invariant under the residual diffeomorphism (2.22) of the background metric (2.11).

These one-point correlators are subject to various Ward identities [31]. In particular, one has the diffeomorphism Ward identity

$$\partial^i \langle T_{ij} \rangle = -\langle \mathcal{O}_3 \rangle \partial_j p_0. \tag{2.38}$$

Of course, when the mass parameter is held constant, this expression reduces to the conservation of energy and momentum in the boundary theory. In the present case, the configurations are independent of the spatial coordinates and so only the $j = t$ component of eq. (2.38) is nontrivial, yielding

$$\partial_t \mathcal{E} = \langle \mathcal{O}_3 \rangle \partial_t p_0. \tag{2.39}$$

With a time-dependent p_0 , the contribution on the right-hand side describes the work done by varying the fermionic mass in the boundary theory.⁵ We also note that this equation is scheme independent, *i.e.*, eqs. (2.38) and (2.39) hold independent of the

⁵Later we will see that $p_0 = \sqrt{2} m_f$.

values of δ_i . Finally we observe that the constraint (2.16) reduces to this identity on the asymptotic boundary $\rho = 0$, *i.e.*, eqs. (2.21) and (2.39) are precisely the same.

We also have the conformal Ward identify

$$\langle T_i{}^i \rangle = -p_0 \langle \mathcal{O}_3 \rangle + \frac{1}{16\pi G_5} \left(\frac{1}{2} p_0 \square p_0 - \frac{1}{12} p_0^4 + \delta \square (p_0^2) \right), \quad (2.40)$$

where

$$\delta = -\delta_2 + 6 \delta_3. \quad (2.41)$$

Examining the right-hand side of this expression, the first term represents the ‘classical’ contribution from breaking conformal invariance by the introduction of a dimensionful coupling p_0 . Note that this term carries an overall factor of $(\Delta - d)$, which happens to be -1 in the present case. The remaining terms can be interpreted as anomalous contributions. The quadratic term is a standard scalar anomaly that was first studied in [33]. In a curved space background, this term would take the form of a Paneitz operator: $p_0(\square - R^\gamma/6)p_0$ [34]. The quartic term was previously observed in [24]. The final term is a scheme dependent total derivative that is induced by the finite counterterms. While the δ_2 and δ_3 counterterms in eq. (2.32) are not conformally invariant, they still respect scale invariance and so can only contribute with a total derivative in eq. (2.40) [35]. Note that with $\delta_3 = \delta_2/6$, these two counterterms combine to form a conformally invariant combination and hence the total derivative contribution above vanishes. Of course, the usual curvature-squared contributions to the trace anomaly [36] do not appear on the right-hand side of eq. (2.40) because we are examining the boundary theory in flat space, *e.g.*, see eq. (2.28).

2.1.2 Renormalization of $m^2 = -4$ bulk scalar

Constructing the transformation between EF and FG coordinates, using (2.23) for $m^2 = -4$, we find

$$\begin{aligned} v &= t - \rho + \mathcal{O}(\rho^5 \ln \rho), \\ r &= \frac{1}{\rho} \left(1 - \frac{1}{2} \rho a_1(t) + \frac{1}{2} \rho^2 a_1'(t) - \frac{1}{4} \rho^3 a_1'(t) + \mathcal{O}(\rho^4 \ln \rho) \right). \end{aligned} \quad (2.42)$$

Note that as in the previous case, we have $v \rightarrow t$ on the asymptotic boundary, *i.e.*, as $\rho \rightarrow 0$.

In this case, we write the relevant boundary counterterms as [24, 31]:

$$I_{ct} = I_{ct}^{divergent} + I_{ct}^{finite}, \quad (2.43)$$

with

$$I_{ct}^{divergent} = \frac{1}{16\pi G_5} \int_{\partial\mathcal{M}_5, \rho=\epsilon} d^4x \sqrt{-\gamma} \left(6 + \phi^2 + \frac{1}{2 \ln \rho} \phi^2 \right), \quad (2.44)$$

$$I_{ct}^{finite} = \frac{1}{16\pi G_5} \int_{\partial\mathcal{M}_5, \rho=\epsilon} d^4x \sqrt{-\gamma} \left(\frac{\delta_1}{\ln^2 \rho} \phi^2 + \frac{\delta_2}{\ln \rho} R^\gamma \phi \right). \quad (2.45)$$

Again we have separated the counterterms which diverge in the limit $\epsilon \rightarrow 0$ from those which remain finite. Further recall that the coefficients δ_i of the finite counterterms (2.45) are arbitrary constants reflecting the ambiguities in the renormalization scheme. Notice that there is a finite counterterm involving the curvature term, *i.e.*, $\frac{1}{\ln \rho} R^\gamma \phi$, even though the divergent counterterm $R^\gamma \phi$ is absent. The absence of such a divergent counterterm was established in [24]. Since the bulk action (2.9) is even in ϕ , all divergences must be even in ϕ as well. However, the candidate counterterm in question is linear in ϕ and so does not occur.

Transforming the expressions in eq. (2.23) to FG form and computing the renormalized one-point functions of $\langle T_{ij} \rangle$ and $\langle \mathcal{O}_2 \rangle$, we find

$$\begin{aligned} 8\pi G_5 \mathcal{E} &= -\frac{5}{18} p_0^l p_0 - \frac{3}{2} a_4 - \frac{5}{54} (p_0^l)^2 - \frac{1}{6} p_0^2 + \mathcal{E}^{ambiguity}, \\ 8\pi G_5 \mathcal{P} &= \frac{13}{54} p_0^l p_0 - \frac{1}{2} a_4 + \frac{17}{324} (p_0^l)^2 - \frac{1}{18} p_0^2 + \mathcal{P}^{ambiguity}, \\ 16\pi G_5 \langle \mathcal{O}_2 \rangle &= -p_0 + \mathcal{O}_2^{ambiguity}, \end{aligned} \quad (2.46)$$

where

$$\begin{aligned} \mathcal{E}^{ambiguity} &= \frac{1}{2} \delta_1 (p_0^l)^2, \\ \mathcal{P}^{ambiguity} &= -\frac{1}{2} \delta_1 (p_0^l)^2 + \delta_2 (p_0^l)'', \\ \mathcal{O}_2^{ambiguity} &= 2\delta_1 p_0^l. \end{aligned} \quad (2.47)$$

As expected, the physical one-point correlation functions in (2.46) are invariant under the residual diffeomorphisms (2.25) of the background metric in eq. (2.11).

Again, the one-point correlators satisfy Ward identities. In particular, the diffeomorphism Ward identity now becomes

$$\partial^i \langle T_{ij} \rangle = -\langle \mathcal{O}_2 \rangle \partial_j p_0^l. \quad (2.48)$$

As in the previous case, this equation contains a single nontrivial component here,⁶

$$\partial_t \mathcal{E} = \langle \mathcal{O}_2 \rangle \partial_t p_0^l. \quad (2.49)$$

⁶Note that we will see $p_0^l = \sqrt{2/3} m_b^2$ below.

As before, this expression is scheme independent, *i.e.*, it holds for arbitrary δ_i , and it is equivalent to the constraint (2.24) when the latter is taken to the asymptotic boundary. The conformal Ward identify becomes

$$\langle T_i{}^i \rangle = -2p_0^l \langle \mathcal{O}_2 \rangle + \frac{1}{16\pi G_5} \left(\frac{1}{2}(p_0^l)^2 - 6\delta_2 \square(p_0^l) \right), \quad (2.50)$$

which has the same general form as described with the fermionic mass operator in the previous subsection.

2.2 High temperature equilibrium thermodynamics

Having established the equations of motion for the bulk theory (2.9) of gravity coupled to a free scalar, as well as the asymptotic expansions required to extract the one-point functions, we apply these results here to examine time-independent or equilibrium configurations. High temperature equilibrium thermodynamics of the $\mathcal{N} = 2^*$ gauge theory has been extensively discussed in [23–25]. In the following, we highlight some of the salient results of these investigations. In particular, this allows us to connect the bulk parameters to those in the $\mathcal{N} = 2^*$ gauge theory, *e.g.*, as given in eqs. (2.62) and (2.63). Note that our nomenclature here should be interpreted as follows: ‘high temperature’ implies that $m_{b,f}/T \ll 1$ while ‘equilibrium’ implies that the bulk gravity solution will be time-independent.

Recall that in the high temperature limit, we are working perturbatively in the amplitude of the bulk scalar. Hence the zero’tth order solution will be a planar AdS black hole with the bulk scalar field set to zero. To leading order in the expansion in $m_{b,f}/T$, it is sufficient to solve the linearized equations for the scalar ϕ in the black hole background. The scalar only backreacts on this background geometry at the quadratic order. Thus given the ansatz (2.11), we write

$$\begin{aligned} \phi(v, r) &= \lambda \phi_1^e(r) + \mathcal{O}(\lambda^3), \\ A(v, r) &= r^2 - \frac{\mu^4}{r^2} + \lambda^2 \mu^2 A_2^e(r) + \mathcal{O}(\lambda^4), \\ \Sigma(v, r) &= r + \lambda^2 \mu \Sigma_2^e(r) + \mathcal{O}(\lambda^4), \end{aligned} \quad (2.51)$$

where we have introduced λ as an expansion counting parameter. Setting $\lambda = 0$ leaves the AdS black hole, where $r = \mu$ is the position of the event horizon. Note that we are using the superscript e above to denote quantities corresponding to the equilibrium (or static) solution.

From eq. (2.13), the linearized scalar equation becomes

$$0 = \partial_{rr}^2 \phi_1^e + \frac{5r^4 - \mu^4}{r(r^4 - \mu^4)} \partial_r \phi_1^e + \frac{m^2 r^2}{r^4 - \mu^4} \phi_1^e. \quad (2.52)$$

It is convenient to introduce a new radial coordinate ρ ,⁷

$$\rho = \frac{\mu}{r}, \quad (2.53)$$

such that the asymptotic boundary ($r \rightarrow \infty$) occurs at $\rho \rightarrow 0$ while the horizon ($r \rightarrow \mu$) is positioned at $\rho \rightarrow 1^-$ (to zero'th order in the λ expansion). In terms of ρ , eq. (2.52) takes the form

$$0 = \partial_{\rho\rho}^2 \phi_1^e - \frac{3 + \rho^4}{\rho(1 - \rho^4)} \partial_\rho \phi_1^e - \frac{m^2}{\rho^2(1 - \rho^4)} \phi_1^e. \quad (2.54)$$

The solutions are readily expressed in terms of hypergeometric functions and then in each case, they take the form:

■ For $m^2 = -3$,

$$\phi_1^e = \pi^{-1/2} \Gamma\left(\frac{3}{4}\right)^2 \rho^3 {}_2F_1\left(\frac{3}{4}, \frac{3}{4}, 1, 1 - \rho^4\right). \quad (2.55)$$

This particular solution is chosen by demanding regularity at the horizon. The overall normalization constant is chosen here in such a way that

$$p_0 = \lambda \mu, \quad (2.56)$$

where p_0 is the leading coefficient in the asymptotic expansion of the scalar given in eq. (2.20). Given the above solution (2.55), we can also extract the next independent coefficient at order ρ^3 ($\propto r^{-3}$) in the latter expansion as

$$p_2 = -\lambda \mu^3 \frac{\Gamma\left(\frac{3}{4}\right)^4}{\pi^2}. \quad (2.57)$$

Further given the linearized solution (2.55), we can choose the asymptotic solution of A_2^e as

$$A_2^e(\rho) = -\frac{1}{6} + \mathcal{C} \rho^2 + O(\rho^3 \ln \rho), \quad (2.58)$$

where \mathcal{C} is an arbitrary constant. With this choice, we identify in eq. (2.20)

$$a_1 = 0, \quad a_4 = -\mu^4 + \lambda^2 \mu^4 \mathcal{C}. \quad (2.59)$$

⁷Note that this radial coordinate is distinct from the the FG radius ρ , which is related to the EF radius r in eqs. (2.29) and (2.42).

As noted at eq. (2.22), $a_1 = 0$ corresponds to an implicit gauge choice that was made in choosing the form of $A_2^e(\rho)$ in eq. (2.58) — compare this expression to the general form in eq. (2.20). Similarly, the constant \mathcal{C} can be chosen arbitrarily with a gauge choice which fixes the position of the horizon, *i.e.*, $r_H^4 = \mu^4 (1 - \lambda^2 \mathcal{C} + \mathcal{O}(\lambda^4))$. In a discussion of the equilibrium thermodynamics, the most convenient choice is to simply set $\mathcal{C} = 0$. However, we will see the analogous constant cannot be avoided in the following studies since the quenches naturally cause the horizon to grow.

Now using eq. (2.36), we can compute the equilibrium expectation values for the energy density \mathcal{E}^e , the pressure \mathcal{P}^e and the fermionic mass operator $\langle \mathcal{O}_3 \rangle^e$:

$$\begin{aligned} 8\pi G_5 \mathcal{E}^e &= \frac{3}{2} \mu^4 (1 - \lambda^2 \mathcal{C}) + \mu^4 \lambda^2 \frac{\Gamma\left(\frac{3}{4}\right)^4}{2\pi^2} + \mathcal{O}(\lambda^4), \\ 8\pi G_5 \mathcal{P}^e &= \frac{1}{2} \mu^4 (1 - \lambda^2 \mathcal{C}) - \mu^4 \lambda^2 \frac{\Gamma\left(\frac{3}{4}\right)^4}{6\pi^2} + \mathcal{O}(\lambda^4), \\ 16\pi G_5 \langle \mathcal{O}_3 \rangle^e &= \mu^3 \lambda \frac{2\Gamma\left(\frac{3}{4}\right)^4}{\pi^2} + \mathcal{O}(\lambda^3). \end{aligned} \quad (2.60)$$

Note that to the order presented, there is no ambiguity in $\{\mathcal{E}^e, \mathcal{P}^e, \langle \mathcal{O}_3 \rangle^e\}$. From eq. (2.37), we can see that for a time independent mass, the ambiguities first arise at order λ^3 in $\langle \mathcal{O}_3 \rangle^e$, while they only arise at order λ^4 in \mathcal{E}^e and \mathcal{P}^e .

Next we compare eq. (2.60) with the energy density and the pressure given in [25]

$$\begin{aligned} \mathcal{E}^e &= \frac{3}{8} \pi^2 N^2 T^4 \left(1 - \frac{2\Gamma\left(\frac{3}{4}\right)^4}{3\pi^4} \frac{m_f^2}{T^2} \right), \\ \mathcal{P}^e &= \frac{1}{8} \pi^2 N^2 T^4 \left(1 - \frac{2\Gamma\left(\frac{3}{4}\right)^4}{\pi^4} \frac{m_f^2}{T^2} \right), \end{aligned} \quad (2.61)$$

for the high-temperature thermodynamics of $\mathcal{N} = 2^*$ gauge theory. This comparison allows us to identify

$$\mu = \pi T \left(1 + \left(\frac{\mathcal{C}}{2\pi^2} - \frac{\Gamma\left(\frac{3}{4}\right)^4}{3\pi^4} \right) \frac{m_f^2}{T^2} + \mathcal{O}\left(\frac{m_f^4}{T^4}\right) \right), \quad \lambda = \frac{\sqrt{2} m_f}{\pi T} \left(1 + \mathcal{O}\left(\frac{m_f^2}{T^2}\right) \right). \quad (2.62)$$

Combining these expressions with eq. (2.56) yields

$$p_0 = \sqrt{2} m_f \left(1 + \mathcal{O}\left(\frac{m_f^2}{T^2}\right) \right). \quad (2.63)$$

Similarly, the equilibrium expectation value of the fermionic mass term in eq. (2.60) becomes

$$\langle \mathcal{O}_3 \rangle^e = \frac{\sqrt{2} \Gamma\left(\frac{3}{4}\right)^4}{4\pi^2} N^2 m_f T^2 \left(1 + \mathcal{O}\left(\frac{m_f^2}{T^2}\right) \right). \quad (2.64)$$

■ For $m^2 = -4$, the linearized solution for the scalar field becomes

$$\phi_1^e = \frac{\pi}{4} \rho^2 {}_2F_1\left(\frac{1}{2}, \frac{1}{2}, 1, 1 - \rho^4\right). \quad (2.65)$$

Again, this particular solution is chosen to be regular at the horizon. Here the overall normalization constant is chosen in such a way that

$$p_0^l = \lambda \mu^2, \quad (2.66)$$

in the asymptotic expansion of the bulk scalar in eq. (2.23). Further, the second independent coefficient in the latter expansion becomes

$$p_0 = -\lambda \mu^2 \ln(\mu/2), \quad (2.67)$$

given the solution (2.65) above. Without loss of generality, we write the asymptotic solution of A_2^e as

$$A_2^e(\rho) = \left(\mathcal{C} + \left(\frac{1}{54} + \frac{2}{9} \ln 2\right) \ln \rho - \frac{1}{9} \ln^2 \rho\right) \rho^2 + \mathcal{O}(\rho^3 \ln \rho), \quad (2.68)$$

where \mathcal{C} is an arbitrary constant. In this case comparing eq. (2.23), we identify

$$a_1 = 0, \quad a_4 = -\mu^4 + \lambda^2 \mu^4 \left(\mathcal{C} + \left(\frac{1}{54} + \frac{2}{9} \ln 2\right) \ln \mu - \frac{1}{9} \ln^2 \mu\right). \quad (2.69)$$

As discussed above, gauge choices are implicitly at work in setting $a_1 = 0$ and fixing a final value for \mathcal{C} .

Using eq. (2.46), we can now compute the equilibrium expectation values for the energy density \mathcal{E}^e , the pressure \mathcal{P}^e and the bosonic mass operator $\langle \mathcal{O}_2 \rangle^e$:

$$\begin{aligned} 8\pi G_5 \mathcal{E}^e &= \frac{3}{2} \mu^4 + \lambda^2 \mu^4 \left(-\frac{3}{2} \mathcal{C} + \frac{1}{4} \ln \mu - \frac{5}{18} \ln 2 - \frac{5}{54} - \frac{1}{6} \ln^2 2\right) + \mathcal{E}_{ambiguity}^e + \mathcal{O}(\lambda^4), \\ 8\pi G_5 \mathcal{P}^e &= \frac{1}{2} \mu^4 + \lambda^2 \mu^4 \left(-\frac{1}{2} \mathcal{C} - \frac{1}{4} \ln \mu + \frac{13}{54} \ln 2 + \frac{17}{324} - \frac{1}{18} \ln^2 2\right) + \mathcal{P}_{ambiguity}^e + \mathcal{O}(\lambda^4), \\ 16\pi G_5 \langle \mathcal{O}_2 \rangle^e &= \lambda \mu^2 \ln \frac{\mu}{2} + \mathcal{O}_{ambiguity}^e + \mathcal{O}(\lambda^3), \end{aligned} \quad (2.70)$$

where

$$\begin{aligned} \mathcal{E}_{ambiguity}^e &= \frac{1}{2} \delta_1 \lambda^2 \mu^4, \\ \mathcal{P}_{ambiguity}^e &= -\frac{1}{2} \delta_1 \lambda^2 \mu^4, \\ \mathcal{O}_{ambiguity}^e &= 2 \delta_1 \lambda \mu^2. \end{aligned} \quad (2.71)$$

Next we compare the energy density and pressure in eq. (2.70) with the analogous expressions in [25]:

$$\begin{aligned}\mathcal{E}^e &= \frac{3}{8}\pi^2 N^2 T^4 \left(1 + \left(\ln \frac{\pi T}{\Lambda} - 1 \right) \frac{m_b^4}{9\pi^4 T^4} \right), \\ \mathcal{P}^e &= \frac{1}{8}\pi^2 N^2 T^4 \left(1 - \ln \frac{\pi T}{\Lambda} \frac{m_b^4}{3\pi^4 T^4} \right),\end{aligned}\tag{2.72}$$

where Λ is an arbitrary scale in the theory. In this way, we identify

$$\begin{aligned}\mu &= \pi T \left(1 + \frac{m_b^4}{972 \pi^4 T^4} (162\mathcal{C} + 3 \ln 2 + 18 \ln^2 2 - 17) \right), \\ \lambda &= \sqrt{\frac{2}{3}} \frac{m_b^2}{\pi^2 T^2}, \quad \delta_1 = -\frac{1}{2} \ln \frac{\Lambda}{2}.\end{aligned}\tag{2.73}$$

Notice that the renormalization scheme ambiguity δ_1 is identified with the ambiguity of choosing the scale Λ in eq. (2.72). Combining these expressions with eq. (2.56) yields

$$p_0^l = \sqrt{\frac{2}{3}} m_b^2 \left(1 + O\left(\frac{m_b^4}{T^4}\right) \right).\tag{2.74}$$

Similarly, the equilibrium expectation value of the fermionic mass term in eq. (2.60) becomes

$$\langle \mathcal{O}_2 \rangle^e = \sqrt{\frac{2}{3}} \frac{N^2}{8\pi^2} m_b^2 \ln \frac{\pi T}{\Lambda} \left(1 + O\left(\frac{m_b^4}{T^4}\right) \right).\tag{2.75}$$

3 Holographic mass quenches at high temperatures

Next we apply our results here to holographic quenches where the mass parameters in the dual gauge theory are varied as in eq. (1.3). Let us sketch the general approach here for $m^2 = -3$:⁸ Choosing a specific time-dependent profile for m_f corresponds to fixing the asymptotic function p_0 according to eq. (2.63). Given this boundary condition, we then numerically solve the scalar field equation (2.13) which allows us to determine the subleading coefficient p_2 . Note that as in the previous section with the high temperature approximation, we are working perturbatively in the amplitude of the scalar and so this equation is solved to linear order in λ with the static black hole background (*i.e.*, setting $A = r^2 - \mu/r^2$ and $\Sigma = r$). Given both p_0 and p_2 , we can evaluate the one-point function $\langle \mathcal{O}_3 \rangle$ using eq. (2.36).⁹ Further, we can integrate the

⁸This discussion extends to the case $m^2 = -4$ in an obvious way.

⁹We will make the gauge choice $a_1 = 0$ to simplify this expression, as well as later calculations.

boundary constraint (2.21) to determine the metric coefficient a_4 . Having calculated the latter, we can evaluate the energy density \mathcal{E} and pressure \mathcal{P} (at order λ^2) using the expressions in eq. (2.36). Note then that we are able to evaluate all of the one-point functions to leading order in the high temperature approximation without actually solving for the time-dependence of bulk metric (*i.e.*, without solving for $A_2(v, r)$ and $\Sigma_2(v, r)$ below). However, the latter will be required to evaluate non-local probes of the quenches [29].

As noted above, we are still investigating the time-dependent configurations in the high-temperature approximation, $m_{f,b}/T \ll 1$. Hence it is still sufficient to first solve the linearized equation for the scalar ϕ with the equilibrium black hole background and then consider the backreaction of the scalar on the geometry at quadratic order. We thus organize the perturbative expansion of the ansatz (2.11) with

$$\begin{aligned}\phi(v, r) &= \lambda \phi_1(v, r) + \mathcal{O}(\lambda^3), \\ A(v, r) &= r^2 - \frac{\mu^4}{r^2} + \lambda^2 \mu^2 A_2(v, r) + \mathcal{O}(\lambda^4), \\ \Sigma(v, r) &= r + \lambda^2 \mu \Sigma_2(v, r) + \mathcal{O}(\lambda^4),\end{aligned}\tag{3.1}$$

which is a simple extension of eq. (2.51) to a time-dependent situation. Then introducing coordinates,

$$\rho = \frac{\mu}{r} \quad \text{and} \quad \tau = \mu v,\tag{3.2}$$

the scalar field equation (2.13) becomes, to linear order in λ :

$$0 = \partial_{\tau\rho}^2 \phi_1 - \frac{1}{2}(1 - \rho^4) \partial_{\rho\rho}^2 \phi_1 - \frac{3}{2\rho} \partial_\tau \phi_1 + \frac{3 + \rho^4}{2\rho} \partial_\rho \phi_1 + \frac{m^2}{2\rho^2} \phi_1.\tag{3.3}$$

Of course, this equation reduces to eq. (2.54) with a time-independent scalar. Further at order λ^2 , the metric equations (2.14) and (2.15) yield

$$\begin{aligned}0 &= \partial_{\tau\rho} \Sigma_2 - \frac{1}{2}(1 - \rho^4) \partial_{\rho\rho}^2 \Sigma_2 - \frac{2}{\rho} \partial_\tau \Sigma_2 + \frac{2}{\rho} \partial_\rho \Sigma_2 + \frac{1}{2} \partial_\rho A_2 + \frac{(3 - \rho^4)}{\rho^2} \Sigma_2 - \frac{1}{\rho} A_2 \\ &\quad - \frac{m^2}{12\rho^3} \phi_1^2, \\ 0 &= \partial_{\rho\rho}^2 A_2 + \frac{2}{\rho} \partial_\rho A_2 + \frac{12(1 - \rho^4)}{\rho^2} \partial_\rho \Sigma_2 - \frac{12}{\rho^2} \partial_\tau \Sigma_2 + \frac{12(1 - \rho^4)}{\rho^3} \Sigma_2 - \frac{6}{\rho^2} A_2 \\ &\quad + \frac{1 - \rho^4}{2\rho^2} (\partial_\rho \phi_1)^2 - \frac{1}{\rho^2} \partial_\rho \phi_1 \partial_\tau \phi_1 - \frac{m^2}{6\rho^4} \phi_1^2,\end{aligned}\tag{3.4}$$

while the constraint equations (2.16) and (2.17) become

$$\begin{aligned}
0 &= \partial_{\tau\tau}^2 \Sigma_2 + \frac{1}{4}(1 - \rho^4)^2 \partial_{\rho\rho}^2 \Sigma_2 - (1 - \rho^4) \partial_{\tau\rho}^2 \Sigma_2 - \frac{1 + \rho^4}{\rho} \partial_\tau \Sigma_2 + \frac{(1 - \rho^4)^2}{2\rho} \partial_\rho \Sigma_2 \\
&\quad + \frac{1}{2} \partial_\tau A_2 - \frac{1 - \rho^4}{6\rho} \partial_\tau \phi_1 \partial_\rho \phi_1 + \frac{(1 - \rho^4)^2}{24\rho} (\partial_\rho \phi_1)^2 + \frac{1}{6\rho} (\partial_\tau \phi_1)^2, \\
0 &= \partial_{\rho\rho}^2 \Sigma_2 + \frac{2}{\rho} \partial_\rho \Sigma_2 + \frac{1}{6\rho} (\partial_\rho \phi_1)^2.
\end{aligned} \tag{3.5}$$

It is now straightforward to find the asymptotic solutions (as $\rho \rightarrow 0$) of eqs. (3.3–3.5).

■ When $m^2 = -3$

$$\begin{aligned}
\phi_1 &= p_{1,0} \rho + p'_{1,0} \rho^2 + \left(p_{1,2} + \frac{1}{2} p''_{1,0} \ln \rho \right) \rho^3 + \mathcal{O}(\rho^4 \ln \rho), \\
\Sigma_2 &= -\frac{1}{12} p_{1,0}^2 \rho - \frac{1}{9} p_{1,0} p'_{1,0} \rho^2 + \mathcal{O}(\rho^3 \ln \rho), \\
A_2 &= -\frac{1}{6} p_{1,0}^2 + \left(a_{2,4} + \frac{1}{6} ((p'_{1,0})^2 - p_{1,0} p''_{1,0}) \ln \rho \right) \rho^2 + \mathcal{O}(\rho^3 \ln \rho).
\end{aligned} \tag{3.6}$$

In addition, the first equation in eq. (3.5) provides the following constraint:

$$0 = a'_{2,4} + \frac{1}{3} (p_{1,0} p'_{1,2} - p'_{1,0} p_{1,2}) + \frac{1}{18} p'_{1,0} p''_{1,0} - \frac{2}{9} p_{1,0} p'''_{1,0}. \tag{3.7}$$

In eqs. (3.6) and (3.7), we have $p_{1,0} = p_{1,0}(\tau)$, $p_{1,2} = p_{1,2}(\tau)$ and $a_{2,4} = a_{2,4}(\tau)$, while the prime ' denotes differentiation with respect to τ .

Comparing eqs. (2.20) and (3.6), we identify

$$\begin{aligned}
p_0 &= \lambda \mu p_{1,0}, & p_2 &= \lambda \mu^3 \left(p_{1,2} + p''_{1,0} \frac{1}{2} \ln \mu \right), \\
a_1 &= 0, & a_4 &= -\mu^4 + \lambda^2 \mu^4 \left(a_{2,4} + \frac{1}{6} ((p'_{1,0})^2 - p_{1,0} p''_{1,0}) \ln \mu \right).
\end{aligned} \tag{3.8}$$

Note that $a_1 = 0$ was an implicit gauge choice made in writing Σ_2 and A_2 in eq. (3.6). Further we note that the boundary constraint (3.7) is precisely the constraint (2.21) evaluated at order λ^2 .

As argued above, it is enough to solve numerically only the scalar field equation (3.3) to compute p_2 for a specified profile p_0 . Then we obtain $a_{2,4}$ by directly integrating the constraint (3.7),

$$a_{2,4} = \mathcal{C}_3 - \frac{1}{3} p_{1,0} p_{1,2} - \frac{5}{36} (p'_{1,0})^2 + \frac{2}{9} p_{1,0} p''_{1,0} + \frac{2}{3} \int_{-\infty}^{\tau} ds p_{1,2}(s) p'_{1,0}(s), \tag{3.9}$$

where \mathcal{C}_3 is an arbitrary integration constant which we will fix to a convenient value below. Now we have determined both $p_{1,2}$ and $a_{2,4}$ for a specific profile $p_{1,0}$ (as well as having set $a_1 = 0$). Thus, as observed above, we have sufficient data to evaluate the one-point correlation functions of T_{ij} and \mathcal{O}_3 using the expressions in eq. (2.36) for a mass quench to $\mathcal{O}(\lambda^2)$.

■ When $m^2 = -4$

$$\begin{aligned}\phi_1 &= - (p_{1,0} + p_{1,0}^l \ln \rho) \rho^2 + \mathcal{O}(\rho^3 \ln \rho), \\ \Sigma_2 &= \mathcal{O}(\rho^3 \ln^2 \rho), \\ A_2 &= \left(a_{2,4} + \left(\frac{1}{54} (p_{1,0}^l)^2 - \frac{2}{9} p_{1,0} p_{1,0}^l \right) \ln \rho - \frac{1}{9} (p_{1,0}^l)^2 \ln^2 \rho \right) \rho^2 + \mathcal{O}(\rho^3 \ln^2 \rho).\end{aligned}\tag{3.10}$$

The first equation in eq. (3.5) now yields the following boundary constraint:

$$0 = a'_{2,4} - \frac{5}{27} p_{1,0}^l p'_{1,0} + \frac{4}{27} (p_0^l)' p_{1,0} + \frac{10}{81} p_{1,0}^l (p_{1,0}^l)' + \frac{2}{9} p_{1,0} p'_{1,0}.\tag{3.11}$$

As before, the boundary profiles are functions of τ , *i.e.*, $p_{1,0}^l = p_{1,0}^l(\tau)$, $p_{1,0} = p_{1,0}(\tau)$ and $a_{2,4} = a_{2,4}(\tau)$ and the prime denotes derivative with respect to τ .

Comparing eqs. (2.23) and (3.10), we identify

$$\begin{aligned}p_0^l &= \lambda \mu^2 p_{1,0}^l, & p_0 &= -\lambda \mu^2 (p_{1,0} + p_{1,0}^l \ln \mu), \\ a_1 &= 0, & a_4 &= -\mu^4 + \lambda^2 \mu^4 \left(a_{2,4} + \left(\frac{1}{54} (p_{1,0}^l)^2 - \frac{2}{9} p_{1,0} p_{1,0}^l \right) \ln \mu - \frac{1}{9} (p_{1,0}^l)^2 \ln^2 \mu \right).\end{aligned}\tag{3.12}$$

Again, note that it suffices to solve numerically only eq. (3.3), which allows us to extract $p_{1,0}$ for a given mass profile specified by $p_{1,0}^l$ and then compute the one-point function $\langle \mathcal{O}_2 \rangle$ using eq. (2.46). These expressions also allow us to evaluate $\langle T_{ij} \rangle$ after we determine $a_{2,4}$ by integrating eq. (3.11):

$$a_{2,4} = \mathcal{C}_2 - \frac{5}{81} (p_{1,0}^l)^2 - \frac{1}{9} p_{1,0}^2 + \frac{5}{27} p_{1,0} p_{1,0}^l - \frac{1}{3} \int_{-\infty}^{\tau} ds p_{1,0}(s) (p_{1,0}^l(s))',\tag{3.13}$$

where \mathcal{C}_2 is another integration constant, for which we make a convenient choice below.

3.1 Physical observables and ambiguities

As already discussed, the physical observables which we track during the quenches are the one-point correlation functions of the stress-energy tensor T_{ij} and the operator

dual to the bulk scalar ϕ which induces the quench, *i.e.*, \mathcal{O}_3 operator for $m^2 = -3$ and \mathcal{O}_2 for $m^2 = -4$. Further we will consider two types of mass quenches: First, we start at $t \rightarrow -\infty$ with the CFT (*i.e.*, $m_{f,b} = 0$) in a thermal equilibrium state at temperature T_i , and after the quench as $t \rightarrow +\infty$, it will equilibrate to a thermal state of the massive theory with a final temperature T_f but still in the regime where $m_{f,b} \ll T_f$. The second scenario will be mass quenches where we start at $t \rightarrow -\infty$ with the massive theory in thermal equilibrium with $m_{f,b} \ll T_i$ and the quench will take the mass in the boundary theory to zero. Hence as $t \rightarrow +\infty$, it equilibrates to a new thermal state now of the CFT with temperature T_f .

3.1.1 $m^2 = -3$

From substituting the expressions in eq. (3.8) into eq. (2.36), we find

$$\begin{aligned}
8\pi G_5 \mathcal{E} &= \frac{3}{2}\mu^4 - \mu^4 \lambda^2 \left(\frac{3}{2}a_{2,4} + \frac{1}{4} \ln \mu (p'_{1,0})^2 + \frac{1}{12}p'^2_{1,0} + \frac{1}{2}p_{1,0}p_{1,2} - \frac{1}{3}p''_{1,0}p_{1,0} \right) \\
&\quad + \mathcal{E}^{ambiguity} + \mathcal{O}(\lambda^4), \\
8\pi G_5 \mathcal{P} &= \frac{1}{2}\mu^4 - \lambda^2 \mu^4 \left(\frac{1}{2}a_{2,4} + \ln \mu \left(-\frac{1}{6}p''_{1,0}p_{1,0} + \frac{1}{12}(p'_{1,0})^2 \right) + \frac{1}{36}(p'_{1,0})^2 \right. \\
&\quad \left. - \frac{1}{6}p_{1,0}p_{1,2} + \frac{1}{18}p''_{1,0}p_{1,0} \right) + \mathcal{P}^{ambiguity} + \mathcal{O}(\lambda^4), \\
16\pi G_5 \langle \mathcal{O}_3 \rangle &= \frac{1}{2}\mu^3 \lambda (p''_{1,0} - 4p_{1,2} - 2 \ln \mu p''_{1,0}) + \mathcal{O}_3^{ambiguity} + \mathcal{O}(\lambda^3),
\end{aligned} \tag{3.14}$$

where:

$$\begin{aligned}
\mathcal{E}^{ambiguity} &= \frac{1}{2}\delta_2 \mu^4 \lambda^2 (p'_{1,0})^2, \\
\mathcal{P}^{ambiguity} &= \mu^4 \lambda^2 \left(\frac{1}{2}\delta_2 (p'_{1,0})^2 - 2\delta_3 ((p'_{1,0})^2 + p''_{1,0}p_{1,0}) \right), \\
\mathcal{O}_3^{ambiguity} &= 2\delta_2 \mu^3 \lambda p''_{1,0}.
\end{aligned} \tag{3.15}$$

As described above, we consider two classes of quenches:

- First, we start with a CFT as $t \rightarrow -\infty$ ($\tau \rightarrow -\infty$) and quench to a massive theory as $t \rightarrow +\infty$ ($\tau \rightarrow +\infty$). This quench is implemented as

$$\lim_{\tau \rightarrow -\infty} p_{1,0} = 0, \quad \lim_{\tau \rightarrow +\infty} p_{1,0} = 1, \quad \lim_{\tau \rightarrow \pm\infty} p'_{1,0} = 0. \tag{3.16}$$

Further, the asymptotic values of $p_{1,2}$ match those in the appropriate thermodynamic equilibrium,

$$\lim_{\tau \rightarrow -\infty} p_{1,2} = 0, \quad \lim_{\tau \rightarrow +\infty} p_{1,2} = -\frac{\Gamma\left(\frac{3}{4}\right)^4}{\pi^2}. \quad (3.17)$$

In particular, the latter is given by comparing to eqs. (2.56) and (2.57). Once the profile $p_{1,0}(\tau)$ is specified, the full function $p_{1,2}(\tau)$ will be determined by numerically integrating the scalar field equation (3.3). The metric function $a_{2,4}$ is then determined by eq. (3.9) but we must first fix the integration constant \mathcal{C}_3 . It turns out that a convenient choice is simply $\mathcal{C}_3 = 0$, which sets $a_{2,4}(\tau = -\infty) = 0$ for the present class of quenches. Matching the $\tau \rightarrow \pm\infty$ limits of T_{ij} with the corresponding equilibrium results, we identify to leading order

$$\mu = \pi T_i, \quad \lambda = \frac{\sqrt{2}m_f^0}{\pi T_i}, \quad m_f(\tau) = m_f^0 p_{1,0}(\tau). \quad (3.18)$$

Further we define two scales, Λ_2 and Λ_3 , to be associated with the ambiguities in the renormalization scheme,

$$\delta_2 = \frac{1}{2} \ln \Lambda_2, \quad \delta_3 = \frac{1}{12} \ln \Lambda_3. \quad (3.19)$$

Now we can rewrite eq. (3.14) in terms of variables of the boundary gauge theory:

$$\begin{aligned} \mathcal{E} &= \frac{3}{8}\pi^2 N^2 T_i^4 \left(1 - \left(2a_{2,4} + \frac{1}{3}(p'_{1,0})^2 \ln \frac{\pi T_i}{\Lambda_2} + \frac{1}{9}(p'_{1,0})^2 - \frac{4}{9}p_{1,0}p''_{1,0} \right. \right. \\ &\quad \left. \left. + \frac{2}{3}p_{1,0}p_{1,2} \right) \frac{(m_f^0)^2}{\pi^2 T_i^2} + \mathcal{O}\left(\frac{(m_f^0)^4}{T_i^4}\right) \right), \\ \mathcal{P} &= \frac{1}{8}\pi^2 N^2 T_i^4 \left(1 - \left(2a_{2,4} + \frac{1}{9}(p'_{1,0})^2 - \frac{2}{3}p_{1,0}p_{1,2} + \frac{2}{9}p_{1,0}p''_{1,0} \right. \right. \\ &\quad \left. \left. - \frac{2}{3}(p_{1,0}p''_{1,0} + (p'_{1,0})^2) \ln \frac{\pi T_i}{\Lambda_3} + (p'_{1,0})^2 \ln \frac{\pi T_i}{\Lambda_2} \right) \frac{(m_f^0)^2}{\pi^2 T_i^2} + \mathcal{O}\left(\frac{(m_f^0)^4}{T_i^4}\right) \right), \\ \mathcal{O}_3 &= -\frac{1}{2\sqrt{2}}N^2 T_i^2 m_f^0 \left(p_{1,2} - \frac{1}{4}p''_{1,0} + \frac{1}{2} \ln \frac{\pi T_i}{\Lambda_2} p''_{1,0} + \mathcal{O}\left(\frac{(m_f^0)^2}{T_i^2}\right) \right). \end{aligned} \quad (3.20)$$

Notice that at the order that we are calculating these quantities, the scheme-dependent ambiguities (the arbitrariness in the choice of Λ_2 and Λ_3) arise only during the evolution. That is, asymptotically $p'_{1,0} = 0 = p''_{1,0}$ and hence the terms involving $\ln \Lambda_{1,2}$ above vanish in the initial and final equilibrium configurations. Of course, this is in agreement with our observation in the previous section that there are no renormalization ambiguities in the one-point functions (2.60) at equilibrium.

Finally, we compute the final temperature and the final energy density/pressure after the quench. Denoting

$$a_{2,4}^\infty = \lim_{\tau \rightarrow +\infty} a_{2,4}(\tau) = \frac{\Gamma\left(\frac{3}{4}\right)^4}{3\pi^2} + \frac{2}{3} \int_{-\infty}^{\infty} ds p_{1,2}(s) p'_{1,0}(s), \quad (3.21)$$

and matching the $\tau \rightarrow +\infty$ limit of the above expressions (3.20) with the equilibrium values in eq. (2.61), we find

$$\begin{aligned} \frac{T_f}{T_i} &= 1 + \left(\frac{\Gamma\left(\frac{3}{4}\right)^4}{3\pi^2} - \frac{1}{2} a_{2,4}^\infty \right) \frac{(m_f^0)^2}{\pi^2 T_i^2} + \mathcal{O}\left(\frac{(m_f^0)^4}{T_i^4}\right), \\ \frac{\mathcal{E}_f}{\mathcal{E}_i} &= 1 + \left(\frac{2\Gamma\left(\frac{3}{4}\right)^4}{3\pi^2} - 2a_{2,4}^\infty \right) \frac{(m_f^0)^2}{\pi^2 T_i^2} + \mathcal{O}\left(\frac{(m_f^0)^4}{T_i^4}\right), \\ \frac{\mathcal{P}_f}{\mathcal{P}_i} &= 1 - \left(\frac{2\Gamma\left(\frac{3}{4}\right)^4}{3\pi^2} + 2a_{2,4}^\infty \right) \frac{(m_f^0)^2}{\pi^2 T_i^2} + \mathcal{O}\left(\frac{(m_f^0)^4}{T_i^4}\right). \end{aligned} \quad (3.22)$$

It is also interesting to consider the entropy of the gauge theory. For either of the asymptotic equilibrium states, we can use the thermodynamic formula: $S = (\mathcal{E} + \mathcal{P})/T$. Further, we have $\mathcal{E}_i = 3\mathcal{P}_i$ for the initial equilibrium of the CFT and so we find

$$\begin{aligned} \frac{S_f}{S_i} &= \frac{T_i}{T_f} \left(\frac{3}{4} \frac{\mathcal{E}_f}{\mathcal{E}_i} + \frac{1}{4} \frac{\mathcal{P}_f}{\mathcal{P}_i} \right) \\ &= 1 - \frac{3}{2} a_{2,4}^\infty \frac{(m_f^0)^2}{\pi^2 T_i^2} + \mathcal{O}\left(\frac{(m_f^0)^4}{T_i^4}\right). \end{aligned} \quad (3.23)$$

This last expression makes clear that the constant $a_{2,4}^\infty$, defined in eq. (3.21), directly parameterizes the entropy production of the mass quench. In our simulations, we find that $a_{2,4}^\infty$ is always negative — see section 5.1 for details. This result is, of course, in agreement with the expectation that the entropy density should always increase.

Let us consider an adiabatic transition in the mass where

$$|p'_{1,0}| \ll 1 \quad (3.24)$$

everywhere. We expect (and later confirm numerically) that

$$p_{1,2}(\tau) \approx p_{1,2}(\tau = +\infty) p_{1,0}(\tau) = -\frac{\Gamma\left(\frac{3}{4}\right)^4}{\pi^2} p_{1,0}(\tau). \quad (3.25)$$

That is, for a very slow transition, the system essentially maintains thermodynamic equilibrium throughout the process and $p_{1,2}(\tau)$ simply tracks $p_{1,0}(\tau)$. Thus, from

eq. (3.21), we have

$$a_{2,4}^\infty \approx \frac{\Gamma\left(\frac{3}{4}\right)^4}{3\pi^2} \left(1 - 2 \int_{-\infty}^{\infty} ds p_{1,0}(s) p'_{1,0}(s)\right) = 0. \quad (3.26)$$

Given this result, eq. (3.23) indicates that the entropy density is constant for slow changes of masses. Of course, from eq. (3.22), we see that these adiabatic processes where the mass is raised still produce an increase in temperature and energy density but a decrease in pressure. This behaviour can be intuitively understood with a quasi-particle picture of a system undergoing such an adiabatic transition.¹⁰ In such an adiabatic process, the occupation number of energy levels is unchanged but increasing mass increases the energy of any given level. Hence the net energy density would increase and further, the occupation number of the states after such a quench would correspond to a higher effective temperature.

Notice that since we expect that $a_{2,4}^\infty$ is always negative, eq. (3.22) indicates that the temperature and energy density always increase, even for rapid mass quenches. However, the change in the pressure can be either a decrease or an increase. We can expect that slow transitions result in the pressure decreasing while rapid quenches, with a large entropy production, should result in an increase in the pressure.

■ For the second type of quenches, we start with a massive theory as $t \rightarrow -\infty$ ($\tau \rightarrow -\infty$) and quench to a CFT as $t \rightarrow +\infty$ ($\tau \rightarrow +\infty$). This quench is implemented as¹¹

$$\lim_{\tau \rightarrow -\infty} \tilde{p}_{1,0} = 1, \quad \lim_{\tau \rightarrow +\infty} \tilde{p}_{1,0} = 0, \quad \lim_{\tau \rightarrow \pm\infty} \tilde{p}'_{1,0} = 0. \quad (3.27)$$

In this case, the asymptotic values of $p_{1,2}$ become

$$\lim_{\tau \rightarrow -\infty} \tilde{p}_{1,2} = -\frac{\Gamma\left(\frac{3}{4}\right)^4}{\pi^2}, \quad \lim_{\tau \rightarrow +\infty} \tilde{p}_{1,2} = 0. \quad (3.28)$$

The metric function $a_{2,4}$ is again determined by eq. (3.9), however, we have the freedom to choose a new value for the integration constant \mathcal{C}_3 . A convenient choice in this case turns out to be

$$\mathcal{C}_3 = \frac{1}{3} [p_{1,0} p_{1,2}]_{\tau=-\infty} = -\frac{\Gamma\left(\frac{3}{4}\right)^4}{3\pi^2}, \quad (3.29)$$

¹⁰Of course, a quasi-particle picture is not valid for strongly coupled $\mathcal{N} = 2^*$ plasma.

¹¹We use an upper symbol \sim to distinguish quenches of this type.

which again ensures that $\tilde{a}_{2,4}(\tau = -\infty) = 0$. Now comparing to eq. (2.61), we match the $\tau \rightarrow -\infty$ limit of T_{ij} to the corresponding equilibrium results by identifying

$$\mu = \pi T_i \left(1 - \frac{\Gamma \left(\frac{3}{4}\right)^4 (m_f^0)^2}{3\pi^4 T_i^2} + \mathcal{O}\left(\frac{(m_f^0)^4}{T_i^4}\right) \right), \quad \lambda = \frac{\sqrt{2}m_f^0}{\pi T_i}, \quad (3.30)$$

$$m_f(\tau) = m_f^0 \tilde{p}_{1,0}(\tau),$$

to leading order. Further we introduce the same scales, Λ_2 and Λ_3 , as in eq. (3.19) to define the renormalization scheme. Then we rewrite eq. (3.14) in terms of field theory parameters:

$$\begin{aligned} \mathcal{E} &= \frac{3}{8}\pi^2 N^2 T_i^4 \left(1 - \left(2\tilde{a}_{2,4} + \frac{4\Gamma \left(\frac{3}{4}\right)^4}{3\pi^2} + \frac{1}{3}(\tilde{p}'_{1,0})^2 \ln \frac{\pi T_i}{\Lambda_2} + \frac{1}{9}(\tilde{p}'_{1,0})^2 - \frac{4}{9}\tilde{p}_{1,0}\tilde{p}''_{1,0} \right. \right. \\ &\quad \left. \left. + \frac{2}{3}\tilde{p}_{1,0}\tilde{p}_{1,2} \right) \frac{(m_f^0)^2}{\pi^2 T_i^2} + \mathcal{O}\left(\frac{(m_f^0)^4}{T_i^4}\right) \right), \\ \mathcal{P} &= \frac{1}{8}\pi^2 N^2 T_i^4 \left(1 - \left(2\tilde{a}_{2,4} + \frac{4\Gamma \left(\frac{3}{4}\right)^4}{3\pi^2} + \frac{1}{9}(\tilde{p}'_{1,0})^2 - \frac{2}{3}\tilde{p}_{1,0}\tilde{p}_{1,2} + \frac{2}{9}\tilde{p}_{1,0}\tilde{p}''_{1,0} \right. \right. \\ &\quad \left. \left. - \frac{2}{3}(\tilde{p}_{1,0}\tilde{p}''_{1,0} + (\tilde{p}'_{1,0})^2) \ln \frac{\pi T_i}{\Lambda_3} + (\tilde{p}'_{1,0})^2 \ln \frac{\pi T_i}{\Lambda_2} \right) \frac{(m_f^0)^2}{\pi^2 T_i^2} + \mathcal{O}\left(\frac{(m_f^0)^4}{T_i^4}\right) \right), \\ \mathcal{O}_3 &= -\frac{1}{2\sqrt{2}}N^2 T_i^2 m_f^0 \left(\tilde{p}_{1,2} - \frac{1}{4}\tilde{p}''_{1,0} + \frac{1}{2} \ln \frac{\pi T_i}{\Lambda_2} \tilde{p}''_{1,0} + \mathcal{O}\left(\frac{(m_f^0)^2}{T_i^2}\right) \right). \end{aligned} \quad (3.31)$$

Once again, the arbitrariness in the choice of Λ_2 and Λ_3 only plays a role during the time-dependent portion of the quench — as already pointed out in eq. (2.60), there are no scheme dependent ambiguities at equilibrium in quenches of the fermionic mass term.

Finally, we compute the final temperature and the final energy density/pressure after the quench. Denoting

$$\tilde{a}_{2,4}^\infty = \lim_{\tau \rightarrow +\infty} \tilde{a}_{2,4}(\tau) = -\frac{\Gamma \left(\frac{3}{4}\right)^4}{3\pi^2} + \frac{2}{3} \int_{-\infty}^{\infty} ds \tilde{p}_{1,2}(s) \tilde{p}'_{1,0}(s), \quad (3.32)$$

and matching the $\tau \rightarrow +\infty$ limit of (3.20) with (2.61) we find

$$\begin{aligned} \frac{T_f}{T_i} &= 1 - \left(\frac{\Gamma \left(\frac{3}{4}\right)^4}{3\pi^2} + \frac{1}{2}\tilde{a}_{2,4}^\infty \right) \frac{(m_f^0)^2}{\pi^2 T_i^2} + \mathcal{O}\left(\frac{(m_f^0)^4}{T_i^4}\right), \\ \frac{\mathcal{E}_f}{\mathcal{E}_i} &= 1 - \left(\frac{2\Gamma \left(\frac{3}{4}\right)^4}{3\pi^2} + 2\tilde{a}_{2,4}^\infty \right) \frac{(m_f^0)^2}{\pi^2 T_i^2} + \mathcal{O}\left(\frac{(m_f^0)^4}{T_i^4}\right), \\ \frac{\mathcal{P}_f}{\mathcal{P}_i} &= 1 + \left(\frac{2\Gamma \left(\frac{3}{4}\right)^4}{3\pi^2} - 2\tilde{a}_{2,4}^\infty \right) \frac{(m_f^0)^2}{\pi^2 T_i^2} + \mathcal{O}\left(\frac{(m_f^0)^4}{T_i^4}\right). \end{aligned} \quad (3.33)$$

Turning to the entropy, it is straightforward to show that

$$\frac{S_f}{S_i} = 1 - \frac{3}{2} \tilde{a}_{2,4}^\infty \frac{(m_f^0)^2}{\pi^2 T_i^2} + \mathcal{O}\left(\frac{(m_f^0)^4}{T_i^4}\right). \quad (3.34)$$

So again the entropy production of these quenches is parameterized by $\tilde{a}_{2,4}^\infty$. Further all of the general comments made above about the transitions from the CFT to the massive theory can be extended to analogous statements about the present class of quenches. In particular, $\tilde{a}_{2,4}^\infty$ vanishes for adiabatic transitions where $|\tilde{p}'_{1,0}| \ll 1$ everywhere.

Notice that if $p_{1,0}(\tau)$ describes a quantum quench from a CFT to a massive theory, then

$$\tilde{p}_{1,0}(\tau) \equiv 1 - p_{1,0}(\tau) \quad (3.35)$$

describes a quench from a massive theory to a CFT. Because we are working perturbatively in the amplitude of the scalar field, in this ‘reverse’ quench, we will also find

$$\tilde{p}_{1,2}(\tau) = p_{2,0}(\tau = +\infty) - p_{2,0}(\tau) = -\frac{\Gamma\left(\frac{3}{4}\right)^4}{\pi^2} - p_{2,0}(\tau). \quad (3.36)$$

Further, comparing eqs. (3.21) and (3.32), we find

$$\tilde{a}_{2,4}^\infty = a_{2,4}^\infty. \quad (3.37)$$

Hence the entropy production of a quench from the CFT to the massive theory is precisely the same as in the reverse quench from the massive theory to the CFT. Again, this result occurs because we are working perturbatively in the high temperature approximation.

3.1.2 $m^2 = -4$

Substituting eq. (2.46) into eq. (3.12), we find

$$\begin{aligned} 8\pi G_5 \mathcal{E} &= \frac{3}{2} \mu^4 - \mu^4 \lambda^2 \left(\frac{3}{2} a_{2,4} - \frac{5}{18} p_{1,0} p_{1,0}^l - \frac{1}{4} (p_{1,0}^l)^2 \ln \mu + \frac{5}{54} (p_{1,0}^l)^2 + \frac{1}{6} p_{1,0}^2 \right) \\ &\quad + \mathcal{E}^{ambiguity} + \mathcal{O}(\lambda^4), \\ 8\pi G_5 \mathcal{P} &= \frac{1}{2} \mu^4 - \mu^4 \lambda^2 \left(\frac{1}{2} a_{2,4} + \frac{13}{54} p_{1,0} p_{1,0}^l + \frac{1}{4} (p_{1,0}^l)^2 \ln \mu - \frac{17}{324} (p_{1,0}^l)^2 + \frac{1}{18} p_{1,0}^2 \right) \\ &\quad + \mathcal{P}^{ambiguity} + \mathcal{O}(\lambda^4), \\ 16\pi G_5 \langle \mathcal{O}_2 \rangle &= \mu^2 \lambda (p_{1,0} + p_{1,0}^l \ln \mu) + \mathcal{O}_3^{ambiguity} + \mathcal{O}(\lambda^3), \end{aligned} \quad (3.38)$$

where:

$$\begin{aligned}
\mathcal{E}^{ambiguity} &= \frac{1}{2} \delta_1 \mu^4 \lambda^2 (p_{1,0}^l)^2, \\
\mathcal{P}^{ambiguity} &= -\frac{1}{2} \delta_1 \mu^4 \lambda^2 (p_{1,0}^l)^2 + \delta_2 \mu^2 \lambda (p_{1,0}^l)'' , \\
\mathcal{O}_2^{ambiguity} &= 2\delta_1 \mu^2 \lambda p_{1,0}^l .
\end{aligned} \tag{3.39}$$

As before, we consider two classes of quenches:

- First, we start with a CFT as $t \rightarrow -\infty$ ($\tau \rightarrow -\infty$) and quench to a massive theory as $t \rightarrow +\infty$ ($\tau \rightarrow +\infty$). This quench is implemented as

$$\lim_{\tau \rightarrow -\infty} p_{1,0}^l = 0, \quad \lim_{\tau \rightarrow +\infty} p_{1,0}^l = 1, \quad \lim_{\tau \rightarrow \pm\infty} (p_{1,0}^l)' = 0. \tag{3.40}$$

In this case, the asymptotic values of $p_{1,0}$ are

$$\lim_{\tau \rightarrow -\infty} p_{1,0} = 0, \quad \lim_{\tau \rightarrow +\infty} p_{1,0} = -\ln 2. \tag{3.41}$$

The metric function $a_{2,4}$ is determined by eq. (3.13) but we must now fix the integration constant \mathcal{C}_2 . With some foresight, we choose

$$\mathcal{C}_2 = \left[-\frac{1}{54} p_{1,0} p_{1,0}^l + \frac{5}{81} (p_{1,0}^l)^2 + \frac{1}{9} p_{1,0}^2 \right]_{\tau=+\infty} = \frac{1}{54} \ln 2 + \frac{5}{81} + \frac{1}{9} \ln^2 2. \tag{3.42}$$

Note that with this choice, $a_{2,4}$ does not vanish for either $\tau \rightarrow \pm\infty$. However, we will see that this choice simplifies our description of the entropy production below. Now matching the $\tau \rightarrow \pm\infty$ limits of \mathcal{E} and \mathcal{P} with the corresponding equilibrium results, we identify to leading order

$$\mu = \pi T_i \left(1 + \frac{1}{6} \mathcal{C}_2 \frac{(m_b^0)^4}{\pi^4 T_i^4} \right), \quad \lambda = \sqrt{\frac{2}{3}} \frac{(m_b^0)^2}{\pi^2 T_i^2}, \quad m_b^2(\tau) = (m_b^0)^2 p_{1,0}^l(\tau). \tag{3.43}$$

Next we introduce two scales, Λ_1 and Λ_2 , that are related to the ambiguities in the renormalization scheme with

$$\delta_1 = -\frac{1}{2} \ln \frac{\Lambda_1}{2}, \quad \delta_2 = \Lambda_2^2. \tag{3.44}$$

Then we can rewrite eq. (3.14) using parameters in the dual field theory:

$$\begin{aligned}
\mathcal{E} &= \frac{3}{8}\pi^2 N^2 T_i^4 \left(1 - \left(\frac{2}{3}a_{2,4} - \frac{2}{3}\mathcal{C}_2 - \frac{10}{81}p_{1,0}^l p_{1,0} - \frac{1}{9}(p_{1,0}^l)^2 \ln \frac{2\pi T_i}{\Lambda_1} \right. \right. \\
&\quad \left. \left. + \frac{10}{243}(p_{1,0}^l)^2 + \frac{2}{27}p_{1,0}^2 \right) \frac{(m_b^0)^4}{\pi^4 T_i^4} + \mathcal{O}\left(\frac{(m_b^0)^8}{T_i^8}\right) \right), \\
\mathcal{P} &= \frac{1}{8}\pi^2 N^2 T_i^4 \left(1 - \sqrt{\frac{8}{3}} \frac{\Lambda_2^2 (m_b^0)^2}{\pi^4 T_i^4} (p_{1,0}^l)'' - \left(\frac{2}{3}a_{2,4} - \frac{2}{3}\mathcal{C}_2 + \frac{26}{81}p_{1,0}^l p_{1,0} \right. \right. \\
&\quad \left. \left. + \frac{1}{3}(p_{1,0}^l)^2 \ln \frac{2\pi T_i}{\Lambda_1} - \frac{17}{243}(p_{1,0}^l)^2 + \frac{2}{27}p_{1,0}^2 \right) \frac{(m_b^0)^4}{\pi^4 T_i^4} + \mathcal{O}\left(\frac{(m_b^0)^8}{T_i^8}\right) \right), \\
\mathcal{O}_2 &= \frac{\sqrt{6}N^2}{24\pi^2} (m_b^0)^2 \left(p_{1,0} + p_{1,0}^l \ln \frac{2\pi T_i}{\Lambda_1} + \mathcal{O}\left(\frac{(m_b^0)^4}{T_i^4}\right) \right).
\end{aligned} \tag{3.45}$$

Note that in our perturbative expansion in powers of $(m_b^0)^2/T_i^2$, the pressure is formally dominated by the term proportional to Λ_2^2 . However, this scheme dependent term vanishes in an equilibrium configuration where $(p_{1,0}^l)'' = 0$.

Now we compute the final temperature and the final energy density/pressure after the quench. Denoting

$$a_{2,4}^\infty = \lim_{\tau \rightarrow +\infty} a_{2,4}(\tau) = -\frac{1}{6} \ln 2 - \frac{1}{3} \int_{-\infty}^{\infty} ds p_{1,0}(s) (p_{1,0}^l)'(s), \tag{3.46}$$

and matching the $\tau \rightarrow +\infty$ limit of the above results (3.45) with the equilibrium values (2.72), we find

$$\begin{aligned}
\frac{T_f}{T_i} &= 1 + \left(\frac{1}{36} - \frac{1}{6}a_{2,4}^\infty \right) \frac{(m_b^0)^4}{\pi^4 T_i^4} + \mathcal{O}\left(\frac{(m_b^0)^8}{T_i^8}\right), \\
\frac{\mathcal{E}_f}{\mathcal{E}_i} &= 1 + \left(\frac{1}{9} \ln \frac{\pi T_i}{\Lambda_1} - \frac{2}{3}a_{2,4}^\infty \right) \frac{(m_b^0)^4}{\pi^4 T_i^4} + \mathcal{O}\left(\frac{(m_b^0)^8}{T_i^8}\right), \\
\frac{\mathcal{P}_f}{\mathcal{P}_i} &= 1 + \left(\frac{1}{9} - \frac{1}{3} \ln \frac{\pi T_i}{\Lambda_1} - \frac{2}{3}a_{2,4}^\infty \right) \frac{(m_b^0)^4}{\pi^4 T_i^4} + \mathcal{O}\left(\frac{(m_b^0)^8}{T_i^8}\right).
\end{aligned} \tag{3.47}$$

Turning to the entropy, since this quench begins with the CFT, we may apply the same expression as given in eq. (3.23) to find

$$\begin{aligned}
\frac{S_f}{S_i} &= \frac{T_i}{T_f} \left(\frac{3}{4} \frac{\mathcal{E}_f}{\mathcal{E}_i} + \frac{1}{4} \frac{\mathcal{P}_f}{\mathcal{P}_i} \right) \\
&= 1 - \frac{1}{2}a_{2,4}^\infty \frac{(m_b^0)^4}{\pi^4 T_i^4} + \mathcal{O}\left(\frac{(m_b^0)^8}{T_i^8}\right).
\end{aligned} \tag{3.48}$$

Hence with the judicious choice of the integration constant made in eq. (3.42), we find that $a_{2,4}^\infty$ directly parameterizes the entropy production in these quenches of the

bosonic mass. As before, our simulations of the bosonic mass quenches seem to indicate that $a_{2,4}^\infty$ is always negative — see section 5.2 for details. Of course, this matches the intuition that the entropy density must always increase.

If we consider an adiabatic transition where

$$|(p_{1,0}^l)'| \ll 1 \quad (3.49)$$

we expect (and later confirm numerically) that

$$p_{1,0}(\tau) \approx p_{1,0}(\tau = +\infty) p_{1,0}^l(\tau) = -\ln 2 p_{1,0}^l(\tau). \quad (3.50)$$

Again, this reflects the expectation that for a very slow transition, the system essentially maintains thermodynamic equilibrium throughout the process and $p_{1,0}(\tau)$ simply tracks $p_{1,0}^l(\tau)$. Thus, from eq. (3.21), we have

$$a_{2,4}^\infty \approx -\frac{1}{6} \ln 2 \left(1 - 2 \int_{-\infty}^{\infty} ds p_{1,0}^l(s) (p_{1,0}^l)'(s) \right) = 0. \quad (3.51)$$

Hence we again find that the entropy density is constant for adiabatic changes of the mass. Notice that in this case, from eq. (3.47), these adiabatic processes always produce an increase in temperature, however, the sign of change in the energy density and the pressure depends on the choice of the renormalization scale Λ_1 , which is needed to describe thermodynamics in the massive theory, *e.g.*, see eq. (2.72). Even with $a_{2,4}^\infty$ always being negative, similar statements still apply for rapid mass quenches.

■ The second type of quench, which we consider, starts with the massive theory as $t \rightarrow -\infty$ ($\tau \rightarrow -\infty$) and makes a transition to the CFT as $t \rightarrow +\infty$ ($\tau \rightarrow +\infty$). These quenches are implemented with¹²

$$\lim_{\tau \rightarrow -\infty} \tilde{p}_{1,0}^l = 1, \quad \lim_{\tau \rightarrow +\infty} \tilde{p}_{1,0}^l = 0, \quad \lim_{\tau \rightarrow \pm\infty} (\tilde{p}_{1,0}^l)' = 0. \quad (3.52)$$

In this case, the asymptotic values of $p_{1,0}$ become

$$\lim_{\tau \rightarrow -\infty} \tilde{p}_{1,0} = -\ln 2, \quad \lim_{\tau \rightarrow +\infty} \tilde{p}_{1,0} = 0. \quad (3.53)$$

The metric function $a_{2,4}$ is determined by eq. (3.13) and we must now fix the integration constant \mathcal{C}_2 . Motivated by the desire for a simple expression for the entropy production, we choose

$$\mathcal{C}_2 = \left[-\frac{1}{6} \tilde{p}_{1,0} \tilde{p}_{1,0}^l \right]_{\tau=-\infty} = \frac{1}{6} \ln 2. \quad (3.54)$$

¹²Here again, we use \sim to distinguish this second class of quenches.

This choice of \mathcal{C}_2 again means that $a_{2,4}$ is nonvanishing for both $\tau \rightarrow \pm\infty$. Now matching the $\tau \rightarrow -\infty$ limit of T_{ij} with the corresponding equilibrium results (2.72), we identify to leading order

$$\mu = \pi T_i \left(1 - \frac{1}{36} \frac{(m_b^0)^4}{\pi^4 T_i^4} \right), \quad \lambda = \sqrt{\frac{2}{3}} \frac{(m_b^0)^2}{\pi^2 T_i^2}, \quad m_b^2(\tau) = (m_b^0)^2 \tilde{p}_{1,0}^l(\tau). \quad (3.55)$$

Finally, we introduce two renormalization scales, Λ_1 and Λ_2 , as in eq. (3.44). Then we can rewrite eq. (3.38) in terms of field theory parameters:

$$\begin{aligned} \mathcal{E} &= \frac{3}{8} \pi^2 N^2 T_i^4 \left(1 - \left(\frac{2}{3} \tilde{a}_{2,4} - \frac{2}{3} \mathcal{C}_2 + \frac{1}{9} + \frac{1}{9} \ln 2 - \frac{10}{81} \tilde{p}_{1,0}^l \tilde{p}_{1,0} - \frac{1}{9} (\tilde{p}_{1,0}^l)^2 \ln \frac{2\pi T_i}{\Lambda_1} \right. \right. \\ &\quad \left. \left. + \frac{10}{243} (\tilde{p}_{1,0}^l)^2 + \frac{2}{27} \tilde{p}_{1,0}^2 \right) \frac{(m_b^0)^4}{\pi^4 T_i^4} + \mathcal{O} \left(\frac{(m_b^0)^8}{T_i^8} \right) \right), \quad (3.56) \\ \mathcal{P} &= \frac{1}{8} \pi^2 N^2 T_i^4 \left(1 - \sqrt{\frac{8}{3}} \frac{\Lambda_2^2 (m_b^0)^2}{\pi^4 T_i^4} (\tilde{p}_{1,0}^l)'' - \left(\frac{2}{3} \tilde{a}_{2,4} - \frac{2}{3} \mathcal{C}_2 + \frac{1}{9} + \frac{1}{9} \ln 2 \right. \right. \\ &\quad \left. \left. + \frac{26}{81} \tilde{p}_{1,0}^l \tilde{p}_{1,0} + \frac{1}{3} (\tilde{p}_{1,0}^l)^2 \ln \frac{2\pi T_i}{\Lambda_1} - \frac{17}{243} (\tilde{p}_{1,0}^l)^2 + \frac{2}{27} \tilde{p}_{1,0}^2 \right) \frac{(m_b^0)^4}{\pi^4 T_i^4} + \mathcal{O} \left(\frac{(m_b^0)^8}{T_b^8} \right) \right), \\ \mathcal{O}_2 &= \frac{\sqrt{6} N^2}{24\pi^2} (m_b^0)^2 \left(\tilde{p}_{1,0} + \tilde{p}_{1,0}^l \ln \frac{2\pi T_i}{\Lambda_1} + \mathcal{O} \left(\frac{(m_b^0)^4}{T_i^4} \right) \right). \end{aligned}$$

Finally, we compute the final temperature and the final energy density/pressure after the quench. Denoting

$$\tilde{a}_{2,4}^\infty = \lim_{\tau \rightarrow +\infty} \tilde{a}_{2,4}(\tau) = \frac{1}{6} \ln 2 - \frac{1}{3} \int_{-\infty}^{\infty} ds p_{1,0}(s) (p_{1,0}^l)'(s), \quad (3.57)$$

and matching the $\tau \rightarrow \infty$ limit of eq. (3.45) with eq. (2.72), we find

$$\begin{aligned} \frac{T_f}{T_i} &= 1 - \left(\frac{1}{36} + \frac{1}{6} \tilde{a}_{2,4}^\infty \right) \frac{(m_b^0)^4}{\pi^4 T_i^4} + \mathcal{O} \left(\frac{(m_b^0)^8}{T_i^8} \right), \\ \frac{\mathcal{E}_f}{\mathcal{E}_i} &= 1 - \left(\frac{1}{9} \ln \frac{\pi T_i}{\Lambda_1} + \frac{2}{3} \tilde{a}_{2,4}^\infty \right) \frac{(m_b^0)^4}{\pi^4 T_i^4} + \mathcal{O} \left(\frac{(m_b^0)^8}{T_i^8} \right), \quad (3.58) \\ \frac{\mathcal{P}_f}{\mathcal{P}_i} &= 1 - \left(\frac{1}{9} - \frac{1}{3} \ln \frac{\pi T_i}{\Lambda_1} + \frac{2}{3} \tilde{a}_{2,4}^\infty \right) \frac{(m_b^0)^4}{\pi^4 T_i^4} + \mathcal{O} \left(\frac{(m_b^0)^8}{T_i^8} \right). \end{aligned}$$

Given these expressions, it is straightforward to shown that the change in the entropy is given by

$$\frac{S_f}{S_i} = 1 - \frac{1}{2} \tilde{a}_{2,4}^\infty \frac{(m_b^0)^4}{\pi^4 T_i^4} + \mathcal{O} \left(\frac{(m_b^0)^8}{T_i^8} \right). \quad (3.59)$$

Hence we again find that $\tilde{a}_{2,4}^\infty$ gives a direct measure of the entropy production in these quenches. Of course, this simple result (3.59) relies on the judicious choice of \mathcal{C}_2 in

eq. (3.54). Furthermore all of the general comments made above about the transitions from the CFT to the massive theory can be extended to analogous statements about the present class of quenches.

Again, we observe that if $p_{1,0}^l(\tau)$ describes a quench from a CFT to a massive theory, then

$$\tilde{p}_{1,0}^l(\tau) \equiv 1 - p_{1,0}^l(\tau) \quad (3.60)$$

will describe a quench from a massive theory to a CFT. Because our calculations are perturbative in the amplitude of the scalar field, we will also have

$$\tilde{p}_{1,0}(\tau) = p_{1,0}(\tau = +\infty) - p_{1,0}(\tau) = -\ln 2 - p_{2,0}(\tau) \quad (3.61)$$

for this ‘reverse’ quench. Thus, comparing eqs. (3.46) and (3.57), we again find

$$\tilde{a}_{2,4}^\infty = a_{2,4}^\infty. \quad (3.62)$$

Hence the entropy production of a quench from the CFT to the massive theory is precisely the same as in the reverse quench from the massive theory to the CFT. Again, this result occurs because we are working perturbatively in the high temperature approximation.

4 Numerical procedure

As described at the beginning of section 3, the focus of our numerical calculations is the linearized scalar wave equation (3.3). The non-normalizable mode of the scalar specifies the time-dependent profile of the corresponding mass parameter in the dual gauge theory. Solving the scalar equation allows us to extract the normalizable mode, with which we can evaluate the one-point function of the corresponding operator. With this information, it is also straightforward to integrate the corresponding boundary constraint, eq. (3.9) or (3.13), which then allows us to calculate the energy density and pressure.

For the sake of clarity, we describe the numerical procedure for the fermionic and bosonic operators, *i.e.*, $m^2 = -3$ and $m^2 = -4$, separately. Below and in the following section, we also focus on the quenches which go from the CFT to the massive theory. As described in the previous section, the reverse quenches going from the massive theory to the CFT are then easily obtained using eqs. (3.35) and (3.36) for $m^2 = -3$ or eqs. (3.60) and (3.61) for $m^2 = -4$.

4.1 $m^2 = -3$

We study mass quenches generated by

$$p_{1,0} = \frac{1}{2} + \frac{1}{2} \tanh \frac{\tau}{\alpha} = \frac{1}{2} + \frac{1}{2} \tanh \frac{t}{\mathcal{T}}, \quad (4.1)$$

where

$$\mathcal{T} = \frac{\alpha}{\mu} = \frac{\alpha}{\pi T_i} \left(1 + \mathcal{O} \left(\frac{(m_f^0)^2}{T_i^2} \right) \right). \quad (4.2)$$

Here we have used the fact that at the boundary $t = v = \frac{\tau}{\mu}$ — see eq. (2.30). By varying the constant α , we are able to study quenches that are much faster or slower than the characteristic thermal time-scale in the corresponding plasma, *i.e.*, $1/T_i$.

Solving the linearized equation (3.3) for ϕ_1 , we are then able to extract the normalizable coefficient $p_{1,2}(\tau)$, which appears as shown in eq. (3.6). In practice, it is more convenient to integrate the evolution of $\hat{\phi}_1(\tau, \rho)$, which we define as

$$\phi_1(\tau, \rho) \equiv \rho p_{1,0} + \rho^2 \partial_\tau p_{1,0} + \frac{1}{2} \rho^3 \ln \rho \partial_{\tau\tau}^2 p_{1,0} + \rho \hat{\phi}_1(\tau, \rho). \quad (4.3)$$

Comparing this definition with eq. (3.6), we see that asymptotically as $\rho \rightarrow 0$,

$$\hat{\phi}_1 = p_{1,2} \rho^2 + \mathcal{O}(\rho^3 \ln \rho). \quad (4.4)$$

Hence organizing the scalar in this way provides for a natural way to enforce the desired boundary condition for $p_{1,0}$ and to deal with a regular field in the numerical implementation. The scalar wave equation (3.3) now becomes

$$0 = \partial_{\tau\rho}^2 \hat{\phi}_1 - \frac{1 - \rho^4}{2} \partial_{\rho\rho}^2 \hat{\phi}_1 - \frac{1}{2\rho} \partial_\tau \hat{\phi}_1 + \frac{1 + 3\rho^4}{2\rho} \partial_\rho \hat{\phi}_1 + \frac{\rho^2}{2} \hat{\phi}_1 + J_0, \quad (4.5)$$

with

$$J_0 = \frac{1}{4} \rho (2 + 3 \ln \rho) \partial_{\tau\tau\tau}^3 p_{1,0} + \frac{3}{4} \rho^4 (2 + 3 \ln \rho) \partial_{\tau\tau}^2 p_{1,0} + 2\rho^3 \partial_\tau p_{1,0} + \frac{1}{2} \rho^2 p_{1,0}. \quad (4.6)$$

From eq. (4.4), the required boundary condition is $\hat{\phi}_1 = 0$.

4.2 $m^2 = -4$

We study mass quenches generated by

$$p_{1,0}^l = \frac{1}{2} + \frac{1}{2} \tanh \frac{\tau}{\alpha} = \frac{1}{2} + \frac{1}{2} \tanh \frac{t}{\mathcal{T}}, \quad (4.7)$$

where

$$\mathcal{T} = \frac{\alpha}{\mu} = \frac{\alpha}{\pi T_i} \left(1 + \mathcal{O} \left(\frac{(m_b^0)^4}{T_i^4} \right) \right). \quad (4.8)$$

We are again using $t = v = \frac{\tau}{\mu}$ at the boundary and we will vary α to study quenches that are much faster or slower than the characteristic thermal time-scale, *i.e.*, $1/T_i$.

Solving the linearized equation (3.3) for ϕ_1 , we extract the normalizable coefficient $p_{1,0}(\tau)$, which appears as shown in eq. (3.10). In this case, it is convenient to introduce $\hat{\phi}_1(\tau, \rho)$ defined as

$$\phi_1(\tau, \rho) = \rho^2 \ln \rho p_{1,0}^l + \rho^3 \ln \rho \partial_\tau p_{1,0}^l + \rho \hat{\phi}_1(\tau, \rho). \quad (4.9)$$

Comparing this definition with eq. (3.10), we see that asymptotically

$$\hat{\phi}_1 = p_{1,0} \rho + \mathcal{O}(\rho). \quad (4.10)$$

Writing the scalar equation (3.3) in terms of $\hat{\phi}_1$, we have

$$0 = \partial_{\tau\rho}^2 \hat{\phi}_1 - \frac{1-\rho^4}{2} \partial_{\rho\rho}^2 \hat{\phi}_1 - \frac{1}{2\rho} \partial_\tau \hat{\phi}_1 + \frac{1+3\rho^4}{2\rho} \partial_\rho \hat{\phi}_1 - \frac{1-\rho^4}{2\rho^2} \hat{\phi}_1 + J_0, \quad (4.11)$$

with

$$J_0 = \frac{1}{2} \rho (2 + 3 \ln \rho) \partial_{\tau\tau}^2 p_{1,0}^l + \frac{3}{2} \rho^4 (2 + 3 \ln \rho) \partial_\tau p_{1,0}^l + 2\rho^3 (1 + \ln \rho) p_{1,0}^l. \quad (4.12)$$

From eq. (4.10), the boundary condition is $\hat{\phi}_1 = 0$ for $\rho \rightarrow 0$.

Eqs. (4.5) and (4.11) were discretized employing second order finite difference approximations as discussed in Appendix A. The normalizable response, *i.e.*, $p_{1,2}$ for $m^2 = -3$ and $p_{1,0}$ for $m^2 = -4$, is then obtained by a straightforward fit from the numerical solutions obtained. Examples of the computed values versus time for the case $\alpha = 1$ are shown in fig. 1, together with the adiabatic responses from eqs. (3.25) and (3.50) for guidance:

$$[p_{1,2}(\tau)]_{adiabatic} = -\frac{\Gamma\left(\frac{3}{4}\right)^4}{\pi^2} p_{1,0}(\tau), \quad (4.13)$$

$$[p_{1,0}(\tau)]_{adiabatic} = -\ln 2 p_{1,0}^l(\tau). \quad (4.14)$$

5 Results

In this section we present the results for a range of different quenches with both the fermionic and bosonic operators. We discuss each case separately.

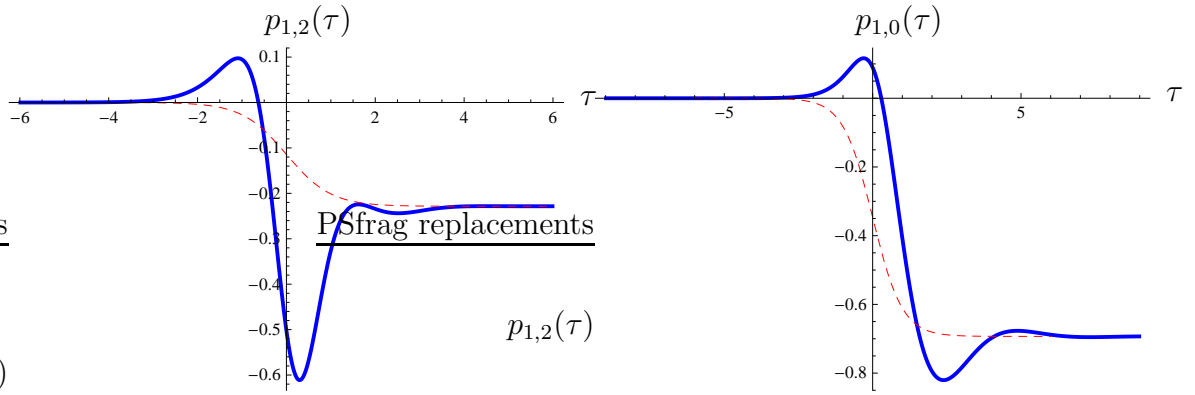


Figure 1: (Colour online) Evolution of the normalizable component $p_{1,2}$ (left panel) and $p_{1,0}$ (right panel) during the quenches in eqs. (4.1) and (4.7), respectively, with $\alpha = 1$. The dashed red lines represent the adiabatic response given by eqs. (4.13) and (4.14), respectively.

5.1 Quenches with \mathcal{O}_3

The source $p_{1,0}$ is given by eq. (4.1) and hence α indicates the characteristic time scale of the quench. The response of the normalizable component $p_{1,2}$ depends crucially on whether the transition is ‘fast’ with $\alpha < 1$ or ‘slow’ with $\alpha > 1$. Our results for both cases are presented in fig. 2. The curves in the left panel present the (rescaled) profile of $p_{1,2}$ as function of $\frac{\tau}{\alpha}$ for fast quenches. As indicated, here we have adopted values $\alpha = \{1, 0.5, 0.1, 0.05, 0.01, 0.005\}$. The right panel we show the evolution of $p_{1,2}$ as a function of $\frac{\tau}{\alpha}$ for slow quenches with $\alpha = \{1, 2.5, 5, 10, 50, 100\}$.

Consider first the fast quenches in the left panel of fig. 2. The response of these quenches deviate very far from the adiabatic response (4.13), which is represented by the red dashed line (with no rescaling). Indeed for the adiabatic response $|p_{1,2}| < 0.3$ while the plots show that the maximum of the response $p_{1,2}$ scales faster than $\frac{1}{\alpha^2}$ for small α . There are three distinct phases in the evolution of $p_{1,2}$. In the infinite past the system starts at equilibrium with $p_{1,0} = 0$ and hence $p_{1,2}(-\infty) = 0$ for all quenches. In the infinite future, the system ends at equilibrium in the massive theory with $p_{1,0} = 1$ and hence $p_{1,2}(+\infty) = -\Gamma\left(\frac{3}{4}\right)^4 / \pi^2$ for all quenches.¹³ The component of $p_{1,2}$ which scales as $1/\alpha^2$ is first excited whenever the source $p_{1,0}$ noticeably deviates from 0, *i.e.*,

¹³Note that the curves in fig. 2 approach different values at large τ because we have rescaled the response with a factor of α^2 in this plot.

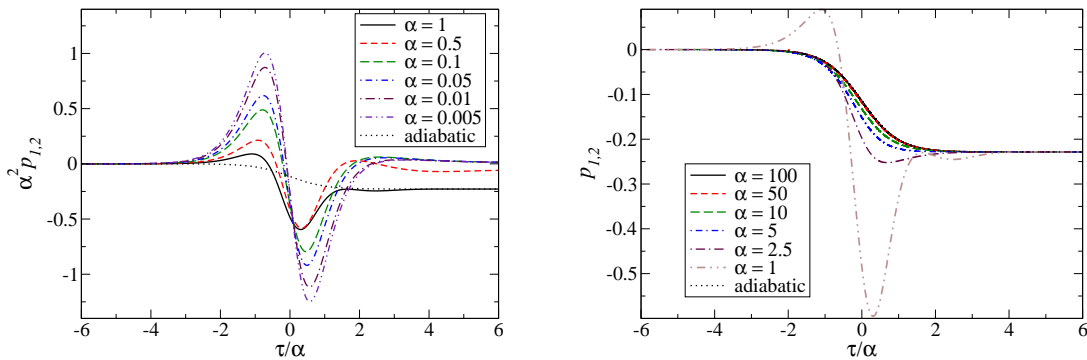


Figure 2: (Colour online) The curves on the left plot represent the evolution of the α -rescaled normalizable component, $\alpha^2 p_{1,2}$, as a function of $\frac{\tau}{\alpha}$ during the quench (4.1) with different values of α . The curves on the right plot represent the evolution of the normalizable component, $p_{1,2}$, as a function of $\frac{\tau}{\alpha}$ during the quench (4.1) for the representative values of α .

whenever $p_{1,0} > 0.01$ which corresponds to $\frac{\tau}{\alpha} > -2.3$. In fig. 2, $\alpha^2 p_{1,2}$ also appears to rapidly approach the asymptotic value¹⁴ for large τ when the source is sufficiently close to 1, *i.e.*, whenever $(1 - p_{1,0}) < 0.01$ and correspondingly $\frac{\tau}{\alpha} > 2.3$. Indeed, most of the variation in $\alpha^2 p_{1,2}$ occurs approximately within the interval $\frac{\tau}{\alpha} \in (-4, 4)$. In this sense, the α^2 -rescaled response *follows* the characteristic time-scale of the source (4.1). That is, faster variations in the source $p_{1,0}$ (smaller values of α) result in both the faster excitation and the faster equilibration of $\alpha^2 p_{1,2}$.

The right panel in fig. 2 presents the evolution of the normalizable component $p_{1,2}$ for slow quenches, *i.e.*, for $\alpha > 1$. Note that we do not rescale $p_{1,2}$ in this plot. Here we see for progressively larger values of α , the profiles come closer to resembling the adiabatic response given by eq. (4.13) — the latter is represented by a barely visible red dashed line.

While it is not surprising that in the limit $\alpha \rightarrow \infty$ the response $p_{1,2}$ follows a universal adiabatic profile (4.13), it is remarkable that the response $p_{1,2}$ is also universal for abrupt quenches, *i.e.*, in the limit $\alpha \rightarrow 0$. In this regard, we first observe that in fig. 2, the profile $\alpha^2 p_{1,2}$ has a relatively simple form for very small α and further

¹⁴As we discuss below, the curves fig. 2 do not allow us to resolve in the details the approach to the final equilibrium.

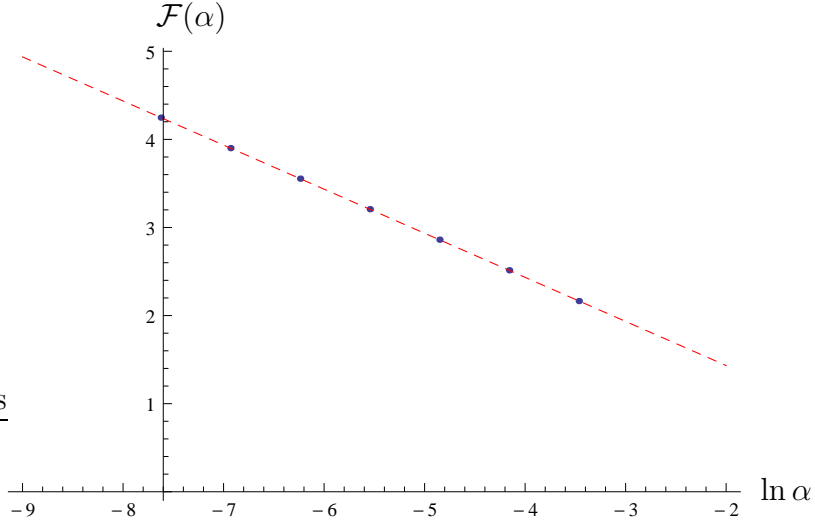


Figure 3: (Colour online) $\mathcal{F}(\alpha)$ quantifies the response $p_{1,2}$ for abrupt quenches, *i.e.*, as $\alpha \rightarrow 0$ — see the definition in eq. (5.1). The blue dots correspond to $\mathcal{F}(\alpha_n)$ for $\alpha_n = 2^{-n}$ with $n = 5, \dots, 11$. The dashed red line represents the linear fit to these points given in eq. (5.2).

that this simple form is remarkably similar to $\alpha^2 p''_{1,0} = -\sinh(\tau/\alpha)/\cosh^3(\tau/\alpha)$. This observation motivated us to define $\mathcal{F}(\alpha)$ as the constant which minimizes the following:

$$\begin{aligned} \|p_{1,2} - \mathcal{F}(\alpha) p''_{1,0}\| &\equiv \int_0^1 d(p_{1,0}) (p_{1,2} - \mathcal{F}(\alpha) p''_{1,0})^2 \\ &= \int_{-\infty}^{\infty} d\tau p'_{1,0} (p_{1,2} - \mathcal{F}(\alpha) p''_{1,0})^2. \end{aligned} \quad (5.1)$$

The first expression defining the norm above was chosen since it seems natural if $\mathcal{F}(\alpha)$ is to describe the universal character of the response. From the second expression, we see that since $p'_{1,0} = 1/(2\alpha \cosh(\tau/\alpha)^2)$, this measure weights most heavily the region in the vicinity of $\tau = 0$, where the peaks in $p_{1,2}$ occur. Fig. 3 shows $\mathcal{F}(\alpha_n)$ for $\alpha_n = 2^{-n}$ with $n = 5, \dots, 11$. As also shown in the figure, these points are very well fit with a simple linear expression which takes the form:

$$\mathcal{F}|_{fit} \simeq 0.43 - 0.50 \ln \alpha. \quad (5.2)$$

This simple result indicates that the leading contribution in response $p_{1,2}$ actually grows as approximately $\alpha^{-2} \ln(1/\sqrt{\alpha})$ as $\alpha \rightarrow 0$, *i.e.*, faster than α^{-2} . Now let us define the

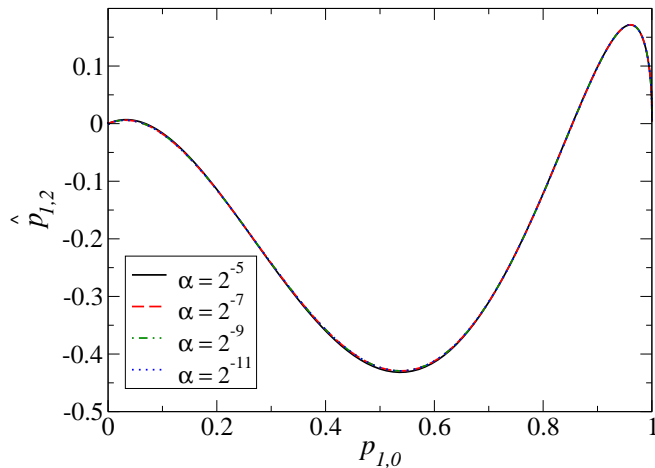


Figure 4: (Colour online) Universality of the subtracted response $\hat{p}_{1,2}$ (defined in eq. (5.3)) for abrupt quenches. The different curves are virtually indistinguishable from each other.

‘subtracted’ response $\hat{p}_{1,2}$ as follows

$$\hat{p}_{1,2} \equiv \alpha^2 (p_{1,2} - \mathcal{F}(\alpha) p''_{1,0}) , \quad (5.3)$$

which is then plotted as a function of $p_{1,0}$ in fig. 4. Remarkably, all four curves in this plot are almost indistinguishable from each other and so we see that $\hat{p}_{1,2}$ also has a simple universal behaviour in the limit $\alpha \rightarrow 0$.

Eqs. (3.22) and (3.23) show the characteristics of the final equilibrium state resulting from the quench, *i.e.*, the temperature T_f , the energy density \mathcal{E}_f , the pressure \mathcal{P}_f and entropy density S_f , relative to the initial state parameters. All of these ratios depend on coefficient $a_{2,4}^\infty$, given in eq. (3.21). As noted in the discussion in section 3.1.1, in the adiabatic limit, $\alpha \rightarrow \infty$, $a_{2,4}^\infty$ vanishes and so the entropy density is constant. Further for these adiabatic transitions from the thermal state of the CFT plasma to the mass-deformed thermal state result in an increase of the temperature $T_f > T_i$ and the energy density $\mathcal{E}_f > \mathcal{E}_i$, while the pressure is decreased $\mathcal{P}_f < \mathcal{P}_i$. In fact, in all of our simulations with finite α , we found that $a_{2,4}^\infty < 0$ and further $|a_{2,4}^\infty|$ grows as α becomes smaller — see below. Of course, in agreement with one’s intuition then, eq. (3.23) indicates that the entropy density increases in a generic quench and in fact, the entropy production grows as the quenches become faster. Further, according to

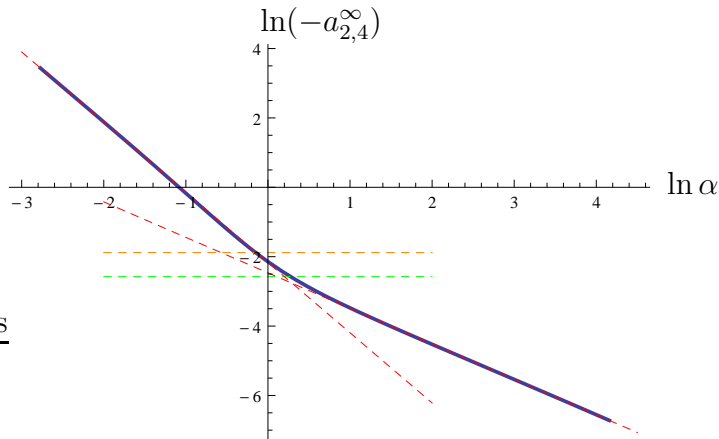


Figure 5: (Colour online) Log-log plot of coefficient $(-a_{2,4}^\infty)$ as a function of α . The dashed red lines represent the linear fits to the data (blue curve) for ‘fast’ quenches with small α ($\ln \alpha \rightarrow -\infty$) and for ‘slow’ quenches with large α ($\ln \alpha \rightarrow +\infty$). The dashed green and orange horizontal lines indicate the thresholds given in eqs. (5.4) and (5.5), respectively. For values of $(-a_{2,4}^\infty)$ above the dashed green line, both classes of quenches produce a final energy density which exceeds the initial energy density. For values of $(-a_{2,4}^\infty)$ above dashed orange line, the final temperature is always larger than the initial temperature for either type of quench. See the discussion in the main text.

eq. (3.22), more rapid quenches result in greater ‘heating’, *i.e.*, the increase in the temperature and the energy density grows as α becomes smaller.

We will consider these results more quantitatively below but first let us consider the properties of quenches which make a transition from a thermal state in the mass-deformed gauge theory to a thermal CFT state. As described in section 3.1.1, we can make a direct translation of any of the previous results to these ‘reverse’ quenches using eqs. (3.35) and (3.36). For these reverse transitions, the characteristics of the final equilibrium relative to the initial state are given by eqs. (3.33) and (3.34) and these ratios are controlled by $\tilde{a}_{2,4}^\infty$, given in eq. (3.32). However, using the previous translation, one finds that, as presented in eq. (3.37): $\tilde{a}_{2,4}^\infty = a_{2,4}^\infty$. In the adiabatic limit, these transition from the mass-deformed theory to the CFT state result in ‘cooling’ of the system. That is, $\tilde{a}_{2,4}^\infty$ vanishes for $\alpha \rightarrow \infty$ and while the entropy density is constant, the temperature and energy density decrease. However, for very rapid transitions, $\tilde{a}_{2,4}^\infty$ becomes large and negative and so eq. (3.33) shows that the quenches are again ‘heating’ the plasma with both $T_f > T_i$ and $\mathcal{E}_f > \mathcal{E}_i$. In fact, we see that the thresholds for

increasing the temperature and energy density are slightly different. Specifically, from (3.33), $\mathcal{E}_f > \mathcal{E}_i$ provided

$$-\tilde{a}_{2,4}^\infty > \frac{\Gamma\left(\frac{3}{4}\right)^4}{3\pi^2}, \quad (5.4)$$

while $T_f > T_i$ requires

$$-\tilde{a}_{2,4}^\infty > \frac{2\Gamma\left(\frac{3}{4}\right)^4}{3\pi^2}. \quad (5.5)$$

As shown in fig. 5, both of these thresholds occur close to $\alpha = 1$:

$$\begin{aligned} \mathcal{E}_f > \mathcal{E}_i &\iff \alpha \lesssim 1.32, \\ T_f > T_i &\iff \alpha \lesssim 0.86. \end{aligned} \quad (5.6)$$

Fig. 5 presents a log-log plot of the coefficient $a_{2,4}^\infty$ as a function of α . The behaviour of the plot reveals simple behaviours in both the ‘slow’ and ‘fast’ regimes with $\alpha \gg 1$ and $\alpha \ll 1$, respectively. In fig. 5, the dashed red lines show the linear fits to the data for these ranges of α . In particular, we find

$$\begin{aligned} \text{slow :} \quad \ln(-a_{2,4}^\infty)|_{fit} &\simeq -2.465 - 1.02 \ln \alpha, & \alpha \gg 1, \\ \text{fast :} \quad \ln(-a_{2,4}^\infty)|_{fit} &\simeq -2.170 - 2.02 \ln \alpha, & \alpha \ll 1. \end{aligned} \quad (5.7)$$

Hence we find that $a_{2,4}^\infty$ vanishes as $\alpha \rightarrow \infty$ with $a_{2,4}^\infty \propto 1/\alpha$. However, we also find that $a_{2,4}^\infty$ is divergent for $\alpha \rightarrow 0$ with $a_{2,4}^\infty \propto 1/\alpha^2$. Let us further observe that the constant term in the ‘fast’ fit seems to match: $\ln\left[\Gamma\left(\frac{3}{4}\right)^4/(2\pi^2)\right] \simeq -2.169\dots$. Hence our numerical results seems to indicate that the leading behaviour as $\alpha \rightarrow 0$ is given by

$$a_{2,4}^\infty \simeq -\frac{\Gamma\left(\frac{3}{4}\right)^4}{2\pi^2} \frac{1}{\alpha^2} + \dots, \quad (5.8)$$

which, of course, calls for an analytic derivation. Unfortunately, at present, we can provide no insight into such a derivation. However, we note that the scaling for slow transitions can, in principle, be deduced analytically from the evolution of ϕ_1 with $\alpha \gg 1$ — see the discussion below at eq. (6.20).

Using eq. (3.22), we can translate the asymptotic behaviour in eq. (5.7) into

$$\frac{\Delta\mathcal{E}}{\mathcal{E}_i} \equiv \frac{\mathcal{E}_f - \mathcal{E}_f^{adiabatic}}{\mathcal{E}_i} \propto \begin{cases} \frac{1}{\alpha} \frac{(m_f^0)^2}{T_i^2} & \text{for } \alpha \gg 1, \\ \frac{1}{\alpha^2} \frac{(m_f^0)^2}{T_i^2} & \text{for } \alpha \ll 1, \end{cases} \quad (5.9)$$

where $\mathcal{E}_f^{adiabatic}$ is the final energy density for an adiabatic transition, *i.e.*,

$$\mathcal{E}_f^{adiabatic} = \mathcal{E}_i \left(1 + \frac{2\Gamma\left(\frac{3}{4}\right)^4}{3\pi^2} \frac{(m_f^0)^2}{\pi^2 T_i^2} + \mathcal{O}\left(\frac{(m_f^0)^4}{T_i^4}\right) \right). \quad (5.10)$$

Note that the same expression (5.9) also applies for $\Delta\mathcal{E}/\mathcal{E}_i$ in the ‘reverse’ quenches describing transitions from the mass-deformed gauge theory to the CFT. Further we can similarly deduce the asymptotic behaviour for the relative change in the temperature and the pressure using eq. (3.22) and the entropy using eq. (3.23). Using eq. (5.8), we have a more precise expression for the limit $\alpha \rightarrow 0$,

$$\frac{\Delta\mathcal{E}}{\mathcal{E}_i} \simeq \frac{\Gamma\left(\frac{3}{4}\right)^4}{\pi^4} \frac{(m_f^0)^2}{T_i^2} \frac{1}{\alpha^2} + \dots \quad (5.11)$$

In particular then, we note that a discontinuous quench with $\alpha = 0$ would seem to produce physical divergences — see further discussion in section 6.

However, let us observe that previously we found that the leading scaling of amplitude of the response was $\alpha^{-2} \ln(1/\alpha)$ — see discussion around eq. (5.2). Hence one might have expected an even stronger divergence in eq. (5.11), which ‘only’ scales like α^{-2} . This behaviour can be understood as follows: The divergence in eq. (5.11) simply reflects the divergence in $a_{2,4}^\infty$ given in eq. (5.8). Now in eq. (3.21) which defines the latter, the integral dominates for small α and so from eq. (5.3), we have

$$\begin{aligned} a_{2,4}^\infty &\simeq \frac{2}{3} \int_{-\infty}^{\infty} ds \left(\mathcal{F}(\alpha) p''_{1,0}(s) - \frac{1}{\alpha^2} \hat{p}_{1,2}(s) \right) p'_{1,0}(s) \\ &= \frac{2}{3\alpha^2} \int_{-\infty}^{\infty} ds \hat{p}_{1,2}(s) p'_{1,0}(s). \end{aligned} \quad (5.12)$$

That is, the specific form of the leading response, *i.e.*, being proportional to $p''_{1,0}$, leads to a total derivative which yields a vanishing contribution above. Hence, only the ‘subtracted’ response (5.3) contributes in the integral to produce the α^{-2} scaling in eq. (5.11).

We conclude this section with more quantitative analysis of the excitation and the equilibration time scales in the evolution of the normalizable component $p_{1,2}(\tau)$. As described above, for an adiabatic transition, the system essentially maintains thermodynamic equilibrium throughout the process and $p_{1,2}(\tau)$ simply tracks $p_{1,0}(\tau)$, as indicated in eq. (3.25) or (4.13). Hence, we define a measure of the deviation from the local equilibrium as follows

$$\delta_{neq}(\tau) \equiv \left| \frac{p_{1,2}(\tau) - [p_{1,2}(\tau)]_{adiabatic}}{p_{1,2}^{equilibrium}} \right|, \quad (5.13)$$

where $[p_{1,2}(\tau)]_{adiabatic}$ is given in eq. (4.13) and

$$p_{1,2}^{equilibrium} = \lim_{\tau \rightarrow +\infty} p_{1,2}(\tau) = -\frac{\Gamma\left(\frac{3}{4}\right)^4}{\pi^2}. \quad (5.14)$$

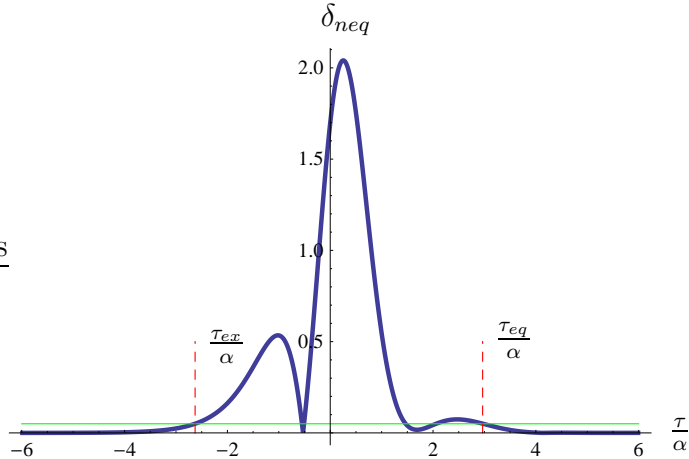


Figure 6: (Colour online) Extraction of the excitation/equilibration rates for $\alpha = 1$ quench. The horizontal green line is the threshold for excitation/equilibration which we define to be 5% away from local equilibrium as determined by δ_{neq} , as given defined in eq. (5.13). The dashed red lines indicate the earliest and latest times of crossing this threshold, which we denote as τ_{ex} (for excitation time) and τ_{eq} (for equilibration time), respectively.

Fig. 6 shows a typical plot of δ_{neq} . We further define the excitation time τ_{ex} as the earliest time in the quench at which δ_{neq} when the latter quantity exceeds a predefined threshold value, which we choose to be $\epsilon = 0.05$, *i.e.*,

$$\delta_{neq} < \epsilon = 0.05, \quad \text{for all } \tau < \tau_{ex}. \quad (5.15)$$

While the choice of the threshold here is somewhat arbitrary, we do not expect that it will greatly effect the following observations. Similarly, we define the equilibration time τ_{eq} as the latest time at which δ_{neq} exceeds the same threshold value, *i.e.*,

$$\delta_{neq} < \epsilon = 0.05, \quad \text{for all } \tau > \tau_{eq}. \quad (5.16)$$

All of these quantities are identified in the sample plot shown in fig. 6. In fig. 7, we show τ_{ex} and τ_{eq} for quenches across a wide range of α .

Examining fig. 6, one sees that δ_{neq} has several the zeros (at finite τ/α) which reflect the fact that $p_{1,2}$ is oscillating about $[p_{1,2}]_{adiabatic}$ — later we will see that these oscillations are described by quasinormal modes of the scalar. The amplitude of oscillations become smaller as α grows and in fact, for α sufficiently large, δ_{neq} will be

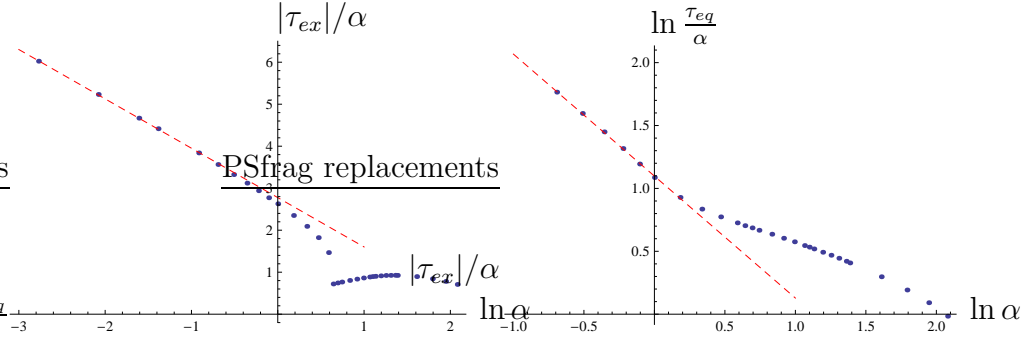


Figure 7: (Colour online) Excitation time τ_{ex} (left panel) and equilibration time τ_{eq} (right panel) as a function of α . The threshold is fixed to be $\epsilon = 0.05$ — see eqs. (5.15) and (5.16). In both cases, a simple linear fit describes the behaviour for small α , as shown with the red dashed lines.

below any fixed threshold ϵ throughout the quench. While we did not try to pinpoint the precise value of α at which this occurs, we did establish that this behaviour sets in before $\alpha = 16$ with $\epsilon = .05$. Further, we see in fig. 7 that τ_{ex} and τ_{eq} behave irregularly for large α . In particular, τ_{ex} is clearly discontinuous for $\alpha \sim 1.8$ and there is a similar discontinuity in τ_{eq} , albeit less profound. Hence, as defined above, these time scales are not useful diagnostics for slow quenches.

On the other hand, both τ_{ex} and τ_{eq} exhibit simple behaviours for small α , as shown with the linear fits in fig. 7. In the left panel, the linear fit for the excitation time is

$$\left. \frac{|\tau_{ex}|}{\alpha} \right|_{fit} \simeq 2.8 - 1.2 \ln \alpha. \quad (5.17)$$

A heuristic understanding of this behaviour is as follows: In the discussion around eqs. (5.1–5.3), we demonstrated that the leading response takes the form

$$p_{1,2}(\tau_{ex}) \simeq \mathcal{F}(\alpha) p''_{1,0}(\tau_{ex}) \simeq -\frac{\ln \alpha}{\alpha^2} e^{2\tau_{ex}/\alpha}, \quad \frac{\tau_{ex}}{\alpha} \rightarrow -\infty. \quad (5.18)$$

where the latter uses the approximate form of $p''_{1,0}$ for large negative τ . Hence if we set a fixed threshold for the response at early times, we should expect that

$$p_{1,2}(\tau_{ex}) \sim \text{const} \quad \implies \quad \frac{|\tau_{ex}|}{\alpha} \sim -\ln \alpha + \mathcal{O}(\ln(-\ln(\alpha))), \quad (5.19)$$

which matches the result given in eq. (5.17). Using eqs. (4.1) and (4.2), this behaviour can be translated to an excitation time in terms of the original boundary time

$$t_{ex} \equiv \mathcal{T} \frac{\tau_{ex}}{\alpha} \simeq \mathcal{T} \ln(1/T_i \mathcal{T}) \quad \text{for } T_i \mathcal{T} \ll 1. \quad (5.20)$$

The scaling of the equilibration time at small α is different. For the right panel on fig. 7, the linear fit was

$$\ln \frac{\tau_{eq}}{\alpha} \Big|_{fit} \simeq 1.1 - 1.0 \ln \alpha. \quad (5.21)$$

Hence we have for the equilibration time in fast quenches

$$\frac{\tau_{eq}}{\alpha} \sim \frac{1}{\alpha}, \quad (5.22)$$

or, in terms of the original boundary time,

$$t_{eq} \equiv \mathcal{T} \frac{\tau_{eq}}{\alpha} \sim \frac{1}{T_i}. \quad (5.23)$$

That is, irrespective of how quickly the system is driven away from the initial equilibrium, the return to the final equilibrium is determined universally by the typical thermal time-scale.

This behaviour seems closely connected to the fact that the late-time response is controlled by the quasinormal modes of the scalar field [37, 38]. The quasinormal oscillations are well illustrated in fig. 8, which shows the late-time evolution of $p_{1,2}$ for a range of small values of α . For all of these fast quenches, a single mode clearly determines the decay of $p_{1,2}$ after a very short time. A rough fit of the oscillation periods and the slopes indicates that in all cases, the decay is governed by a quasinormal mode with $\omega/(2\pi T_i) \simeq (1.095 + i0.87)$. This value is consistent with the expected frequency $(1.099 + i0.879)$, found in [38]. Beyond this fundamental mode, the first overtone can also be extracted for about one oscillation period and a rough fit yields real and imaginary parts of its frequency which agree with the expected values to within approximately 25%.

5.2 Quenches with \mathcal{O}_2

Our discussion of the results for quenching the bosonic mass operator will be shorter, as it parallels the previous discussion of quenches of the fermionic mass operator. However, we will see that the physical characteristic of these types of quenches differ in many respects. For the present quenches, the profile of the source $p_{1,0}^l$ is given by eq. (4.7). Again, the characteristics of response in the normalizable component $p_{1,0}$ depend on whether the transition is ‘fast’ with $\alpha < 1$ or ‘slow’ with $\alpha > 1$. Our results for both cases are presented in fig. 9. The curves in the left and right panels present $p_{1,0}$ as function of $\frac{\tau}{\alpha}$ for fast and slow quenches, respectively. We present fast quenches with $\alpha = \{1, 0.5, 0.1, 0.05, 0.01, 0.005\}$ and slow quenches with $\alpha = \{1, 2.5, 5, 10, 50, 100\}$.

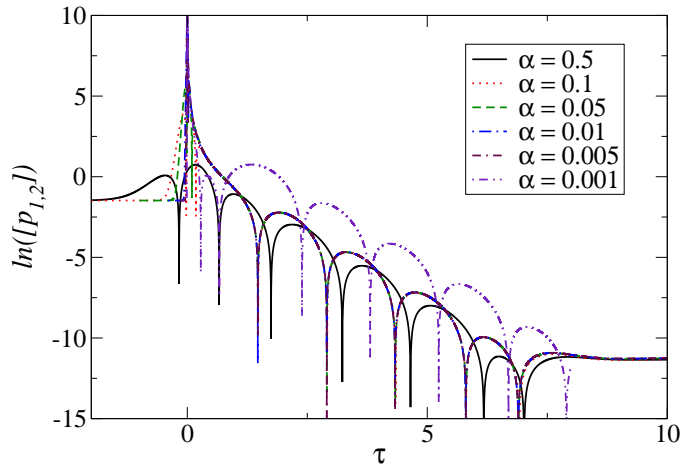


Figure 8: (Colour online) Behaviour of the response coefficient versus time for different fast quenches. Note that on the vertical axis, we have defined $[p_{1,2}] \equiv p_{1,2} + \Gamma(3/4)^4 \pi^{-2}$. In all cases, the same quasinormal mode governs the dynamics very soon after the quench.

First we consider the slow quenches, *i.e.*, with $\alpha > 1$ in the right panel. As found before with quenches of \mathcal{O}_3 operator, progressively larger values of α result in profiles that more closely resemble the adiabatic response given here by eq. (4.14). The latter profile ‘appears’ in the plot as a black dotted line, but for the most part, it is covered by the profiles for $\alpha = 50$ and 100 which track this adiabatic response.

Now we turn to the fast quenches in the left panel. The response shown there is very far from the adiabatic curve, which corresponds to eq. (4.14). Although the maximum amplitude of the response grows as α becomes smaller and the quenches become faster, comparing to fig. 2, we see that the present increase is not as nearly as dramatic as found for quenches of \mathcal{O}_3 in the previous section. Notice that neither the response $p_{1,0}$ nor the time τ is scaled for fast quenches in fig. 9, in contrast to the corresponding plot in fig. 2. With this slower grow, there is no distinctive profile that emerges here for $p_{1,0}$ in this limit. Hence to determine if the response is scaling with α , we first simply consider the peak value of this normalizable component, *i.e.*,

$$\mathcal{F}_0(\alpha) = \max_{\tau \in (-\infty, +\infty)} |p_{1,0}|. \quad (5.24)$$

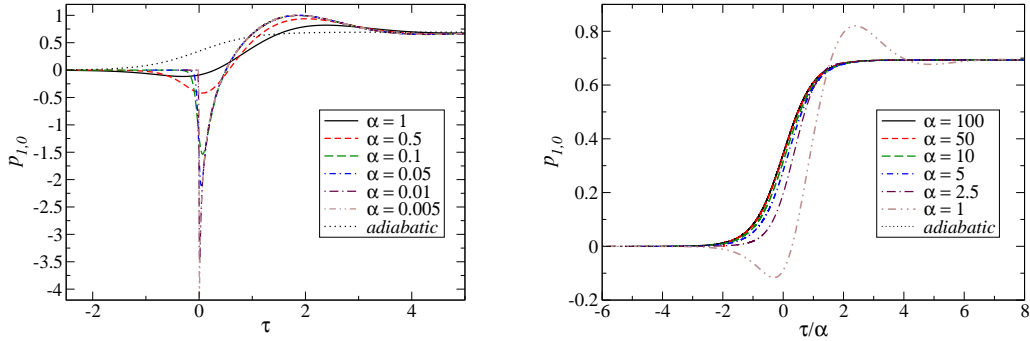


Figure 9: (Colour online) Normalizable component $p_{1,0}$ as a function of τ for fast and slow quenches is shown in the left and the right panels, respectively.

The left panel in fig. 10 shows $\mathcal{F}_0(\alpha_n)$ for a select set of values, $\alpha_n = \{1/32, 1/64, 1/128, 0.0025, 0.0001, 0.00001\}$. As the red dashed line in the figure shows, these points are quite well fit with a simple linear expression which takes the form

$$\mathcal{F}_0|_{fit} \simeq -0.80 - 0.94 \ln \alpha. \quad (5.25)$$

The rescaled response, $\hat{p}_{1,0} \equiv -p_{1,0}/\mathcal{F}_0(\alpha)$, is then shown in the left panel of fig. 11 as a function of $p_{1,0}^l$. It seems that these curves are slowly converging to a straight line such that in the limit $\alpha \rightarrow 0$, the profile of this rescaled response is simply given by $\hat{p}_{1,0} = p_{1,0}^l$, which is represented by a dotted orange line in the figure. That is, in the limit of very fast quenches, the rescaled response simply tracks the source. We must clarify this claim, which seems to suggest that profile of $p_{1,0}$ should approach a simple step function as $\alpha \rightarrow 0$. Clearly, the latter is at odds with the profiles shown in fig. 9. However, note that in fig. 11, we are plotting rescaled response as a function of $p_{1,0}^l$ and with the profile in eq. (4.7), this source varies across 90% of its range within $-3\alpha/2 \leq \tau \leq 3\alpha/2$. Hence in this plot, we are really focussing the behaviour of $p_{1,0}$ in a very narrow range around $\tau = 0$ when α is small.¹⁵ Further, this observation

¹⁵To see more clearly that as $\alpha \rightarrow 0$, $p_{1,0}$ is approaching this step function in time, one can plot $p_{1,0}$ as a function of τ/α – rather than just τ , as was done in fig. 9. However, as is evident from fig. 11, the response still falls off rapidly for $\tau/\alpha > 3/2$ for the values of α shown there.

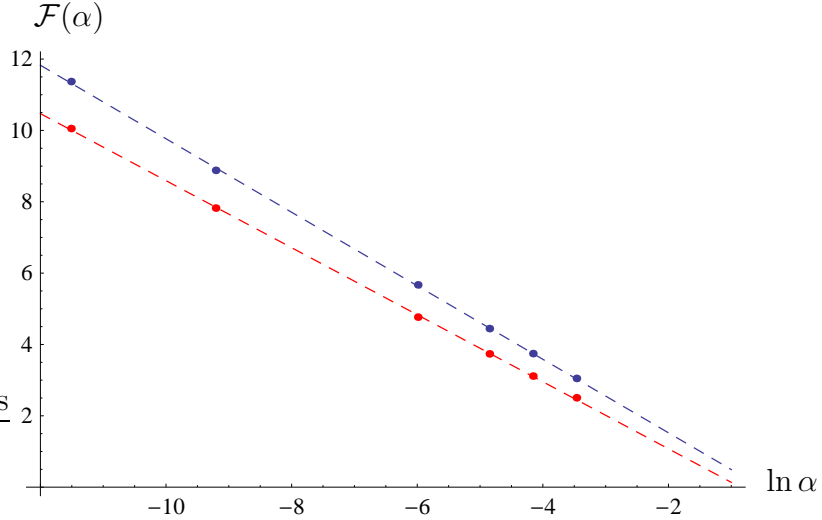


Figure 10: (Colour online) $\mathcal{F}(\alpha)$ quantifies the response $p_{1,0}$ for abrupt quenches, *i.e.*, as $\alpha \rightarrow 0$. The red dots correspond to $\mathcal{F}_0(\alpha_n)$ (defined in eq. (5.24)) for $\alpha_n = \{1/32, 1/64, 1/128, 0.0025, 0.0001, 0.00001\}$. The dashed red line represents the linear fit to these points given in eq. (5.25). The blue dots correspond to $\mathcal{F}_1(\alpha_n)$ (defined in eq. (5.26)) for the same α_n . The dashed blue line represents the linear fit to the latter points given in eq. (5.27).

motivated us to define $\mathcal{F}_1(\alpha)$ as the constant which minimizes the following norm:

$$\begin{aligned} \|p_{1,0} - \mathcal{F}_1(\alpha) p_{1,0}^l\| &\equiv \int_0^1 d(p_{1,0}^l) (p_{1,0} - \mathcal{F}_1(\alpha) p_{1,0}^l)^2 \\ &= \int_{-\infty}^{\infty} d\tau (p_{1,0}^l)' (p_{1,0} - \mathcal{F}_1(\alpha) p_{1,0}^l)^2, \end{aligned} \quad (5.26)$$

in analogy with eq. (5.1) for the dimension-3 operator. As before, the factor $(p_{1,0}^l)' = (2\alpha \cosh(\tau/\alpha)^2)^{-1}$ in the last expression weights most heavily the integration in a narrow range around $\tau = 0$ for small α . The right panel in fig. 10 shows $\mathcal{F}_1(\alpha_n)$ for the the same values α_n used above. The blue dashed line in the figure indicates a simple linear fit to these points, which takes the form

$$\mathcal{F}_1|_{fit} \simeq -0.54 - 1.03 \ln \alpha. \quad (5.27)$$

In this case, the rescaled response, $\tilde{p}_{1,0} \equiv -p_{1,0}/\mathcal{F}_1(\alpha)$, is then shown in the right panel of fig. 11 and again the results suggest a slow convergence towards $\tilde{p}_{1,0} = p_{1,0}^l$ as $\alpha \rightarrow 0$. Hence, with both definitions of the scaling factor in eqs. (5.25) and (5.26), the results

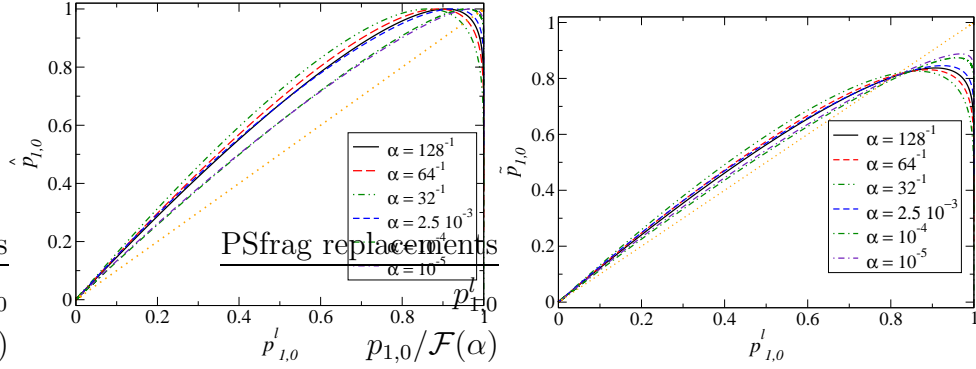


Figure 11: (Colour online) Limiting behaviour of the rescaled response for abrupt quenches with $\hat{p}_{1,0} \equiv -p_{1,0}/\mathcal{F}_0(\alpha)$ in the left panel and $\tilde{p}_{1,0} \equiv -p_{1,0}/\mathcal{F}_1(\alpha)$ in the right panel. In both cases, the curves suggest a slow convergence towards straight line where the rescaled response simply follows the source, *e.g.*, $\hat{p}_{1,0} = p_{1,0}^l$ on the left, as $\alpha \rightarrow 0$.

suggest that the same scaling of the ‘prompt’ response with $p_{1,0} \simeq \log \alpha p_{1,0}^l$ for fast quenches, *i.e.*, with small α .

The reduced response of the present quenches with \mathcal{O}_2 will also become evident below when we consider the properties of the final equilibrium state. Finally, we reiterate that neither $p_{1,0}$ nor τ is scaled in fig. 9 for the fast quenches. Hence we observe that the relaxation of the system after a fast quench is almost ‘universal’, *i.e.*, it is essentially independent of α .

We now turn to eqs. (3.47) and (3.48), which give the characteristics of the final equilibrium state relative to those of the initial equilibrium, *i.e.*, T_f/T_i , $\mathcal{E}_f/\mathcal{E}_i$, $\mathcal{P}_f/\mathcal{P}_i$ and S_f/S_i . All of these ratios depend on coefficient $a_{2,4}^\infty$ given in eq. (3.46). In particular, this coefficient was defined to give a direct measure of the entropy production during the quench, as shown in eq. (3.48). This coefficient is shown for a wide range of α in fig. 12. One simple observation is that in our numerical simulations, we always found $a_{2,4}^\infty \leq 0$, which must intuitively be the case from eq. (3.48) in order that $S_f \geq S_i$. We might also observe that $|a_{2,4}^\infty|$ is becoming very small for large α , which agrees with the discussion in section 3.1 where we argued that $a_{2,4}^\infty \rightarrow 0$ for $\alpha \rightarrow \infty$. Let us add here that according to eq. (3.47), we may describe the quenches going from the CFT to the mass-deformed gauge theory as always ‘heating’ the system. That is, we always have $T_f > T_i$, even in the adiabatic system. On the other hand, according to eq. (3.58) for ‘reverse’ quenches going from the mass-deformed gauge theory to the CFT, the system

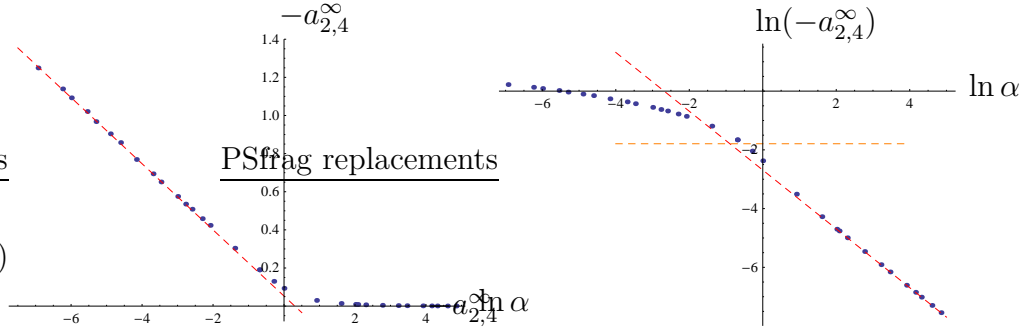


Figure 12: (Colour online) Coefficient $a_{2,4}^\infty$ as a function of α . The dashed red lines represent the linear fits to the data (blue points) for fast (left panel) and slow (right panel) quenches. Values of $(-a_{2,4}^\infty)$ above dashed orange line in the right panel always result in quenches where the final temperature exceeds the initial temperature.

‘cools’ if the transition is sufficiently slow, *i.e.*, $a_{2,4}^\infty$ is sufficiently small. However, as the quenches become faster, $a_{2,4}^\infty$ becomes large and negative resulting in $T_f > T_i$ again. Specifically, from (3.58), $T_f > T_i$ requires¹⁶

$$-a_{2,4}^\infty > \frac{1}{6}. \quad (5.28)$$

As shown in the right panel of fig. 12, this threshold occurs close to $\alpha = 1$:

$$T_f > T_i \quad \Longleftrightarrow \quad \alpha \lesssim 0.58. \quad (5.29)$$

In certain respects, the results for $a_{2,4}^\infty$ in fig. 12 for quenches induced by the bosonic mass term are similar to those in fig. 5 for quenches induced by the fermionic mass term. In particular, both figures show a simple behaviour for both $\alpha \gg 1$ and $\alpha \ll 1$ and a clear transition between these two around $\alpha \sim 1$. However, there is one striking difference in that the fast quenches are shown in the left panel of fig. 12 which shows $-\hat{a}_{2,4}^\infty$ (rather than $\ln(-\hat{a}_{2,4}^\infty)$) as a function of $\ln \alpha$. The simple fits for the fast and slow quenches then take the form

$$\begin{aligned} \text{slow :} \quad & \ln(-a_{2,4}^\infty)|_{fit} \simeq -2.688 - 1.00 \ln \alpha, \quad \alpha \gg 1, \\ \text{fast :} \quad & -a_{2,4}^\infty|_{fit} \simeq 0.05 - 0.17 \ln \alpha, \quad \alpha \ll 1. \end{aligned} \quad (5.30)$$

¹⁶Here we are using eq. (3.62) which states that $\tilde{a}_{2,4}^\infty = a_{2,4}^\infty$ for the reverse quenches described by eqs. (3.60) and (3.61).

Using eq. (3.47), we can translate the asymptotic behaviour in eq. (5.30) into

$$\frac{\Delta\mathcal{E}}{\mathcal{E}_i} \equiv \frac{\mathcal{E}_f - \mathcal{E}_f^{adiabatic}}{\mathcal{E}_i} \propto \begin{cases} \frac{1}{\alpha} \frac{(m_b^0)^4}{T_i^4} & \text{for } \alpha \gg 1, \\ \ln(1/\alpha) \frac{(m_b^0)^4}{T_i^4} & \text{for } \alpha \ll 1, \end{cases} \quad (5.31)$$

where

$$\mathcal{E}_f^{adiabatic} = \mathcal{E}_i \left(1 - \frac{1}{9} \ln \frac{\pi T_i (m_b^0)^4}{\Lambda_1 \pi^4 T_i^4} + \mathcal{O} \left(\frac{(m_b^0)^8}{T_i^8} \right) \right). \quad (5.32)$$

Of course, we can also determine the asymptotic behaviour for the relative change in the temperature and the pressure using eq. (3.47) and the entropy using eq. (3.48). In particular then, we note that a discontinuous quench with $\alpha = 0$ would again seem to produce physical divergences. However, we are again seeing a weaker response here for the quenches induced by \mathcal{O}_2 . Recall that the analogous divergence in eq. (5.11) was proportional to $1/\alpha^2$ for the quenches with \mathcal{O}_3 .

Further, we note that the scaling of $a_{2,4}^\infty$ for $\alpha \rightarrow 0$ shown in eq. (5.30) is slower than the scaling of the amplitude of the response for the fast quenches found in our previous discussion — this was also found for the analogous results with \mathcal{O}_3 . However, if we assume the ‘prompt’ response takes the form $p_{1,0} \simeq \log \alpha p_{1,0}^l$ as discussed above, then the arguments given for the \mathcal{O}_3 case around eq. (5.12) would in fact indicate that both $a_{2,4}^\infty$ and $p_{1,0}$ scale in the same way. Hence the reasons for the discrepancy in the scaling of these two quantities must be more subtle here than before.

We now turn to the excitation and the equilibration time scales in the evolution of the normalizable component $p_{1,0}(\tau)$. By analogy to eq. (5.13), we define

$$\delta_{neq}(\tau) \equiv \left| \frac{p_{1,0}(\tau) - [p_{1,0}(\tau)]_{adiabatic}}{p_{1,0}^{equilibrium}} \right|, \quad (5.33)$$

where $[p_{1,0}(\tau)]_{adiabatic}$ is given in eq. (4.14) and

$$p_{1,0}^{equilibrium} = \lim_{\tau \rightarrow +\infty} p_{1,0}(\tau) = -\ln 2. \quad (5.34)$$

A typical behaviour of δ_{neq} is presented in fig. 13. We define the excitation and equilibration times τ_{ex} and τ_{eq} precisely as before in eqs. (5.15) and (5.16). We indicate these times in fig. 13, as well as the threshold $\epsilon = 0.05$. We extracted τ_{ex} and τ_{eq} for a wide range of α and our results are shown in fig. 14. As in the previous discussion, we only expect these time scales to be a useful diagnostic of fast quenches with $\alpha < 1$. For example, while we did not pinpoint the precise value of α such that $\delta_{neq} < \epsilon$ for all $\tau \in (-\infty, +\infty)$, we did establish that such a value of α occurs prior to $\alpha = 16$.

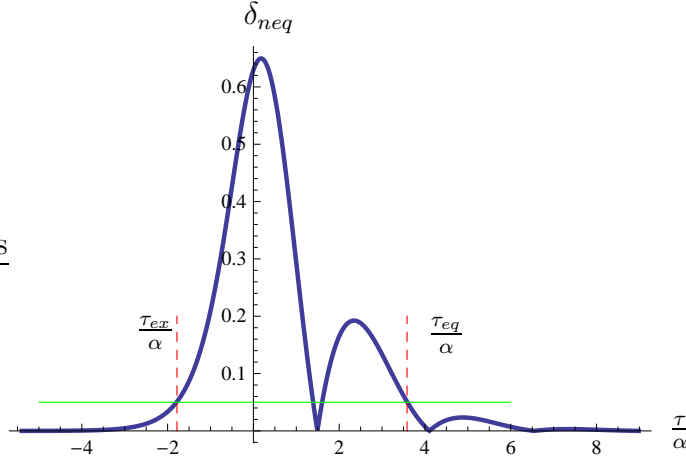


Figure 13: (Colour online) Extraction of the excitation/equilibration rates for $\alpha = 1$ quench. The horizontal green line is the threshold for excitation/equilibration which we define to be 5% away from local equilibrium as determined by δ_{neq} , as given defined in eq. (5.33). The dashed red lines indicate the earliest and latest times of crossing this threshold, which we denote as τ_{ex} (for excitation time) and τ_{eq} (for equilibration time), respectively.

The left panel of fig. 14 suggests that, in the limit $\ln \alpha \rightarrow -\infty$,

$$\frac{\tau_{ex}}{\alpha} \sim \ln(-\ln \alpha), \quad (5.35)$$

however, we must say that our results in this regime were not accurate enough to definitively fix this scaling. According to eq. (4.7), the scaling (5.35) would translate to

$$t_{ex} \sim \mathcal{T} \ln \ln(1/T_i \mathcal{T}) \quad \text{for } \alpha \ll 1. \quad (5.36)$$

In the right panel of fig. 14, we see the scaling of the equilibration time for small α is

$$\ln \frac{\tau_{eq}}{\alpha} \Big|_{fit} \simeq 1.5 - 1.0 \ln \alpha. \quad (5.37)$$

Hence for very fast quenches, $\tau_{eq}/\alpha \propto 1/\alpha$ or in terms of the original boundary time, we have

$$t_{eq} \equiv \mathcal{T} \frac{\tau_{eq}}{\alpha} \propto \frac{1}{T_i}. \quad (5.38)$$

Much like for quenches of \mathcal{O}_3 , here we find that irrespective of how quickly the system was driven away from the initial equilibrium, the return to the final equilibrium is

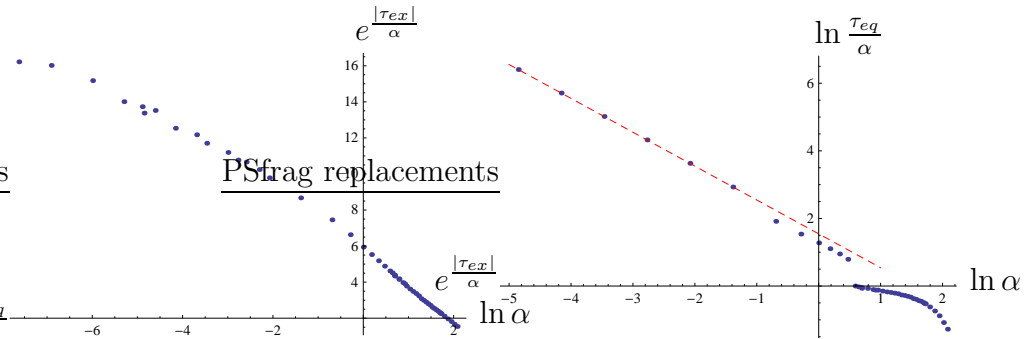


Figure 14: (Colour online) Excitation time τ_{ex} (left panel) and equilibration time τ_{eq} (right panel) as a function of α . The threshold is fixed to be $\epsilon = 0.05$ — see eqs. (5.15) and (5.16). In the left panel, it seems like $|\tau_{ex}|/\alpha \sim \ln(-\ln \alpha)$ in the limit $\ln \alpha \rightarrow -\infty$. In the right panel, the behaviour of $\ln(\tau_{eq}/\alpha)$ is linear in $\ln \alpha$ for small α , as shown with the red dashed line.

determined universally by the thermal time scale $1/T_i$. As with the previous quenches, here again the response is essentially controlled by a single quasinormal mode of the scalar field at a short time after the quench. This behaviour is well illustrated in fig. 15, which displays the evolution of $[p_{1,0}] \equiv p_{1,0} - p_{1,0}^{equilibrium} = p_{1,0} + \ln(2)$. A rough fit to the oscillation periods and slopes indicates that the corresponding quasinormal mode has $\omega/(2\pi T_i) \simeq (0.64 + i 0.4)$, which is consistent with the expected value of $(0.644 + i 0.411)$ found in [38]. As in the previous section, the first overtone can be extracted for about one oscillation period and once again, a rough fit yields real and imaginary parts of the quasinormal frequency which agree to within 25% of the expected ones.

6 Conclusions

In this paper, we initiated a program to study quantum quenches in strongly coupled quantum field theories using holography. We used gauge-gravity correspondence [6] to translate the problem of quenching the coupling λ_Δ of a relevant operator \mathcal{O}_Δ in planar $\mathcal{N} = 4$ SYM, as given in eq. (1.2), to a classical problem in Einstein gravity coupled to a massive scalar field in asymptotically AdS_5 spacetime. Here, we focused on two cases where $\Delta = 2$ and 3 but our analysis is readily extended to considering general values of Δ [29]. Our discussion also only considered ‘thermal quenches’ where the system begins in a thermal state of the gauge theory plasma and was limited to a

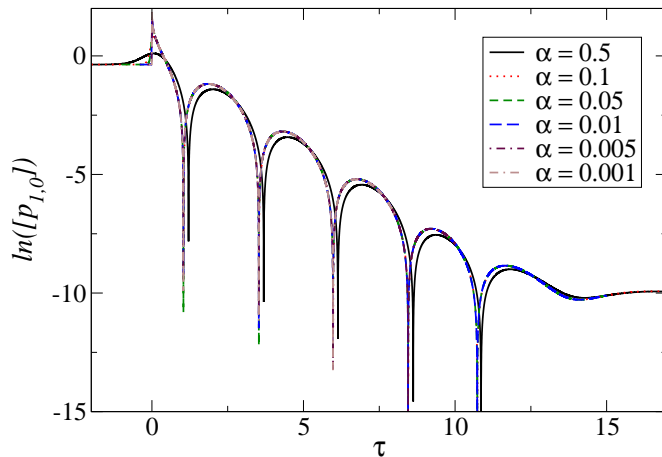


Figure 15: (Colour online) Behaviour of the response coefficients versus time for representative fast quenches. As is evident in the picture, the same quasinormal mode governs the dynamics very quickly after the quench.

high temperature limit. That is, during the quench, λ_Δ is always small compared to the temperature of the initial state T_i , *i.e.*,

$$|\lambda_\Delta| \ll T_i^{4-\Delta}. \quad (6.1)$$

The latter means that our calculations were *perturbative* in the coupling λ_Δ . However, there was no restriction on the time scale \mathcal{T} governing the rate of change of the coupling in the transition. In particular, we considered profiles of the form given in eq. (1.3) and our results were described in terms of the dimensionless parameter: $\alpha = \pi T_i \mathcal{T}$. In our analysis, we considered arbitrary values of α and in particular, we examined the limits of adiabatic transitions with $\alpha \rightarrow \infty$ and abrupt quenches with $\alpha \rightarrow 0$. As indicated in eq. (1.3), we discussed both the quenches from the conformal SYM theory to the mass-deformed gauge theory (with the plus sign for which $\lambda_\Delta(t \rightarrow -\infty) \rightarrow 0$) and the *reverse* quenches from the mass-deformed gauge theory to the conformal gauge theory (with the minus sign). In all of these quenches, we computed, to leading order in the coupling, the response of some basic gauge invariant observables, namely, the one-point correlators of the stress tensor $\langle T_{ij} \rangle$ and the mass operator $\langle \mathcal{O}_\Delta \rangle$. A detailed discussion of the results is given in section 5.

One of the most interesting results coming from our analysis is that the ‘infinitely fast’ quenches seem to be ill-defined because of divergences appearing in the limit $\alpha \rightarrow 0$. These divergences appear most dramatic for quenches of \mathcal{O}_3 , the fermionic mass operator, in expressions such as eqs. (5.9) or (5.11) which indicate that the energy of the final state diverges as $1/\alpha^2$ as $\alpha \rightarrow 0$. This result is of particular note since it is precisely such ‘infinitely fast’ quenches are studied in the seminal work on the topic [4, 5]. In their description of these quenches, the evolution from $t = -\infty$ to 0^- is essentially regarded as preparing the system in the ground state of the initial Hamiltonian and then this ground state is used as the initial condition at $t = 0^+$ as the system evolves forward with the new ‘quenched’ Hamiltonian. In our more physical approach to describing fast quenches, the transition from the initial to the final Hamiltonian is accompanied by an enormous response in the infinitesimal interval around $t = 0$, as can be seen in the scaling of $p_{2,0}$ for \mathcal{O}_3 and of $p_{1,0}$ for \mathcal{O}_2 as $\alpha \rightarrow 0$. Hence one might worry that our results call into question the approach of these early studies. Of course, an important difference between these studies and our work is that the former considered free or weakly coupled field theories whereas we are studying a strongly coupled field theory.

However, we must insert a word of caution with respect to our discussion above. The framework considered here treats the bulk scalar field perturbatively. In particular, we scaled the amplitude of the field by a factor λ , which was then gave a perturbative expansion of the results for the boundary theory in terms of m_f^0/T_i or $(m_b^0)^2/T_i^2$, using eq. (3.18) or (3.43), respectively. However, this approach only properly accounts for the backreaction of the bulk scalar on the background spacetime as long as the quench is not too fast. Looking at the gravitational equations, we find terms containing time-derivatives of the scalar, *i.e.*, terms proportional to $(\partial_v\phi)^2$ in eq. (2.16), as well as to $\partial_v\phi\partial_r\phi$ in both eqs. (2.15) and (2.16). Hence heuristically we should say that in order to ensure the full backreaction of the bulk scalar remains small, we must in fact fix $\lambda/\alpha \ll 1$. In other words, our perturbative calculations only yield reliable results, *e.g.*, in eqs. (5.9) or (5.11), as long as $\frac{1}{\alpha^2} \left(\frac{m_f^0}{T_i}\right)^2$ remains small. This issue is also evident in the observation that with a very high final temperature (in particular, much larger than the mass scale of the operator in the quench), T_f/T_i , $\mathcal{E}_f/\mathcal{E}_i$ and S_f/S_i can not all diverge in precisely the same way, as would naively be the case with our perturbative treatment. Rather, the divergences (or scalings) must arrange themselves such that $\mathcal{E}_f/\mathcal{E}_i \propto (T_f/T_i)^4$ and $S_f/S_i \propto (T_f/T_i)^3$. Hence it is clear that our present analysis does

not provide the final story and to properly understand the behaviour of the ‘infinitely fast’ quenches, we must turn to a full nonlinear analysis of the bulk gravitational equations of motion (2.13–2.17) [29]. However, to close this discussion, let us note that the nonlinear analysis of [13] do yield divergent results in the limit $\alpha \rightarrow 0$.

Further, we wish to stress that the above discussion does not invalidate the various universal scaling properties and profiles that were found in section 5 for $\alpha \rightarrow 0$. Rather these should be interpreted in terms of choosing $\lambda \ll \alpha_{min}$ for some small value α_{min} . Then for such a sufficiently small amplitude, the universal behaviours will still correctly describe the physics of quenches in the regime $\alpha_{min} < \alpha \ll 1$.

Allowing the couplings of the boundary gauge theory to vary in space and time introduces a variety of new ultraviolet divergences into the quantum field theory. The power of holography is that it provides a well-defined framework for the renormalization of the boundary theory, even in the presence of these space-time varying couplings. As discussed in section 2.1, the bulk gravity theory provides a natural geometric construction which regulates the new divergences and allows us to identify the appropriate counterterms to renormalize them in a covariant way. Recall that roughly, the expectation value of the quenching operator \mathcal{O}_Δ and its coupling λ_Δ are encoded as normalizable and non-normalizable coefficients (correspondingly) of the dual bulk scalar,¹⁷ $\phi_\Delta = \phi_\Delta(t, \rho)$,

$$\begin{aligned} \phi_\Delta &\sim \lambda_\Delta \rho^{4-\Delta} + \mathcal{O}_\Delta \rho^\Delta && \text{for } 2 < \Delta < 4, \\ \phi_2 &\sim \lambda_2 \rho^2 \ln \rho + \mathcal{O}_2 \rho^2 && \text{for } \Delta = 2, \end{aligned} \tag{6.2}$$

where ρ is the usual Fefferman-Graham coordinate (2.26) in the asymptotically AdS spacetime. In particular, examining eq. (2.32) for the fermionic mass operator, we see that there are additional counterterms proportional to $(\partial\lambda_3)^2$ and $R\lambda_3^2$, which play a role in backgrounds where λ_3 varies in time (and/or space). We note that this is completely analogous to placing the boundary theory in a curved background spacetime, which creates the necessity of including additional counterterms which are functionals of the background curvatures [40]. We also note that some of the new UV divergences, *e.g.*, those associated with the two counterterms above, are logarithmic in the cut-off scale and as a result, new scheme dependent ambiguities are inevitable in the renormalization procedure — we return to this issue below.

¹⁷We focus here on relevant operators (with $\Delta < 4$). We can also consider operators with $1 \leq \Delta < 2$ using the ‘alternate quantization’ of the holographic theory [39]. For these, the powers of ρ associated with the two coefficients are interchanged in eq. (6.2).

Through Einstein's equations (2.7), the bulk scalar backreacts on the geometry at least at the quadratic order and hence the renormalized boundary stress-energy tensor must depend on the (non-)normalizable coefficients of ϕ_Δ at least quadratically. Simple dimensional arguments imply that for a constant coupling the boundary stress-energy tensor (having dimension four) can always depend on the bilinear $\lambda_\Delta \mathcal{O}_\Delta$ for any Δ . This combination is seen to explicitly appear in the energy tensor and the pressure given in eqs. (2.36) and (2.46) for $\Delta = 3$ and 2 , respectively. Continuing these dimensional arguments for constant coupling, the stress tensor can also depend on

$$\begin{aligned} \lambda_\Delta^n & \quad \text{for } \Delta = 4 - \frac{4}{n} \text{ with } n = 2, 3, 4, \dots, \\ \mathcal{O}_\Delta^m & \quad \text{for } \Delta = \frac{4}{m} \text{ with } m = 2, 3, 4. \end{aligned} \tag{6.3}$$

For $\Delta = 2$ and 3 , the dependence as in (6.3) was indeed established in [24, 25] and can again be explicitly seen in eqs. (2.36) and (2.46).

Once λ_Δ depends on time, additional combinations involving time-derivatives of λ_Δ or \mathcal{O}_Δ can appear in boundary stress tensor, as long as the dependence has the correct mass-dimension four (and is at least quadratic in these coefficients). In particular, the stress tensor may depend on

$$\begin{aligned} \lambda_\Delta^{n-2} \partial_t \lambda_\Delta \partial_t \lambda_\Delta, \lambda_\Delta^{n-1} \partial_{tt}^2 \lambda_\Delta & \quad \text{for } \Delta = 4 - \frac{2}{n} \text{ with } n = 2, 3, 4, \dots, \\ \partial_t \mathcal{O}_\Delta \partial_t \mathcal{O}_\Delta, \mathcal{O}_\Delta \partial_{tt}^2 \mathcal{O}_\Delta & \quad \text{for } \Delta = 1. \end{aligned} \tag{6.4}$$

Here we have restricted our attention on relevant operators (with $\Delta < 4$). We also only consider the possibility of an even number of time-derivatives because otherwise the corresponding operator could not be extended to a covariant expression. Again, these additional terms are explicitly seen in eq. (2.36) for the $\Delta = 3$ operator. Further, as indicated by eq. (6.4), no such contributions appear in eq. (2.46) for $\Delta = 2$.

Returning to the possibility that rapid quenches may produce singular behaviour, the additional contributions to the boundary stress-energy tensor involving time derivatives of the couplings λ_Δ , as in eq. (6.4), should be worrisome. In particular, these terms suggest that instantaneous changes in the corresponding couplings will produce a singular response in the stress tensor. Alternatively, if such a singularity is to be avoided, the response of the normalizable coefficient \mathcal{O}_Δ should be 'finely correlated' to cancel the potential divergence, *e.g.*, through the contributions of the $\lambda_\Delta \mathcal{O}_\Delta$ terms. While in section 5, we saw that for both operators the specific profile of the leading

response was closely related to that for the coupling, *e.g.*, see eq. (5.1), we must reiterate that our perturbative calculations can not fully address the question of such a cancellation.

Of course, rapid quenches also displayed interesting (potentially divergent) scalings in the physical properties of the final state, *e.g.*, the energy density as shown in eqs. (5.9) and (5.31).¹⁸ These scalings do not depend on the derivatives of the couplings as we set $\partial_t \lambda_\Delta(t \rightarrow \pm\infty) \rightarrow 0$ to ensure that the system begins at equilibrium and eventually settles into a new equilibrium state. Rather these scalings can be associated with the behaviour of the expectation value of \mathcal{O}_Δ itself, as follows: Recall the basic observation that when the boundary theory has a time-varying coupling $\lambda_\Delta(t)$, the stress-energy tensor is not longer conserved, *i.e.*, see eqs. (2.38) and (2.48). Instead, the diffeomorphism Ward identity states that for our quenches:

$$\partial_t \mathcal{E} = \langle \mathcal{O}_\Delta \rangle \partial_t \lambda_\Delta. \quad (6.5)$$

That is, the time-variation of the coupling is performing work on a system. Of course, eq. (6.5) can be written in an integral form as

$$\mathcal{E}_f = \mathcal{E}_i + \int \langle \mathcal{O}_\Delta \rangle d\lambda_\Delta. \quad (6.6)$$

Since we only considered quenches where the change in the coupling was finite, the (divergent) scaling in this expression for fast quenches must come from $\langle \mathcal{O}_\Delta \rangle$.

From the above perspective, the integral appearing, *e.g.*, eq. (3.21) defining $a_{2,4}^\infty$ can be seen to describe the total work done on the system. In fact, in the subsequent expression for $\mathcal{E}_f/\mathcal{E}_i$ appearing in eq. (3.22), the extra constant terms cancel and so we recover precisely eq. (6.6), *i.e.*, an integral form of eq. (6.5). With respect to the comments above, recall that the leading scaling in the response was slightly stronger for fast quenches than that found for $a_{2,4}^\infty$. That is, the integral in eq. (6.6) tempers the scaling of the response to fast quenches, as was discussed in detail in section 5. We have made some preliminary steps towards extending our present work to quenches with a generic relevant (or marginal) operator with dimension Δ [29]. This work suggests that our previous results generalize in a simple fashion with

$$a_{2,4}^\infty \propto \begin{cases} \alpha^{-(2\Delta-4)}, & 2 < \Delta \leq 4, \\ \ln(1/\alpha), & \Delta = 2, \end{cases} \quad (6.7)$$

¹⁸As noted in section 5, the same scalings appear for the temperature, pressure and entropy density of the final state.

for fast quenches with $\alpha \ll 1$. Here we might note that the scaling above with $\Delta = 4$ matches that found in [13].

It is well-known that the renormalization procedure in QFT is scheme-dependent. In the context of gauge/gravity duality, such scheme-dependence manifests itself with the appearance of finite counterterms in the holographic renormalization. In this paper, we carefully enumerated all of the finite counterterms for the situation where the couplings for \mathcal{O}_2 and \mathcal{O}_3 vary in time (or space) for the mass-deformed version of $\mathcal{N} = 4$ SYM theory. It is worth noting that the scheme-dependence in holographic renormalization does not introduce any ambiguity in the diffeomorphism Ward identity (6.5) — see also eqs. (2.38) and (2.48). That is, in general, both the stress tensor and the expectation value $\langle \mathcal{O}_\Delta \rangle$ are scheme-dependent but these ambiguities cancel in eq. (6.5) and this Ward identity is still true as written in any scheme. This might be contrasted with the conformal Ward identity, where the scheme-dependent terms can make an explicit appearance, as shown in eqs. (2.40) and (2.50).

As our analysis showed, the number of scheme-dependent parameters introduced in renormalization of a general deformation (1.2) depends on the choice of Δ , the dimension of the operator. Specifically, we found three ambiguity coefficients in eq. (2.37) for $\Delta = 3$ and two such coefficients in eq. (2.47) for $\Delta = 2$.¹⁹ We would like to emphasize that these ambiguity coefficients are actually necessary to properly interpret the bulk gravitational data in the language of the boundary gauge theory. As a simple example, consider the case $\Delta = 2$ with a constant coupling. As illustrated in eq. (2.72), already to leading order in λ_2 in our high temperature expansion, the energy density and pressure of $\mathcal{N} = 4$ SYM plasma are modified by a term of the form $m_b^4 \ln T$ — see [25] for more discussion. Further, a similar term appears in the expectation value $\langle \mathcal{O}_2 \rangle$ as shown in eq. (2.75). To make sense of the $\ln T$, one has to introduce an arbitrary scale in the theory, as shown in eq. (2.72). The arbitrariness associated with the scale Λ is encoded in the arbitrariness of the scheme-dependent coefficient δ_1 in eq. (2.47). We note that the analogous δ_1 term in eq. (2.37) would produce a similar effect for $\Delta = 3$, *e.g.*, the energy density would be modified by a term proportional to $m_f^4 \ln T$, but clearly such contributions would only occur at quartic order in the high temperature expansion and so were not studied here.

Of course, the above example illustrates that the time variation of the couplings is

¹⁹Note that for the case $\Delta = 3$, this means there are two extra coefficients compared to renormalization of the theory with static couplings, while one extra coefficient appears for $\Delta = 2$.

not intrinsic to scheme-dependence appearing various natural ‘observables’. However, once we consider time-dependent couplings, one can expect new contributions to the energy density or pressure proportional to $\ln T$ with coefficients involving time-derivatives of the coupling λ_Δ . In particular, the latter must form dimension four operators and so can be read off from the first line of eq. (6.4). Hence there are precisely two such contributions for $\Delta = 3$:

$$(\partial_t \lambda_3)^2 \ln T, \quad \lambda_3 \partial_t^2 \lambda_3 \ln T. \quad (6.8)$$

As in static case, the proper interpretation of these $\ln T$ terms requires introduction of two new independent scales, Λ_2 and Λ_3 , as appear in eqs. (3.20) and (3.31). As shown in eq. (3.19), the ambiguity in the choice of these scales is then precisely accounted for with the two new scheme-dependent coefficients, δ_2 and δ_3 , appearing in the finite counterterms in eq. (2.37).

Of course, our description of quenches with \mathcal{O}_2 contains the same $\ln \frac{T}{\Lambda}$ ambiguity which appeared in the equilibrium thermodynamics. However, these quenches also contain a novel power law ambiguity arising from the finite counterterm proportional to $R^\gamma \phi$ in eq. (2.45). This counterterm contributes a term proportional to the dimension four operator $(p_{1,0}^l)'' \sim \partial_t^2 \lambda_2$ in the pressure, as shown in eqs. (3.45) and (3.56). However, this term carries a pre-factor $\Lambda_2^2 (m_b^0)^2 / T_i^4$ here. This makes this contribution novel in two respects: First of all, the renormalization scale Λ_2 appears with a power, rather than in a logarithm. Note that we are therefore free to set this scale to zero, which may be the most natural choice in this case. Second, this term carries a factor of $(m_b^0)^2 / T_i^2$ and so appears at first order in the high temperature expansion, in contrast to all of the other perturbative corrections, *e.g.*, in eq. (3.45) which are second order in this expansion. Hence (if $\Lambda_2 \neq 0$), this term formally dominates the behaviour of the pressure while the mass coupling λ_2 is varying. Here we might note that all of the new ambiguities discussed here only play a role while the couplings are varying. Hence, for example, they are not important after the coupling has achieved its final value but the system is still relaxing to its final equilibrium state. Further, they do not appear in expressions relating the properties of the final and initial equilibrium states, *e.g.*, in eq. (3.22).

In standard QFT, the scheme-dependence associated with choosing renormalization scales can typically be eliminated with a judicious choice of observables or by choosing a physical reference point. For example, calculating the overall vacuum energy density

in a QFT typically yields a result depending on some cut-off scale and so which is scheme-dependent. However, any excited stationary state has a definite energy as measured with respect to this vacuum energy. A similar strategy might be used in considering the thermal ensemble of the mass-deformed gauge theory with \mathcal{O}_2 . That is, we could choose a particular reference temperature $T_0 (\neq 0)$ and compare, *e.g.*, the energy density of a given thermal ensemble to that of the reference ensemble at T_0 . This prescription would then yield a result for the equilibrium energy density which is independent of the renormalization scale Λ ,

$$\tilde{\mathcal{E}}(T, T_0) \equiv \mathcal{E}(T) - \mathcal{E}(T_0) = \frac{3}{8}\pi^2 N^2 \left(T^4 - T_0^4 + \frac{m_b^4}{9\pi^4} \ln \frac{T}{T_0} \right). \quad (6.9)$$

Unfortunately, this approach does not extend naturally to quenches where the mass coupling varies in time. However, another strategy that is available, at least in this case of the dimension two operator, is to formulate a new scheme-independent observable by combining \mathcal{E} and $\langle \mathcal{O}_2 \rangle$. That is, although both of these quantities are individually scheme-dependent, as shown in eq. (3.45), the following combination is independent of both Λ_1 and Λ_2 :

$$\tilde{\mathcal{E}}(\tau) \equiv \mathcal{E}(\tau) + \frac{(m_b^0)^2}{\sqrt{6}} p_{1,0}^l(\tau) \langle \mathcal{O}_2(\tau) \rangle. \quad (6.10)$$

In particular, this scheme-independence extends to the situation where the mass coupling varies in time. However, it is not clear if this definition applies or can be extended to higher orders in the high temperature expansion. Further, it is not possible to extend this strategy to define scheme-independent pressure. Similarly, no such definitions of scheme-independent observables seem possible in the case of quenches with \mathcal{O}_3 .

Hence it seems like that situation here for the holographic QFT's with time dependent couplings is similar in many respects to QFT in curved spacetime [27]. In a generic background without any special symmetries, one simply finds that $\langle T_{ij} \rangle$ is ambiguous. In this context, an 'axiomatic' approach has been developed in which general physically reasonable properties are imposed on the renormalized stress-energy tensor, without reference to any particular renormalization techniques [27,41,42]. Three of these conditions would naturally carry over to a general discussion of quenches, or more generally time-dependent couplings, in QFT. Namely, the conditions related to causality, finite matrix elements for orthogonal states and recovering standard results in Minkowski space or here in the limit of time-independent couplings [41]. The first condition, however, was covariant conservation of the stress tensor and in the present context

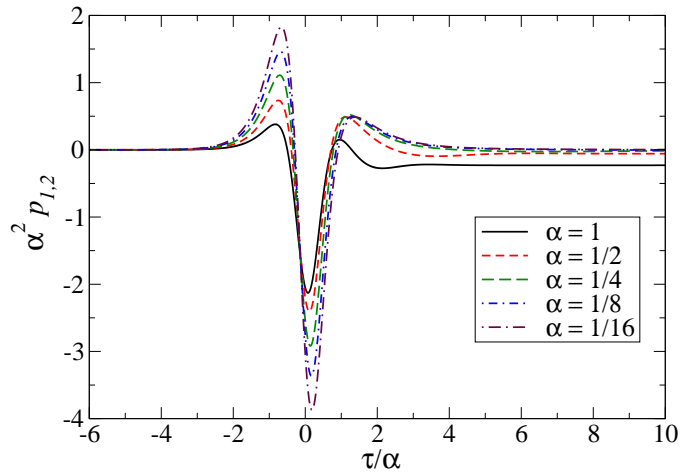


Figure 16: (Colour online) The evolution of the α -rescaled normalizable component, $\alpha^2 p_{1,2}$, as a function of τ/α during quenches with the profile given in eq. (6.11) with different values of α .

this would have to be changed to incorporate work terms induced by the time-varying couplings, as found in eqs. (2.38) and (2.48). We re-iterate that the latter were diffeomorphism Ward identities, which naturally appear without any scheme-dependence in the present holographic renormalization. We might add that the appearance of scheme-dependent contributions in the trace anomaly is not resolved by the axiomatic approach discussed above [42] and this feature is also evident in the present holographic analysis with eqs. (2.40) and (2.50).

Given the ambiguities in the observables, \mathcal{E} , \mathcal{P} and $\langle \mathcal{O}_\Delta \rangle$, we demonstrate that some care must be taken in defining the excitation and equilibration times. As an example, we focus on the equilibration time for quenches with \mathcal{O}_3 and consider a profile of the mass coupling which given by

$$p_{1,0} = \left(\frac{1}{2} + \frac{1}{2} \tanh \frac{\tau}{\alpha} \right) \left(1 + \frac{1}{1 + \frac{\tau^2}{\alpha^2}} \right). \quad (6.11)$$

With this profile, there is still an exponential turn on of the coupling at early times but the approach to the final equilibrium value is now controlled by a power law, *i.e.*, $p_{1,0} \simeq 1 + \frac{\alpha^2}{\tau^2} + \dots$ as $\tau \rightarrow +\infty$. Fig. 16 shows the response of the normalizable component $p_{1,2}$ in these quenches for select values of $\alpha = \{1, \frac{1}{2}, \frac{1}{4}, \frac{1}{8}, \frac{1}{16}\}$. If we use

the same definitions as before, *i.e.*, eqs. (5.13), (5.14) and (5.16), the results for the equilibration time scale are essentially unchanged. That is, $\tau_{eq} \sim 1$ or $t_{eq} \sim 1/T_i$ and for $\tau \gtrsim \tau_{eq}$, $p_{1,2}$ follows the adiabatic response (4.13).²⁰ Now we may also consider defining the equilibration time scale $\tau_{eq}^{\mathcal{O}}$ directly in terms of a more physical quantity such as the expectation value of \mathcal{O}_3 — similar remarks would apply using \mathcal{E} or \mathcal{P} below. That is, we would replace our previous definitions with

$$\delta_{neq}^{\mathcal{O}}(\tau) \equiv \left| \frac{\mathcal{O}_3(\tau) - \mathcal{O}_3^{adiabatic}(\tau)}{\mathcal{O}_3^{equilibrium}} \right|, \quad (6.12)$$

where

$$\mathcal{O}_3^{equilibrium} = \lim_{\tau \rightarrow +\infty} \mathcal{O}_3(\tau) = \frac{\Gamma(3/4)^4}{2\sqrt{2}\pi^2} N^2 T_i^2 m_f^0. \quad (6.13)$$

Then the equilibration time $\tau_{eq}^{\mathcal{O}}$ would be defined as the latest time at which $\delta_{neq}^{\mathcal{O}}$ exceeds some threshold, *i.e.*, $\delta_{neq}^{\mathcal{O}}(\tau > \tau_{eq}^{\mathcal{O}}) < \epsilon$. Unfortunately, this approach would lead to ambiguous results because of the scheme-dependent contribution in the expression for \mathcal{O}_3 given in eq. (3.20). In particular, we find

$$\delta_{neq}^{\mathcal{O}}(\tau) \Big|_{ambiguity} \propto p_{1,0}'' \ln \frac{\pi T_i}{\Lambda_2} \sim \frac{\alpha^2}{\tau^4} \ln \frac{\pi T_i}{\Lambda_2} \sim \left(\frac{\tau_{eq}}{\tau} \right)^4 \alpha^2 \ln \frac{\pi T_i}{\Lambda_2}, \quad (6.14)$$

where τ_{eq} is the previously defined equilibration time. This ambiguity could substantially affect the computation of the relaxation time $\tau_{eq}^{\mathcal{O}}$ (*i.e.*, making it longer than the thermal time scale) if the renormalization scheme is such that

$$\alpha^2 \ln \frac{\pi T_i}{\Lambda_2} \gg 1. \quad (6.15)$$

Of course, one may regard the real source of the issue here to be the power law behaviour of the profile (6.11) at late times. The latter was introduced precisely to enhance the importance of the scheme-dependent terms in eq. (3.20), as these issues would not have occurred with the exponential fall-off of the original profile (4.1). Still this example stands as a cautionary note in studying the excitation and equilibration times in generic time-dependent settings.

Further it is interesting that, in some cases, the renormalization scheme ambiguities can be used to remove the divergent scaling behaviour appears in the one-point correlators because of the rapid variation of the couplings in these observables.²¹ Consider

²⁰We also explicitly checked that the essentially same QNM behaviour occurs for these quenches (6.11) as shown in fig. 8.

²¹These divergences should be distinguished from that in the expectation value of the corresponding operator \mathcal{O}_Δ , as discussed above.

a quench of \mathcal{O}_3 where the coupling λ_3 exhibits a power law growth in the vicinity of $t \geq 0$ with

$$\lambda_3(t) = t^\beta, \quad 0 < \beta < 1. \quad (6.16)$$

From eq. (2.36), we can see that for generic values of the scheme-dependent coefficients δ_2 and δ_3 , the observables of the theory would diverge as $t \rightarrow 0$. The divergence introduced by the time variation of the coupling $p_0 \propto \lambda_3$ is given by

$$\begin{aligned} 8\pi G_5 \mathcal{E} \Big|_{\text{coupling-divergence}} &= -\frac{1}{12}(p'_0)^2 + \frac{1}{3}p_0 p''_0 + \frac{1}{2}\delta_2(p'_0)^2 \\ &\propto t^{2(\beta-1)}(3\beta - 4 + 6\beta\delta_2), \\ 8\pi G_5 \mathcal{P} \Big|_{\text{coupling-divergence}} &= -\frac{1}{36}(p'_0)^2 - \frac{1}{18}p_0 p''_0 - 2\delta_3(p'_0)^2 - 2\delta_3 p_0(p''_0) + \frac{1}{2}\delta_2(p'_0)^2 \\ &\propto t^{2(\beta-1)}(-144\delta_3\beta + 72\delta_3 - 3\beta + 2 + 18\delta_2\beta), \\ 16\pi G_5 \langle \mathcal{O}_3 \rangle \Big|_{\text{coupling-divergence}} &= \frac{1}{2}p''_0 + 2\delta_2 p''_0 \propto t^{\beta-2}(1 + 4\delta_2). \end{aligned} \quad (6.17)$$

Here again, without loss of generality, we have set $a_1 = 0$. Hence by choosing

$$\delta_2 = -\frac{1}{2} + \frac{2}{3\beta}, \quad \delta_3 = \frac{7 - 6\beta}{36(2\beta - 1)}, \quad (6.18)$$

we would remove the divergences in the energy density and the pressure. However, the expectation value of the operator \mathcal{O}_3 would still be divergent. Alternatively, one can remove these coupling-induced divergences in the pressure and $\langle \mathcal{O}_3 \rangle$, with the energy density remaining divergent as $t \rightarrow 0$. Presumably, this example illustrates that it is more useful to consider the scaling behaviour of observables characterizing the final equilibrium state.

Our analysis revealed that for rapid quenches with $\mathcal{T}T_i \ll 1$, the system relaxes, almost universally, on thermal scales $\sim 1/T_i$ — see eqs. (5.23) and (5.38). Such a response might be an artifact of our treatment of the quenches perturbatively in the amplitude of the coupling, effectively about its zero value. It would be interesting to study the full nonlinear problem where not only the rate change of the coupling but also the amplitude of the coupling (and its variation over the history of a quench) can be arbitrary. From figs. 2 and 9, it is clear that even though the relaxation time scale for fast quenches of λ_3 and λ_2 couplings is roughly the same, the amplitude of the response due to quenches of λ_3 is quadratically enhanced (in the rate of change) compared to that for quenches of λ_2 . In this sense, the quenches due to \mathcal{O}_3 operator

more closely follow the intrinsic time-scale of its coupling. Given our perturbative analysis of the quenches here, we could treat quenches due to λ_2 and λ_3 separately. It would be interesting to study “supersymmetric” quenches with

$$\lambda_2(t) = \lambda_3(t)^2, \quad (6.19)$$

which would necessarily require a full nonlinear analysis.

Another regime of the quenches which exhibited interesting universal behaviour was $\alpha \gg 1$, corresponding to slow nearly adiabatic quenches. Recall that for fast quenches ($\alpha \ll 1$), the normalizable mode of the bulk scalar relaxes to its final equilibrium with a quasinormal mode behaviour, *e.g.*, see figs. 8 and 15. In contrast, the relaxation in the nearly adiabatic regime occurs without excitation of any quasinormal modes. Rather for $\alpha \gtrsim 1$, the deviation from the purely adiabatic evolution in eq. (4.13) is governed entirely by derivatives of the source profile, *e.g.*, $\alpha \partial_\tau p_{1,0}(\tau/\alpha)$ for \mathcal{O}_3 quenches or by $\alpha \partial_\tau p_{1,0}^l(\tau/\alpha)$ for \mathcal{O}_2 quenches. Indeed, in either case with an arbitrary source $p_0 = p_0(\tau/\alpha)$ and $\alpha \gg 1$, we can solve the bulk scalar wave equation (3.3) perturbatively in $1/\alpha$:

$$\phi_1 = p_0(\tau/\alpha) \phi_1^e(\rho) + \sum_{n=1}^{\infty} \alpha^{-n} \phi_1^{(n)}(\tau/\alpha, \rho), \quad (6.20)$$

where $\phi_1^e(\rho)$ is the equilibrium solution normalized such that the leading coefficient in the asymptotic expansion is one. For example, for the $m^2 = -3$ scalar, the latter would be the solution given in eq. (2.55) divided by a factor of $\lambda\mu$. Now for $n = 1$, we find

$$\phi_1^{(1)}(\tau/\alpha, \rho) = \alpha \partial_\tau p_0(\tau/\alpha) g^{(1)}(\rho), \quad (6.21)$$

where $g^{(1)}$ satisfies the inhomogeneous equation

$$-\frac{1}{2}(1 - \rho^4) \partial_{\rho\rho}^2 g^{(1)} + \frac{3 + \rho^4}{2\rho} \partial_\rho g^{(1)} + \frac{m^2}{2\rho^2} g^{(1)} = \frac{3}{2\rho} \phi_1^e - \partial_\rho \phi_1^e. \quad (6.22)$$

Similarly, successively higher derivatives of p_0 appear at higher orders in this expansion. Hence the entire dynamics of the linearized solution is simply governed by the nearly adiabatic driving source.

Quantum quenches from a thermal initial state were discussed previously in [5]. The major difference between this seminal study and our present analysis is that we are considering a strongly coupled field theory while the authors of [5] investigated

quantum quenches of a free scalar field. Effectively, the momentum modes in the latter theory reduce to a collection of decoupled simple harmonic oscillators (SHO's). In [5], it was shown that a(n instantaneous) quench of an individual SHO from an initial frequency ω_i and temperature T_i to a final frequency ω_f results in an effective thermal final state with temperature T_f

$$T_f = \frac{1}{2} \left(1 + \frac{\omega_f^2}{\omega_i^2} \right) T_i, \quad \text{for} \quad T_i \gg \omega_i. \quad (6.23)$$

A striking result here is that if we also choose $\omega_f \ll \omega_i$, then the final temperature is one-half the initial temperature. Quite generally, $\omega_f < \omega_i$ results in $T_f < T_i$, *i.e.*, the system cools! A similar cooling effect was found for quenches of the mass in the field theory where $T_i \gg m_i \gg m_{fin}$, using an effective temperature determined by averaging over all of the momentum modes. In fact, $T_f = T_i/2$ was found for such quenches in $d = 2$ and 3. However, in $d = 4$, the effective temperature was dominated by high momentum modes and they found $T_f = T_i$.

Recall that our analysis also applies to the same high temperature regime, *e.g.*, $T_i \gg m_{f,b}^0$. Hence it is interesting to compare the above results to those for our quenches from the massive gauge theory to the CFT, in which case we also satisfy $m_i \gg m_{fin}$. The expressions for T_f/T_i are given in eqs. (3.33) and (3.58) for these quenches with \mathcal{O}_3 and \mathcal{O}_2 , respectively. Recall that in section 3, we argued that $a_{2,4}^\infty \sim 0$ for $\alpha \gg 1$ — see the discussion around eqs. (3.26) and (3.51) — and hence it is clear that these quenches are indeed cooling the system provided the transition was sufficiently slow. However, as the characteristic time scale of a quench becomes shorter than a typical thermal scale $1/T_i$, we also saw that $a_{2,4}^\infty$ grows large and so the corresponding quenches always result in an increase of the temperature. The precise thresholds between the cooling and heating regimes are given in eqs. (5.6) and (5.29). Of course, since our analysis applies for the high temperature regime, any changes in the temperature are perturbatively small in $m_{b,f}^0/T_i$ and so much like the result of [5] for $d = 4$, we have $T_f \simeq T_i$ to leading order. Hence we may conclude that the thermal quenches studied in [5] for a free field and those studied here for a strongly interacting QFT share certain similar features. Of course, we pointed out above that for fast quenches, the behaviour of these two systems is qualitatively dissimilar.

We would like to contrast our framework with previous analytic investigations using the AdS-Vaidya solution [10]. These studies investigated issues related to thermalization of a holographic plasma by considering the gravitational collapse of a thin shell

of ‘null dust’. Of course, the latter scenarios might also be regarded as a holographic quantum quenches. However, we would note that by design, the null dust does not excite any local gravitational degrees of freedom, in particular, on the horizon. For example, the spacetime becomes that of a static black hole immediately beyond the boundary where the bulk stress tensor goes to zero. In the dual description then, this scenario injects energy into the gauge theory with an ‘exotic’ probe which does not excite any of the local degrees of freedom in the holographic plasma. Hence this approach may be useful to study questions related to the formation and growth of the horizon, however, it can not address many aspects of the holographic quench. For example, it does not reveal the scaling behaviour of the response or the quasinormal response of the horizon. Our analysis indicates that both of these features play an important role in the equilibration of the system. It is interesting that the Vaidya solutions seem to be a good approximation to a quench induced with a massless bulk scalar in a small amplitude expansion [9], similar to that used in our analysis. The analytic approach of [9] also allows one to systematically improve the gravitational description within this expansion.

There are numerous aspects of the holographic quenches described here that are left for future analysis. First and foremost, we would like to extend our perturbative treatment to a full nonlinear analysis of the gravitational equations of motion. However, let us outline a few other potentially interesting extensions:

- In this paper, we only considered the response as measured by a few simple one-point correlators. These are representatives of *local* physical observables in the holographic theory. An open question remains to analyze the behaviour, in particular the relaxation, of *non-local* physical observables, such as higher-point correlation functions, Wilson lines or entanglement entropy. Previous studies [10] indicate that these non-local observables equilibrate more slowly than the local observables and so it will be interesting to see if this effect persists in the present framework which accounts the full quasinormal response of the horizon.
- Our present analysis was restricted to quenches which are spatially isotropic and homogeneous. As a result, we eliminated²² some of the potentially important relaxation channels of the system, namely, the sound and the shear modes in off-equilibrium gauge theory plasma. In a more general anisotropic or inhomogeneous quench where such modes are excited, one may expect that the hydrodynamic modes will have much

²²We would like to thank Rob Leigh for raising this issue.

slower decay rates than the quasinormal modes of the bulk scalar found in the present work. Inevitably then, these new modes would dominate the late-time behaviour of the system, however, their influence on the equilibration time would still depend on how efficiently they are produced during the quench. We defer the consideration such inhomogeneous quenches to future work.

- We focused on the properties of the energy density and the pressure of gauge theory plasma undergoing a quench. We pointed out that both of these observables are renormalization scheme dependent. It is interesting to address the question of ambiguities in the entropy density away from equilibrium [43]. In particular then, it would be interesting to explore how a choice of a renormalization scheme affects the definition of the entropy density.

Acknowledgments

We would like to thank Colin Denniston, Carlos Hoyos, Romuald Janik, Pavel Kovtun, Sung-Sik Lee, Rob Leigh, Jorma Louko, David Mateos, Anton van Niekerk, João Penedones, Eric Poisson, Misha Smolkin and Toby Wiseman for useful discussions. Research at Perimeter Institute is supported by the Government of Canada through Industry Canada and by the Province of Ontario through the Ministry of Research & Innovation. AB, LL and RCM gratefully acknowledge support from NSERC Discovery grants. Research by LL and RCM is further supported by funding from the Canadian Institute for Advanced Research.

A Discretization of the evolution equation

We describe here the basic strategy employed to discretize the evolution equation. The schematic structure of such equation, for a field $f(\tau, \rho)$, takes the form:

$$0 = \partial_{\tau\rho} f - A_{\rho\rho} \partial_{\rho\rho}^2 f - A_{\tau} \partial_{\tau} f + A_{\rho} \partial_{\rho} f + A_0 f + J_0, \quad (\text{A.1})$$

for suitably defined multiplicative factors A_{\dots} , and a source term J_0 , all explicit functions of (τ, ρ) . Notice the principal part of the system, *i.e.*,

$$0 = (\partial_{\tau\rho} - A_{\rho\rho} \partial_{\rho\rho}^2) f, \quad (\text{A.2})$$

is a second order partial differential equation admitting two propagating modes. One of them has a characteristic speed given by $A_{\rho\rho}$ while the other propagates instantly

inwards from the boundary (a consequence of having chosen incoming characteristics to foliate the spacetime). Further, notice that for a scenario with a black hole present from the start, as is the case for our studies here, $A_{\rho\rho} > 0$ (< 0) outside (inside) the horizon. Thus *only one boundary condition* can be prescribed at the AdS boundary.

A natural strategy to discretize the system, taking advantage of the characteristic structure explicitly displayed by equation (A.1), has been presented in [44] (and further extended in [45] to include dissipation and in [46] to allow for adaptive meshes). In our implementation, we follow this approach to obtain a second order accurate implementation in the following way. We introduce a uniform discrete spatial grid covering the domain $\rho \in [0, L_\rho]$ with $N_\rho + 1$ points located at $\rho_i = (i - 1)d\rho$ ($d\rho \equiv L_\rho/(N_\rho)$). Discrete, evenly spaced, time levels are introduced as $\tau_n = \tau_o + (n - 1)d\tau$ (with $d\tau = \alpha d\rho$). The continuous function $f(\tau, \rho)$ is then represented by values on this grid structure as $f(\tau_n, \rho_i) \equiv f_i^n$. Only two time levels are required for discretizing our target equation as follows. Consider f is known at level n , *i.e.*, all values f_i^n are known, as well as those at level $n + 1$ for $\rho < \rho_i$, to obtain the value of f_i^{n+1} a centered discretization at the virtual point $(n + 1/2, i - 1/2)$ is achieved by discretizing the terms involved as,

$$\partial_{\tau\rho} f|_i^{n+1/2} = \frac{f_i^{n+1} - f_{i-1}^{n+1} - f_i^n + f_{i-1}^n}{d\rho d\tau}, \quad (\text{A.3})$$

$$\partial_\rho^2 f|_i^{n+1/2} = \frac{f_i^{n+1} - f_{i-1}^{n+1} + f_{i-1}^{n+1} + f_{i+1}^n - 2f_i^n + f_{i-1}^n}{2d\rho^2}, \quad (\text{A.4})$$

$$\partial_\tau f|_i^{n+1/2} = \frac{f_i^{n+1} + f_{i-1}^{n+1} - f_i^n - f_{i-1}^n}{2d\tau}, \quad (\text{A.5})$$

$$\partial_\rho f|_i^{n+1/2} = \frac{f_i^{n+1} - f_{i-1}^{n+1} + f_i^n - f_{i-1}^n}{2d\rho}, \quad (\text{A.6})$$

$$f|_i^{n+1/2} = \frac{f_{i-1}^{n+1} + f_i^n}{2}. \quad (\text{A.7})$$

The coefficients $A_{..}$ and the source J_0 are evaluated analytically at the virtual point. Plugging these expressions into the equation and solving for f_i^{n+1} defines the scheme employed. Notice the resulting scheme is thus an inwards “marching” algorithm that provides the value of f_i^{n+1} . Further the “slanted” nature of this scheme (*i.e.*, the forward offset of the second derivative at level n) is simply a reflection of the characteristic structure of the system. Since initial data is given at an initial hypersurface, and boundary conditions at $\rho_1 = 0$, this scheme suffices to integrate all points with the

exception of $\rho_2, \rho_{N_{\rho+1}}$ where the simple change,

$$\partial_\rho^2 f|_2^{n+1/2} = \frac{f_3^n - 2f_2^n + f_1^n}{d\rho^2}, \quad (\text{A.8})$$

$$\partial_\rho^2 f|_{N_{\rho+1}}^{n+1/2} = \frac{f_{N_{\rho+1}}^{n+1} - f_{N_\rho}^{n+1} + f_{N_{\rho-1}}^{n+1} + f_{N_{\rho+1}}^n - 2f_{N_\rho}^n + f_{N_{\rho-1}}^n}{2d\rho^2}, \quad (\text{A.9})$$

suffices to provide a first accurate order approximation which does not affect the overall second order convergence of the solution.

We specify the characteristic initial data $f^{initial}(\rho)$ at initial time $\tau = \tau_1$:

$$f(\tau = \tau_1, \rho) = f^{initial}(\rho), \quad (\text{A.10})$$

and the boundary data $f^{boundary}$ at $\rho_1 = 0$,

$$f(\tau, \rho = \rho_1) = f^{boundary}(\tau). \quad (\text{A.11})$$

As a representative test of the code's convergence behaviour, we consider the bosonic case and obtain solutions for different grid sizes $N_\rho = 2^p \times 100$ ($p = 0, \dots, 4$) and simulate the system until equilibration. We monitor the (L_2 norm of the) difference of solutions with successive values of p (defining $e_p \equiv \|\phi_{p+1} - \phi_p\|_2$) as well as the convergence rate q calculated as,

$$2^q = \frac{\|\phi_{p+1} - \phi_p\|_2}{\|\phi_{p+2} - \phi_{p+1}\|_2} = \frac{e_p}{e_{p+1}}. \quad (\text{A.12})$$

The results are shown in figure 17, the left panel illustrates how e_p decreases as the resolution is improved while the right one the convergence rate q illustrating second order convergence behaviour.

As a last remark, we stress that in the general case metric variables governed by an evolution equation (*e.g.*, Σ determined by eq. (2.14)) can be integrated using the same strategy described above. Thus, this algorithm together with straightforward integration along the radial direction (*e.g.*, for A determined by eq. (2.15)) suffice for implementing the complete system provided consistent boundary conditions are provided at the boundary. For other strategies see [13] (employing also a characteristic formulation of the equations) and [16, 18]) (for works implementing a Cauchy formulation).

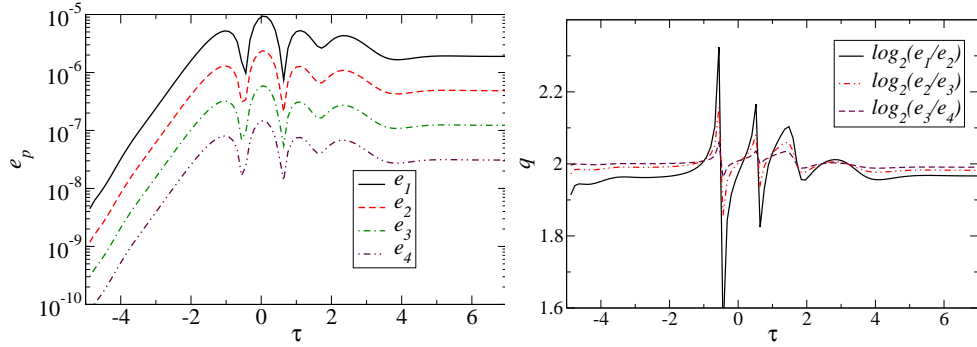


Figure 17: (Colour online) Convergence tests. (Left panel) L_2 norm of the difference between solutions obtained halving the discretization length. (Right panel) Estimated convergence rate from the numerical solution, indicating the numerical solution indeed converges to second order as expected.

References

- [1] L. D. Landau and E. M. Lifshitz, *Quantum Mechanics*, Course of Theoretical Physics, Volume 3, 1989.
- [2] C. Itzykson and J. B. Zuber, *Quantum field theory*, McGraw-Hill International Book Co., 1980.
- [3] For example, see the following reviews:
 - S. Mondal, D. Sen and K. Sengupta, “Non-equilibrium dynamics of quantum systems: order parameter evolution, defect generation, and qubit transfer,” arXiv:0908.2922;
 - J. Dziarmaga, “Dynamics of a quantum phase transition and relaxation to a steady state,” *Adv. Phys.* **59**, 1063 (2010) [arXiv:0912.4034 [cond-mat.quant-gas]];
 - A. Polkovnikov, K. Sengupta, A. Silva and M. Vengalattore, “Nonequilibrium dynamics of closed interacting quantum systems,” *Rev. Mod. Phys.* **83**, 863 (2011) [arXiv:1007.5331 [cond-mat.stat-mech]];
 - A. Lamacraft and J.E. Moore, “Potential insights into non-equilibrium behavior from atomic physics,” arXiv:1106.3567.
- [4] P. Calabrese and J. L. Cardy, “Evolution of entanglement entropy in one-dimensional systems,” *J. Stat. Mech.* **0504**, P04010 (2005) [cond-mat/0503393];

- P. Calabrese and J. L. Cardy, “Time-dependence of correlation functions following a quantum quench,” *Phys. Rev. Lett.* **96**, 136801 (2006) [cond-mat/0601225];
- P. Calabrese and J. Cardy, “Quantum Quenches in Extended Systems,” *J. Stat. Mech.* **0706**, P06008 (2007) [arXiv:0704.1880 [cond-mat.stat-mech]];
- S. Sotiriadis and J. Cardy, “Quantum quench in interacting field theory: A Self-consistent approximation,” *Phys. Rev. B* **81**, 134305 (2010) [arXiv:1002.0167 [quant-ph]];
- S. Sotiriadis and J. Cardy, “Inhomogeneous Quantum Quenches,” *J. Stat. Mech.* P11003 (2008) [arXiv:0808.0116 [cond-mat.stat-mech]].
- [5] S. Sotiriadis, P. Calabrese and J. Cardy, “Quantum quench from a thermal initial state,” *EPL* **87**, 20002 (2009) [arXiv:0903.0895v2 [cond-mat.stat-mech]].
- [6] J. M. Maldacena, “The large N limit of superconformal field theories and supergravity,” *Adv. Theor. Math. Phys.* **2**, 231 (1998) [*Int. J. Theor. Phys.* **38**, 1113 (1999)] [arXiv:hep-th/9711200];
- O. Aharony, S. S. Gubser, J. M. Maldacena, H. Ooguri and Y. Oz, “Large N field theories, string theory and gravity,” *Phys. Rept.* **323**, 183 (2000) [arXiv:hep-th/9905111].
- [7] S. R. Das, T. Nishioka and T. Takayanagi, “Probe Branes, Time-dependent Couplings and Thermalization in AdS/CFT,” *JHEP* **1007**, 071 (2010) [arXiv:1005.3348 [hep-th]];
- P. Basu and S. R. Das, *JHEP* **1201**, 103 (2012) [arXiv:1109.3909 [hep-th]];
- S. R. Das, “Holographic Quantum Quench,” *J. Phys. Conf. Ser.* **343**, 012027 (2012) [arXiv:1111.7275 [hep-th]].
- [8] U. H. Danielsson, E. Keski-Vakkuri and M. Kruczenski, “Spherically collapsing matter in AdS, holography, and shellons,” *Nucl. Phys. B* **563**, 279 (1999) [hep-th/9905227];
- U.H. Danielsson, E. Keski-Vakkuri and M. Kruczenski, “Black hole formation in AdS and thermalization on the boundary,” *JHEP* **0002**, 039 (2000) [hep-th/9912209];
- S.B. Giddings and S.F. Ross, “D3-brane shells to black branes on the Coulomb branch,” *Phys. Rev. D* **61**, 024036 (2000) [hep-th/9907204];

- S. B. Giddings and A. Nudelman, “Gravitational collapse and its boundary description in AdS,” JHEP **0202**, 003 (2002) [hep-th/0112099].
- [9] S. Bhattacharyya and S. Minwalla, “Weak Field Black Hole Formation in Asymptotically AdS Spacetimes,” JHEP **0909**, 034 (2009) [arXiv:0904.0464 [hep-th]].
- [10] J. Abajo-Arrastia, J. Aparicio and E. Lopez, “Holographic Evolution of Entanglement Entropy,” JHEP **1011**, 149 (2010) [arXiv:1006.4090 [hep-th]];
T. Albash and C. V. Johnson, “Evolution of Holographic Entanglement Entropy after Thermal and Electromagnetic Quenches,” New J. Phys. **13**, 045017 (2011) [arXiv:1008.3027 [hep-th]];
H. Ebrahim and M. Headrick, “Instantaneous Thermalization in Holographic Plasmas,” arXiv:1010.5443 [hep-th];
V. Balasubramanian *et al.*, “Thermalization of Strongly Coupled Field Theories,” Phys. Rev. Lett. **106**, 191601 (2011) [arXiv:1012.4753 [hep-th]];
V. Balasubramanian *et al.*, “Holographic Thermalization,” Phys. Rev. D **84**, 026010 (2011) [arXiv:1103.2683 [hep-th]];
V. Balasubramanian, A. Bernamonti, N. Copland, B. Craps and F. Galli, “Thermalization of mutual and tripartite information in strongly coupled two dimensional conformal field theories,” Phys. Rev. D **84**, 105017 (2011) [arXiv:1110.0488 [hep-th]];
J. Aparicio and E. Lopez, “Evolution of Two-Point Functions from Holography,” JHEP **1112**, 082 (2011) [arXiv:1109.3571 [hep-th]];
A. Allais and E. Tonni, “Holographic evolution of the mutual information,” JHEP **1201**, 102 (2012) [arXiv:1110.1607 [hep-th]];
V. Keranen, E. Keski-Vakkuri and L. Thorlacius, “Thermalization and entanglement following a non-relativistic holographic quench,” Phys. Rev. D **85**, 026005 (2012) [arXiv:1110.5035 [hep-th]];
D. Galante and M. Schvellinger, “Thermalization with a chemical potential from AdS spaces,” arXiv:1205.1548 [hep-th];
E. Caceres and A. Kundu, “Holographic Thermalization with Chemical Potential,” arXiv:1205.2354 [hep-th].
- [11] R. A. Janik and R. B. Peschanski, “Gauge/gravity duality and thermalization of a boost-invariant perfect fluid,” Phys. Rev. D **74**, 046007 (2006) [hep-th/0606149];

- R. A. Janik, “Viscous plasma evolution from gravity using AdS/CFT,” *Phys. Rev. Lett.* **98**, 022302 (2007) [hep-th/0610144].
- [12] S. Lin and E. Shuryak, “Toward the AdS/CFT Gravity Dual for High Energy Collisions. 3. Gravitationally Collapsing Shell and Quasiequilibrium,” *Phys. Rev. D* **78**, 125018 (2008) [arXiv:0808.0910 [hep-th]].
- [13] P.M. Chesler and L.G. Yaffe, “Horizon formation and far-from-equilibrium isotropization in supersymmetric Yang-Mills plasma,” *Phys. Rev. Lett.* **102**, 211601 (2009). [arXiv:0812.2053 [hep-th]].
- [14] P. M. Chesler and L. G. Yaffe, “Boost invariant flow, black hole formation, and far-from-equilibrium dynamics in $N = 4$ supersymmetric Yang-Mills theory,” *Phys. Rev. D* **82**, 026006 (2010) [arXiv:0906.4426 [hep-th]].
- [15] D. Garfinkle and L. A. Pando Zayas, “Rapid Thermalization in Field Theory from Gravitational Collapse,” *Phys. Rev. D* **84**, 066006 (2011) [arXiv:1106.2339 [hep-th]];
D. Garfinkle, L. A. Pando Zayas and D. Reichmann, “On Field Theory Thermalization from Gravitational Collapse,” *JHEP* **1202**, 119 (2012) [arXiv:1110.5823 [hep-th]].
- [16] H. Bantilan, F. Pretorius and S. S. Gubser, “Simulation of Asymptotically AdS5 Spacetimes with a Generalized Harmonic Evolution Scheme,” arXiv:1201.2132 [hep-th].
- [17] M. P. Heller, D. Mateos, W. van der Schee and D. Trancanelli, “Strong coupling isotropization simplified,” arXiv:1202.0981 [hep-th].
- [18] M.P. Heller, R.A. Janik and P. Witaszczyk, “A numerical relativity approach to the initial value problem in asymptotically Anti-de Sitter spacetime for plasma thermalization – an ADM formulation,” arXiv:1203.0755 [hep-th].
- [19] J. Bhaseen, B. Simons, j. Sonner, J. Gauntlett and T. Wiseman, “Quenches in Holographic Superconductors,” in preparation (see: <http://pirsa.org/12060027/>).
- [20] K. Pilch and N. P. Warner, “ $N=2$ supersymmetric RG flows and the IIB dilaton,” *Nucl. Phys. B* **594**, 209 (2001) [hep-th/0004063];

- A. Khavaev, K. Pilch and N. P. Warner, “New vacua of gauged N=8 supergravity in five-dimensions,” *Phys. Lett. B* **487**, 14 (2000) [hep-th/9812035].
- [21] A. Buchel, A.W. Peet and J. Polchinski, “Gauge dual and noncommutative extension of an N = 2 supergravity solution,” *Phys. Rev. D* **63**, 044009 (2001) [arXiv:hep-th/0008076].
- [22] N.J. Evans, C.V. Johnson and M. Petrini, “The Enhanced and N=2 gauge theory: Gravity RG flows,” *JHEP* **0010**, 022 (2000) [hep-th/0008081].
- [23] A. Buchel and J.T. Liu, “Thermodynamics of the N=2* flow,” *JHEP* **0311**, 031 (2003) [hep-th/0305064].
- [24] A. Buchel, “N = 2* hydrodynamics,” *Nucl. Phys. B* **708**, 451 (2005) [arXiv:hep-th/0406200].
- [25] A. Buchel, S. Deakin, P. Kerner and J. T. Liu, “Thermodynamics of the N=2* strongly coupled plasma,” *Nucl. Phys. B* **784**, 72 (2007) [hep-th/0701142].
- [26] C. Hoyos, S. Paik and L. G. Yaffe, “Screening in strongly coupled N=2* supersymmetric Yang-Mills plasma,” *JHEP* **1110**, 062 (2011) [arXiv:1108.2053 [hep-th]].
- [27] N. D. Birrell and P. C. W. Davies, *Quantum Fields In Curved Space*, Cambridge, UK: University Press (1982) 340p.
- [28] S. Bhattacharyya, V. E. Hubeny, S. Minwalla and M. Rangamani, “Nonlinear Fluid Dynamics from Gravity,” *JHEP* **0802**, 045 (2008) [arXiv:0712.2456 [hep-th]];
V. E. Hubeny, S. Minwalla and M. Rangamani, “The fluid/gravity correspondence,” arXiv:1107.5780 [hep-th].
- [29] A. Buchel, L. Lehner, R.C. Myers and A. van Niekerk, work in progress.
- [30] C. Fefferman and C. R. Graham, “Conformal Invariants,” in *Elie Cartan et les Mathématiques d’aujourd’hui (Astérisque, 1985)* 95;
C. Fefferman and C. R. Graham, “The Ambient Metric,” arXiv:0710.0919 [math.DG].
- [31] M. Bianchi, D. Z. Freedman and K. Skenderis, “Holographic renormalization,” *Nucl. Phys. B* **631**, 159 (2002) [arXiv:hep-th/0112119];

- M. Bianchi, D. Z. Freedman and K. Skenderis, “How to go with an RG flow,” JHEP **0108**, 041 (2001) [arXiv:hep-th/0105276].
- [32] O. Aharony, A. Buchel and A. Yarom, “Holographic renormalization of cascading gauge theories,” Phys. Rev. D **72**, 066003 (2005) [arXiv:hep-th/0506002].
- [33] A. Petkou and K. Skenderis, “A Nonrenormalization theorem for conformal anomalies,” Nucl. Phys. B **561**, 100 (1999) [arXiv:hep-th/9906030].
- [34] C.R. Graham and M. Zworski, “Scattering Matrix in Conformal Geometry,” arXiv:math/0109089 [math.DG].
- [35] J. Wess, “The Conformal Invariance in Quantum Field Theory,” Nuovo Cim. **18**, 1086 (1960);
S. R. Coleman and R. Jackiw, “Why dilatation generators do not generate dilatations?,” Annals Phys. **67**, 552 (1971).
- [36] M. Henningson and K. Skenderis, “The holographic Weyl anomaly,” JHEP **9807**, 023 (1998) [arXiv:hep-th/9806087];
M. Henningson and K. Skenderis, “Holography and the Weyl anomaly,” Fortsch. Phys. **48**, 125 (2000) [arXiv:hep-th/9812032].
- [37] E. Berti, V. Cardoso and A. O. Starinets, “Quasinormal modes of black holes and black branes,” Class. Quant. Grav. **26**, 163001 (2009) [arXiv:0905.2975 [gr-qc]].
- [38] A. Nunez and A. O. Starinets, “AdS / CFT correspondence, quasinormal modes, and thermal correlators in N=4 SYM,” Phys. Rev. D **67**, 124013 (2003) [hep-th/0302026].
- [39] I. R. Klebanov and E. Witten, “AdS/CFT correspondence and symmetry breaking,” Nucl. Phys. B **556**, 89 (1999) [arXiv:hep-th/9905104].
- [40] For example, see:
R. Emparan, C. V. Johnson and R. C. Myers, “Surface terms as counterterms in the AdS/CFT correspondence,” Phys. Rev. D **60**, 104001 (1999) [hep-th/9903238].
- [41] R.M. Wald, “Axiomatic Renormalization of the Stress Tensor of a Conformally Invariant Field in Conformally Flat Space-Times,” Annals Phys. **110**, 472 (1978).

- [42] R.M. Wald, “Trace Anomaly of a Conformally Invariant Quantum Field in Curved Space-Time,” *Phys. Rev. D* **17**, 1477 (1978).
- [43] See, for example:
I. Booth, M. P. Heller and M. Spalinski, “Black brane entropy and hydrodynamics: The Boost-invariant case,” *Phys. Rev. D* **80**, 126013 (2009) [arXiv:0910.0748 [hep-th]];
I. Booth, M. P. Heller and M. Spalinski, “Black Brane Entropy and Hydrodynamics,” *Phys. Rev. D* **83**, 061901 (2011) [arXiv:1010.6301 [hep-th]];
I. Booth, M. P. Heller, G. Plewa and M. Spalinski, “On the apparent horizon in fluid-gravity duality,” *Phys. Rev. D* **83**, 106005 (2011) [arXiv:1102.2885 [hep-th]].
- [44] R. A. Isaacson, J. S. Welling and J. Winicour, “Null Cone Computation Of Gravitational Radiation,” *J. Math. Phys.* **24**, 1824 (1983).
- [45] L. Lehner, “A Dissipative algorithm for wave - like equations in the characteristic formulation,” gr-qc/9811095.
- [46] F. Pretorius and L. Lehner, “Adaptive mesh refinement for characteristic codes,” *J. Comput. Phys.* **198**, 10 (2004) [gr-qc/0302003].